



Meniscus regeneration by 3D printing technologies: Current advances and future perspectives

Elena Stocco^{1,2}, Andrea Porzionato^{1,2} , Enrico De Rose¹ ,
Silvia Barbon^{1,2}, Raffaele De Caro^{1,2} and Veronica Macchi^{1,2}

Abstract

Meniscal tears are a frequent orthopedic injury commonly managed by conservative strategies to avoid osteoarthritis development descending from altered biomechanics. Among cutting-edge approaches in tissue engineering, 3D printing technologies are extremely promising guaranteeing for complex biomimetic architectures mimicking native tissues. Considering the anisotropic characteristics of the menisci, and the ability of printing over structural control, it descends the intriguing potential of such vanguard techniques to meet individual joints' requirements within personalized medicine. This literature review provides a state-of-the-art on 3D printing for meniscus reconstruction. Experiences in printing materials/technologies, scaffold types, augmentation strategies, cellular conditioning have been compared/discussed; outcomes of pre-clinical studies allowed for further considerations. To date, translation to clinic of 3D printed meniscal devices is still a challenge: meniscus reconstruction is once again clear expression of how the integration of different expertise (e.g., anatomy, engineering, biomaterials science, cell biology, and medicine) is required to successfully address native tissues complexities.

Keywords

Meniscal tears, 3D printing and bioprinting, printable biomaterials, ultrastructure, tissue engineering

Date received: 18 August 2021; accepted: 24 November 2021

Introduction

The menisci are critical components of a healthy knee joint^{1,2} as exerting a pivotal role in preserving the knee homeostasis³ and biomechanics through load transmission, shock absorption, stability, nutrition, joint lubrication, and proprioception.^{4–6} Consequently, meniscal damage affects knee equilibrium, progressively contributing to cartilage disruption up to osteoarthritis (OA) responsible of pain, loss of joint function, and musculoskeletal morbidity.^{5,7,8} To date, considering meniscal poor-self healing potential,⁹ its repair represents a formidable challenge to orthopedic surgeons.

Efforts in biomechanical/clinical research require a meniscus-preserving strategy instead of meniscus-resection^{10,11} which often lead to poorer clinical outcomes up to total knee arthroplasty.⁶ In particular, degenerative changes showed to be directly proportional to the amount of

meniscus removed; which, in consideration of this, should be minimized preferring a repairing or a replacing approach.^{4,12} Surgical techniques and allograft transplantation were the primary attempts to meniscus repair^{13–15}; however, these procedures display intrinsic limitations in clinical practice as, often, the occurrence of partial or even total meniscal resection is an imminent need.

To counteract the increasing incidence rate of meniscal injury, innovative, and effective repair strategies are required¹⁶

¹Department of Neuroscience, Section of Human Anatomy, University of Padova, Padova, Italy

²L.i.f.e.L.a.b. Program, Consorzio per la Ricerca Sanitaria, Padova, Italy

Corresponding author:

Andrea Porzionato, Department of Neuroscience, Section of Human Anatomy, University of Padova, Via Aristide Gabelli 65, Padova 35121, Italy.

Email: andrea.porzionato@unipd.it



and among vanguard approaches, 3D printing technologies seem to be intriguing and promising. Reviewing the literature, the interest that 3D printing/bioprinting applied to tissue engineering is gaining, appears particularly evident. Development of bone and cartilage scaffolds,^{17,18} thyroid cartilage supports,¹⁹ engineered nasal cartilage implants,²⁰ dentin-pulp substitutes,²¹ devices for adipose tissue regeneration,²² as well as hydrogel systems for biomedical applications²³ are only few examples. As highlighted by Rongen et al.²⁴ in an interesting review article focusing on biomaterials for meniscus substitutes, the ideal scaffold should satisfy some basic requirements. These include mechanical and tribological properties, resembling that of the native meniscus; an adequate shape and size (preferably customized according to patient needs); biocompatibility of the materials used for scaffolds fabrication without leading to cytotoxicity during resorption; biomimicry; favorable porosity satisfying both mechanical stability and cell colonization requirements; adequate degradation profile. Despite still far from clinic, printing approaches for meniscus reconstruction are rapidly developing and great attempts are currently ongoing to meet the criteria above. In particular, extensive research is directed toward the identification of biomaterials, ink/bioinks formulations, cell types able to guarantee for satisfactory outcomes, and future translation to clinic.

Considering this scenario, the aim of this systematic revision of the literature is to provide the state of the art on 3D printing technologies for the manufacture of meniscal substitutes; as the key for successful devices resides on the ability to replicate anatomy, a framework on meniscus macroscopic and microscopic organization is preliminary presented to focus the target tissue and describe the peculiar characteristics that must be sought. Thus, after considering the common meniscal ruptures and currently available approaches (with their limits), an overview on 3D printing technologies is provided to get a basic understanding of 3D printing.

Meniscal scaffolds must assure a balance of shape, biomechanical function, and biocompatibility to guarantee tissue replacement success. Four different categories of devices may be recognized considering the main characteristics of the 3D printed/3Dbioprinted supports reported in the literature: (a) synthetic 3D printed bare scaffolds; (b) synthetic 3D printed conditioned scaffolds; (c) 3D bioprinted scaffolds; (d) synthetic 3D printed + 3D bioprinted composite scaffolds.

To date, the choice and the identification of the most adequate meniscal substitute still represent a challenge and an unmet need.²⁵

The menisci: From anatomy to function

An engineered meniscus should mimic the structural and biochemical organization of the native tissue to assure for

the proper environment and mechanical support able to guide functional regeneration^{26,27}; thus, knowledge of macroscopic and microscopic anatomy is imperative for successful reproduction of the tissue-specific characteristics through vanguard technological approaches²⁸ (Figure 1). Additionally, considering 3D bioprinting strategies including cellular elements in bioinks formulations, consciousness on resident cells phenotype, and peculiar spatial organization may guide in developing effective bioprinted devices.

Macroscopic and microscopic anatomy

In the knee joint, the lateral meniscus (C-shaped) and the medial meniscus (more semicircular shape) are fibrocartilaginous structures, roughly triangular in cross section. They cover approximately the 70% of the tibial plateau articular surface⁵ and they show a unique composition and structure.²⁹ The peripheral, vascular border of each meniscus is thick, convex, and attached to the joint capsule. The innermost border recedes to form a thin free edge. Superiorly, the menisci articulate with the convex femoral condyles, inferiorly they accommodate the tibial plateau.^{30,31}

The menisci receive blood supply by the branches of the popliteal artery, the medial, and the lateral middle geniculate arteries, respectively.^{29,31,32} Vascularization allows to identify here three distinct zones: the vascularized red-red zone, located in the outer edge of the meniscus; the partially vascularized red-white zone, located in the middle; the avascular white-white zone, in the innermost area of the meniscus.²⁹ Only 10%–30% of the medial meniscus and 10%–25% of the lateral meniscus are directly vascularized.^{31,33,34} Nutrition of the central portions of the menisci (i.e. white-white and red-white zones) depends on synovial fluid diffusion, a mechanism sustained by the intermittent loading/release of stress mediated through body weight and muscular force.^{29,35}

Innervation of the menisci has the same distribution of vascularization; the capsule of the knee is penetrated by the branches of the posterior tibial nerve, obturator nerve, femoral nerve, and the common peroneal nerve.^{29,32,36,37} Nociceptive free nerve endings are contained in the peripheral two-thirds of the menisci, while different mechanoreceptors are identifiable in the anterior and posterior horns^{29,32,37} suggesting a proprioceptive function.

According to meniscal anatomical organization, in case of injury, while repair of the outer region is successful, meniscal lesions affecting the inner portion of the tissue often lead to partial meniscectomy.³⁸

As for menisci resident cells, three main subpopulations have been identified according to the different meniscal regions and specific cell morphology³⁹: (a) fibroblast-like cells with elongated morphology in the outer meniscal area, (b) chondrocyte-like cells with oval to round shape in the inner region, and (c) fusiform cells

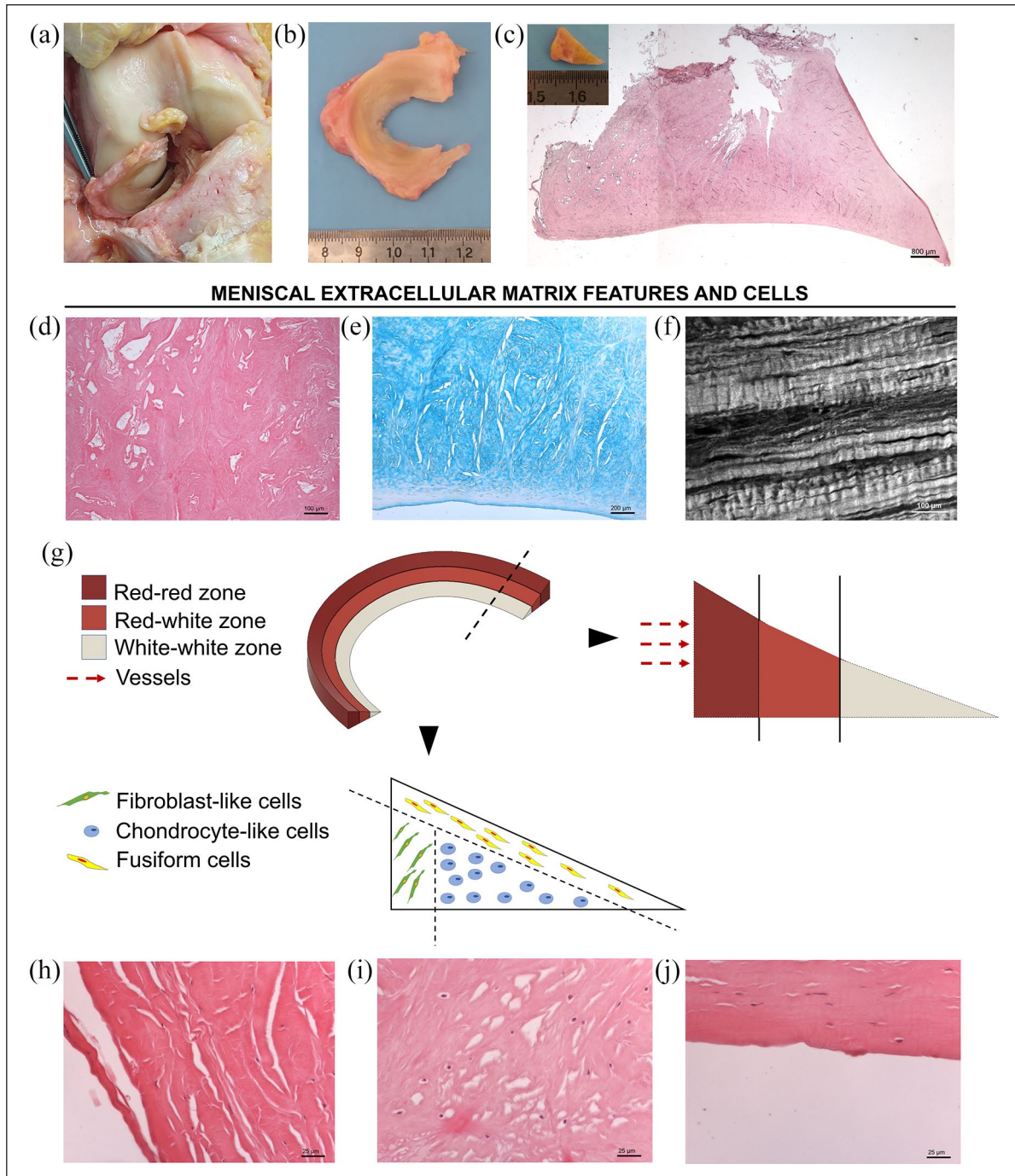


Figure 1. Representative macroscopic and microscopic anatomy of the lateral meniscus (LM). (a) Anterior view of human right knee in flexion. After dissection and removal of patellar ligament and patella, the knee was subluxated showing the LM position between the femoral condyle and the tibial plateau. (b) Gross appearance of the LM soon after excision (superior view), showing its typical crescent C-shape profile, thicker peripherally. (c) Representative section of the LM stained with Hematoxylin and Eosin (H&E). Insert: gross appearance of the tissue in cross-section showing its characteristic triangular shape. (d and e) Extracellular matrix details by H&E (d) and Alcian Blue (e) staining for tissue organization and sulfated glycosaminoglycans/glycoproteins identification, respectively; (f) meniscal tissue appearance by Second Harmonic Generation Microscopy showing the specific orientation of collagen fibrils within the tissue through a label-free approach. (g) Schematic diagram representing the three different areas identifiable in the meniscus, according to vessels distribution: red-red zone; red-white zone; white-white zone; moreover, also specific cells distribution is represented, distinguishing localization of fibroblast-like cells, in the outer zone; chondrocyte-like cells, in the center of the meniscal tissue; fusiform cells, in correspondence of the superficial margin of the meniscus. (h–j) Histological appearance of meniscal cells by H&E. (h) Fibroblast-like cells display long cell extensions; (i) chondrocyte-like cells show a round shape; (j) fusiform cells has no cell extensions (scale bars: 800 μm (c); 100 μm (d and f); 200 μm (f); 25 μm (h–j)).

aligned parallel to the meniscal surface in the superficial zone. Meniscal cells can be detected as isolated, in pairs or in short rows, being either randomly arranged or aligned in longitudinal rows between dense collagen fibers; while the outer two-thirds of meniscal area resemble fibrocartilage organization (cells interconnected by gap junctions), the inner one-third of the tissue presents hyaline cartilage arrangement, with unconnected cells.⁴⁰

While most meniscal cells exhibit a CD34⁻/CD31⁻ phenotype, the fusiform cells of the superficial area were found to be CD34⁺, suggesting that they might be specific progenitors responsible for therapeutic and regenerative effects.^{41,42} In fact, CD34 is acknowledged as a marker of mesenchymal stem cells (MSCs) with high regenerative potential, also expressing alpha-smooth muscle actin (α -SMA).^{43,44} Based on that, CD34⁺/ α -SMA⁺ meniscus cells have been proposed to participate in the reparative process of pathological menisci.⁴²

The ECM composition of normal human menisci mainly consists of water (70%–80%); as for the remaining portion (20%–30%), it is represented by collagen (50%–75%) and glycosaminoglycans (GAGs) (15%–30%).³⁹ Type I collagen constitutes more than 90% of collagen content, being distributed throughout the whole meniscus, from the peripheral to inner area, and organized in circumferential fibers.^{45,46} On the other hand, collagen type II is predominantly localized in the inner avascular zone, showing an organized network of circumferential and radial fibers.⁴⁶ Variable amounts of types III, IV, V, and VI collagen can also be detected within the meniscus.⁴⁵ Collagens were demonstrated to be primarily responsible for the tensile strength of menisci.³⁰

Besides collagen, other matrix proteins include fibronectin, which is known to regulate many cellular processes (i.e. tissue repair, embryogenesis, blood clotting, and cell migration/adhesion) and elastin, which is supposed to interact with collagen to ensure for tissue resiliency.³⁹

Proteoglycans form an organized network mainly localized in the inner zone of the meniscal tissue. The glycosaminoglycan profile of the normal adult human meniscus consists of chondroitin-6-sulfate (40%–60%), chondroitin-4-sulfate (10%–20%), dermatan sulfate (20%–30%), keratan sulfate (15%), and hyaluronic acid (3%).³⁹ Adhesion glycoproteins like fibronectin and thrombospondin connect meniscal cells with the surrounding ECM.⁴⁶ GAGs are more concentrated in the meniscal horns and inner zone of the tissue, which correspond to the primary weightbearing areas.³⁰ Being characterized by high specialized structure, high fixed-charge density, and charge-charge repulsion forces, proteoglycans in the meniscal ECM are suggested to be responsible for tissue hydration, as well as its ability to bear compressive loads, providing the meniscus with the typical viscoelastic mechanical behavior.^{30,39}

Menisci function and biomechanics

During normal daily activities, the knee joint is loaded by up to five times body weight⁴⁷ withstanding different types of forces including shear, tension, compression, and hydrostatic pressure.^{1,48} The menisci, by virtue of their specific wedge-shape, can bear this total joint load (from 45% to 75%) with variations associated to the degree of joint flexion and the health of the tissue.⁴⁹ In particular, the horn attachments allow for conversion of the vertical compressive forces to horizontal hoop stresses.¹

Joint load and mechanical factors play a key role in meniscus homeostasis, orchestrating the biological activity of meniscal cells in both physiological and pathological conditions.⁴⁸ It descends that a profound consciousness about the mechanobiology of the meniscus is fundamental not only to manage the onset and eventual progression of meniscal degeneration but also for the identification, design, and manufacture of optimal meniscal replacements to restore normal tibiofemoral contact pressure in the knee joint.^{50,51}

For a true classification of meniscal tissue properties, avoiding variability among species, human meniscal specimens have specifically to be considered.⁵⁰ The meniscus resists axial compression with an aggregate modulus of 100–150 kPa. As for the tensile modulus of the tissue, it is about 100–300 MPa in circumferential direction and 10-fold lower radially. Finally, the shear modulus of the meniscus is approximately 120 kPa.¹ The menisci also enable effective articulation between the femoral condyles and the tibial plateau⁵ leaving 1 mm space in the articulating surface, with only 10% of contact between femur/tibia; this anatomical organization allows controlling stress on the articular cartilage⁵² and is necessarily altered when meniscectomies occur. Studies considering the biomechanical effects of meniscectomies within the joint showed an increase of 235%–335% in peak local contact load in case of total removal of the lateral meniscus⁵³; >350% in contact forces on the articular cartilage in partial (16%–34%) meniscectomy⁵⁴; and overall increase in contact forces by two to three times, following total meniscectomy.⁵⁵

To effectively maintain their load-bearing function, the menisci can partly move when the knees are in flexion. For human weight-bearing knees, the reported displacements (medial/lateral meniscus, mean \pm SD) are anterior-posterior displacement of the anterior horn $7.1 \pm 2.5/9.5 \pm 4.0$ mm and that of the posterior horn $3.9 \pm 1.8/5.6 \pm 2.8$ mm and a radial displacement of 3.6 ± 2.3 mm/ 3.7 ± 1.7 mm.²⁴

Other functions associated to the menisci are shock absorption (mediated by their ligamentous fixation to the femur and the tibia),⁵⁶ lubrication of the knee joint, nutrition supply to the articular cartilage and proprioception.^{57–59}

Ligaments (i.e. medial collateral ligament, the transverse ligament, and the meniscofemoral ligaments) good shape and tight are a prerogative to assure an effective meniscal function.⁵⁶

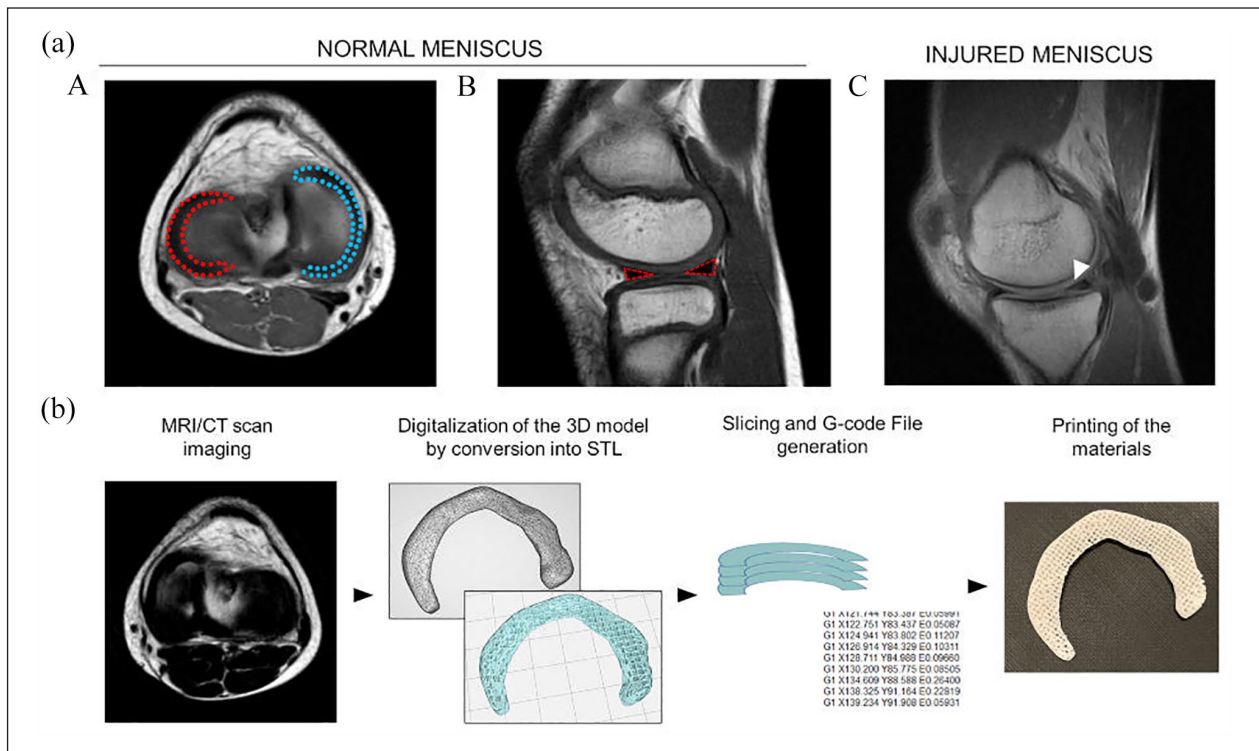


Figure 2. (a) Magnetic resonance imaging of the knee. (A and B) Normal menisci (lateral meniscus: red-dotted; medial meniscus: blue-dotted) and (C) injured meniscus. Specifically, sagittal T1 weighted image reveals a horizontal tear of the posterior horn of the medial meniscus (white arrow). (b) Flow-diagram describing the methodological steps required to print a tissue (i.e. meniscal tissue) from Magnetic Resonance Imaging (MRI)/Computed Tomography (CT). STL: Standard Triangulation Language.

Tears and current treatment options overview

Meniscal tears, showing a bimodal age distribution in young and elderly people, have an incidence per year of 60–70 per 100,000 population.⁵ As for etiopathogenesis, it can be either (a) acute traumatic: mainly in healthy knee joint, if left untreated may lead to secondary OA⁶⁰; (b) chronic degenerative (can also be asymptomatic): mainly in elderly people, within compromised or abnormal joints/menisci. OA is surely a predisposing factor being account as a “whole joint disease”.^{61–63} Additionally, age alone is a critical (and unavoidable) risk factor too.^{64–68}

Typical meniscal tears distinguish five patterns clearly recognizable through Magnetic Resonance Imaging (MRI); these include radial, horizontal longitudinal, vertical longitudinal, oblique, and a complex combination of multiple patterns. The healthy meniscus typically experiences longitudinal tears, bucket-handle tears (vertical split and in line with the orientation of the circumferential collagen fibers), or radial tears (perpendicular split to the long axis). Degenerative meniscal tears are mainly horizontal-cleavage lesions or complex characterized by thin, lesioned, and fibrillated margins (Figure 2).⁶⁰

Treatment options range from non-surgical interventions (i.e. physical therapy) to surgical interventions

including meniscectomy (total and partial performed open or arthroscopically), meniscal repair, and meniscal reconstruction.^{69,70} Nowadays, total meniscectomy is never performed as a primary procedure as predisposing to degenerative changes up to early OA.^{69,71,72} Partial meniscectomy is suggested in case of radial tears at the white-white zone and degenerative meniscal tears displaying mechanical symptoms with no response after 3–6 months to non-surgical approach and after radiological evaluation.⁷³ Therefore, in accordance with data based on clinical experience, meniscal repair, or non-removal procedures in traumatic tears should be the recommended choice to achieve tissue healing.^{69,74}

Considering repair approaches, different suture types can be adopted^{69,75–77} and biological approaches (augmentation techniques) can also be used in combination to enhance the healing response (augmentation by platelet rich plasma (PRP) and platelet rich fibrin (PRF) clot derivatives^{78,79}; trephination, abrasion, and rasping; wrapping^{80,81}). The main drawback with conventional suture techniques relies on long operating time and difficulties in surgery. Therefore, meniscal allograft transplantation (MAT) or more recent meniscal scaffolds have been developed to overcome these issues.

MAT, mimicking the typical loading pattern of the knee, significantly reduces compartment contact pressures

thus protecting from cartilage degeneration.⁵³ However, they are not free from limitations (allografts preparation/preservation,⁸² meniscus sizing,^{82,83} possible graft failure, extrusion, infection, arthrofibrosis, the need for reoperation, aseptic synovitis, hematoma, limited range of motion, joint effusion, and bone plug loosening⁸⁴). Moreover, MAT is not the preferred approach following partial meniscal resection as meniscal scaffolds can induce fibrocartilage tissue.⁸⁵

Commercial scaffolds

To date, three commercial scaffolds are available to reconstruct the segmental meniscus defects⁸⁶ and they belong to two categories: collagen-based implants (Menaflex—ReGen, USA, also known as the collagen meniscus implant CMI®—Ivy Sports Medicine, Germany) and synthetic polymer-based implants (Actifit®—Orteq Ltd., London, UK; NUsurface®—Active Implants, LLC., Memphis, TN, USA).

Menaflex CMI® is crescent-shaped spongy device which can be adjusted to fit the meniscal defect area prior to be sutured to the remaining native meniscus in arthroscopy. It is made of lyophilized and cross-linked purified type I collagen from bovine Achilles tendon, enriched with hyaluronic acid and chondroitin sulfate.^{87,88} The Actifit® is a biodegradable, synthetic, acellular implant in aliphatic polyurethane and polycaprolactone.^{88,89} It has meniscal shape; prior to be arthroscopically implanted and sutured to the meniscal wall and residual meniscus, Actifit® can be cut to match the size of the defect.⁹⁰ Both Menaflex CMI® and Actifit® are adequate in case of partial meniscectomy. Their implant occurs without prior cell seeding; however, they have a proper ultrastructure allowing for optimal resident cells colonization and fibrocartilage ingrowth in turn reducing risk of OA development. After tissue reconstitution, degradation of the implant progressively occurs.^{87,89} NUsurface® Meniscus Implant is a non-anatomically discoid-shaped, free floating and non-anchored meniscal prosthesis designed for total replacement of the medial meniscus. It is made from polycarbonate-urethane (PCU) reinforced with high tensile Ultra High Molecular Weight Polyethylene (UHMWPE) fibers, allowing to mimic and restore the natural contact pattern of pressure distribution within the medial meniscus.⁹¹

Although these scaffolds are designed to stimulate the growth of new tissues or mimic the function of the natural meniscus, the best meniscal scaffold type remains controversial^{92–94} and additional research is required.⁷⁰

Clinical failure (e.g. infections, mechanical failure, chronic synovitis development, need for a second surgery) is reported in up to 8% and 32% for the CMI and Actifit®, respectively. As for NUsurface® Meniscus Implant evidence-based clinical data are still largely absent and FDA approval for it is still pending.¹¹

To date, there is consensus that only a substitute which closely matches normal meniscal tissue properties can re-establish meniscal functions.⁹⁵ Improvement in structure and material design is the direction for advances in surgical meniscal treatment assuring for stable devices that, while bearing the load, also promote meniscal repair and reconstruction.

From additive manufacturing technologies to 3D bioprinting strategies for tissues customization

3D printing technologies, also known as additive manufacturing (AM) technologies or 3D rapid prototyping technologies (i.e. binder jetting, directed energy deposition, material extrusion, material jetting, powder bed fusion, sheet lamination, and vat photopolymerization) represent interesting and emerging approaches to mimic key structural and functional properties of different human tissues from a patient's own medical images,^{96,97} thus overcoming the limits of the traditional methods for manufacturing 3D scaffolds (electrospinning, freeze-drying, gas foaming, particle/porogen leaching).

However, due to inability of AM technologies to print cell-loaded materials, 3D bioprinting methods emerged as intriguing alternatives, distinguishing for a more biological approach to design/manufacture 3D scaffolds.

3D bioprinter technologies can print cell-free natural polymers—the “bio-paper,” cell aggregates, cells encapsulated in hydrogels, or cell-seeded microcarriers formulated as “bioinks”.^{98,99} Typically, biomaterials for 3D bioprinting are soft and mechanically weak hydrogels with thermo-sensitive properties but endowed with intrinsic biological properties allowing for cell colonization. Fusion chambers, prior used to melt polymer filaments, are here converted in pneumatic-based extruders; print head can be equipped with heating/cooling elements to guarantee for tunable print conditions according to different types of bioinks. Nozzles are substituted with needles and piezoelectric elements, while print beds are equipped with cooling and UV light elements to avoid collapsing of low viscosity bioinks.^{99–103}

In bioprinting, different technologies can be identified according to the bioink dispensing method: inkjet-based 3D bioprinting, extrusion-based 3D bioprinting, laser-assisted 3D bioprinting,^{104–108} vat photopolymerization-based bioprinting^{109,110} (Figure 3).

Inkjet-based 3D bioprinting

Inkjet-based methods employ cells or biomaterials instead of the ink used in the existing commercial inkjet printers; moreover, a moving stage is present instead of paper.

According to the actuator type, inkjet-based 3D bioprinters distinguish the thermal jetting systems and the piezoelectric jetting systems.¹¹¹ The actuator generates a

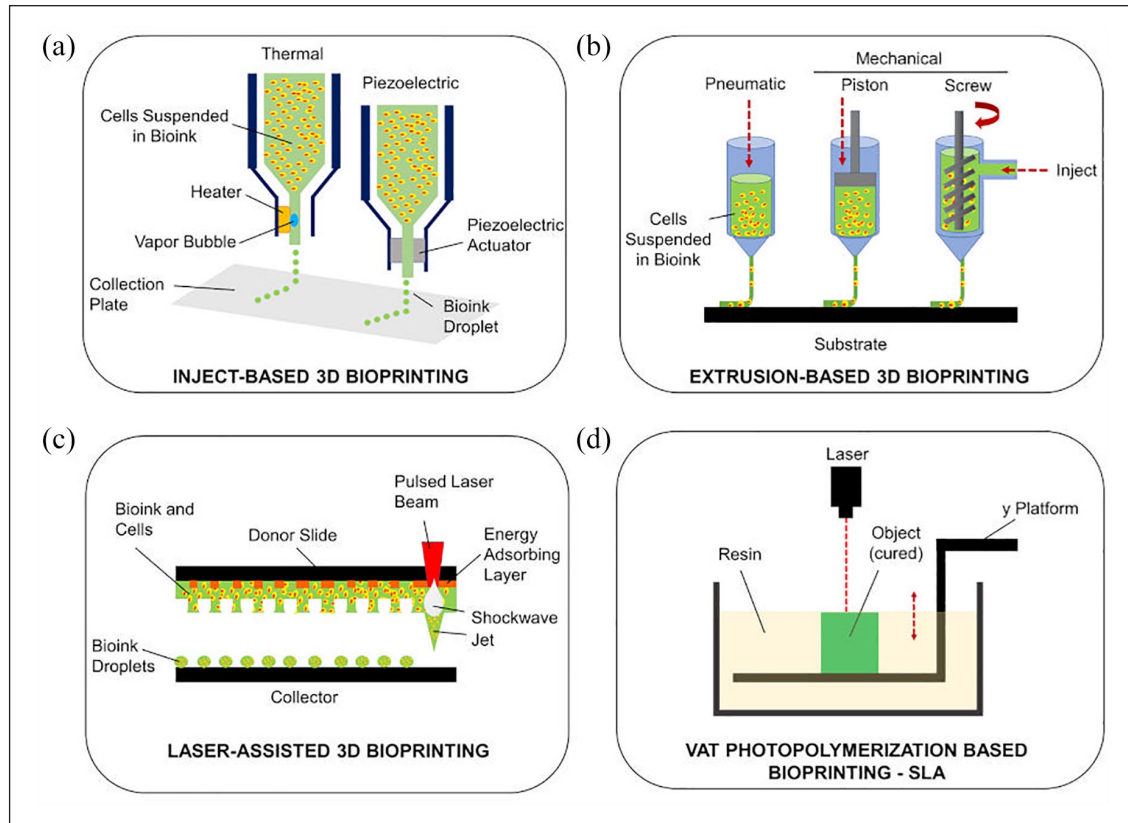


Figure 3. 3D bioprinting technologies. Schematic representation of the main technologies identifiable in 3D bioprinting: (a) inkjet-based 3D bioprinting, (b) extrusion-based 3D bioprinting, (c) laser assisted 3D bioprinting, and (d) vat photopolymerization-based bioprinting (SLA: stereolithography).

pressure overcoming the surface tension at the nozzle opening, thus inducing the ejection of the bioink droplets ($10\ \mu\text{m}$) deposited in a “bottom-up” manner. Bioinks are required to show low viscosities ($10\text{--}100\ \mu\text{Pa}\cdot\text{s}$) to avoid small nozzle clogging. Cell density cannot be high; a shear viscosity of $30\ \text{MPa}\cdot\text{s}$ is the upper boundary of what is “safely” printable through this approach.¹¹²

In the thermal heater method (or bubble-jet method) the materials are turned into ink droplets at the nozzle by heat. Heating generates small air bubbles in the printhead and their collapse allows for ink drops ejection.¹¹³ Controlling temperature and/or modulating pressure pulses frequency it is possible to exert control over droplets size and volume. This approach is adequate for structures requiring high control over ultrastructure.

In the piezoelectric actuator method, ink droplets are created through voltage application to the piezoelectric elements. Despite this approach guarantees for great control over droplets size, the cells are likely affected by the physical impact thus compromising cell membrane integrity. Considering this issue, thermal jetting is often preferred over the piezoelectric-based method.¹¹²

The inkjet method is low cost and it guarantees for short fabrication time (printing speed: $1\text{--}10,000$ droplets/s).

Unfortunately, the obtained products are stiff, and the layers cannot be stacked very high. Moreover, denaturalization of the biomaterials and inconsistent ink droplets can also occur.^{108,112,114,115}

The use of different materials has been reported, these include in example alginate, gelatin, collagen type I, fibrin, polyethylene glycol, gelatin methacrylate (GelMA).

Extrusion-based 3D bioprinting

Extrusion-based methods work dispensing bioink in a continuous filament to produce a 3D structure organized in a layer-by-layer manner¹¹²; printing speed is set at $0.1\text{--}150\ \text{mm/s}$ ¹⁰⁸ According to the dispensing method, pneumatic-extrusion bioprinters or mechanical-extrusion bioprinters can be distinguished; moreover, the mechanical-extrusion bioprinters can also be divided in piston-systems or screw-driven systems.¹¹⁶

In general, extrusion methods can print materials within a viscosity range value of $30\text{--}25 \times 10^3\ \text{MPa}\cdot\text{s}$. Applying the pressure, it is expected a reduction in bioink viscosity, thus allowing its deposition, followed by a prompt increase in viscosity soon after the removal of the shear force. Gelation must occur immediately after deposition to guarantee for

scaffold structure maintenance; however, this depends on the hydrogel solution. In fact, in presence of high water content, the bioink may flow after printing leading to low resolution structures (40–1200 μm). To overcome this limit, affecting resolution, hydrogels with high viscosity or with self-assembling characteristics can be adopted; in parallel, cross-linking during extrusion, the use of a co-extrusion or thermoplastic reinforcement or the extrusion of bioinks in a secondary structure called suspension bath (providing support during gelation) can be adopted.¹¹² Other critical issues include frequent blockage of the nozzles and shear-induced cell death (cell viability ranging from 60% to 90%).^{108,117}

Highly viscous materials are generally approached with screw-driven systems; piston- or pneumatic-based extrusion systems are typically used with lower viscosities.

Extrusion-based approaches have been reported in example with alginate, gelatin, gellan gum, guar gum, methylcellulose, collagen type I, matrigel, fibrinogen, collagen methacrylate, GelMA, elastin, polycaprolactone (PCL), polyethylene glycol (PEG), polyvinyl alcohol (PVA), and polyvinyl acetate.¹⁰⁸

Laser-assisted 3D bioprinting

Laser-assisted methods allow to obtain different structures through a laser, without presence of a nozzle. Together with the pulsed laser source, the other components include a ribbon, serving as a support for the printing material, and a support to collect the printed material. Briefly, the ribbon is a thin absorbing layer of metal (e.g. gold or titanium) coated onto a laser transparent support (i.e. glass). The bioink is deposited at the surface of the metal film; once the laser pulse induces metal film vaporization, the bioink reaches the collector in the form of droplets.¹¹²

Printed materials can be both solid and liquid even though hydrogels are preferred. Despite the existence of possible issues in cells viability ascribable to high levels of thermal energy, controlling intensity/extent of laser exposure guarantees for good performances (viability, $\geq 90\%$) associated to high printing speed (1–2000 mm/s) and resolution (40–100 μm). Low efficiency has been encountered in fabricating high 3D layering.^{108,118}

Vat polymerization-based bioprinting

Vat polymerization-based bioprinting, the most common of which is stereolithography (SLA), is constituted by a building platform, a vat of photopolymer resin, and a light source for resin irradiation. Specifically, according to the irradiation approach, two methods can be recognized: the vectorwise and the mask irradiation. Both a top-down printing and bottom-up printing can be adopted.^{109,119}

In the vectorwise, scanning galvanometers scan the resin surface through a ultraviolet (UV), infrared (IR), or visible

light laser beam. Photopolymerization occurs at the scanned regions thus leading to resin solidification. Once the first layer is built, the building platform descends inside the vat to allow for recoating with resin and subsequent photopolymerization. Each layer is built one by one.^{109,112,118}

In the mask irradiation approach the entire resin surface is irradiated, solidifying in a single step. This strategy allows for more complex structures than vectorwise SLA. Many different photopolymers and cell-laden hydrogels can be used when adopting this bioprinting technique: no particular rheological characteristics are required (upper suspension viscosity limit, 5 Pa s; lower limit, sufficient enough to prevent cells homogeneous and stable distribution).^{109,112,119}

To promote photopolymerization, specific crosslinking agents can be included within the bioink (e.g. methacrylates, azides). Moreover, careful attention must be paid to the gelation strategies as cells viability may be affected by them. To overcome this issue, two-photon polymerization (2PP) has been introduced to fast this phase. 2PP guarantees for high control over ultrastructure.¹¹²

Among the materials used in SLA can be recognized acrylated PEG, PVA, chitosan, GelMA, Allylated gelatin (GelAGE), methacrylated hyaluronic acid, silk fibroin (SF).^{109,119}

Bioinks formulations and critical issues

3D bioprinting technology mainly relies on advanced 3D bioprinters (for details on 3D printing methods see the paragraphs above) and effective cell-laden bioinks.¹²⁰

Cell-laden bioinks are based on polymeric materials (with/without additives and/or crosslinking agents); besides cells encapsulation they are required to assure for their viability, homogeneous distribution and proliferation. Thus, they do not act as an inert carrier, but they constitute the microenvironment which will significantly affect cells behavior within the 3D structure and the leading agent responsible for 3D structure integrity.^{121–123}

To guide the formulation of an ideal bioink, consciousness is mandatory on the characteristics that it is expected to be endowed with. Specifically, these include adequate rheological features, ability to provide a proper biocompatible micro-environment mimicking the target tissue, a controlled biodegradability compatible with dynamic cellular remodeling of the construct. Moreover, due to cellular presence, it is also expected a certain control over shear-thinning behavior (for minimal stress to cells during extrusion), sol-gel transition, and extrudability without clogging the nozzle. Thus, the printed structure is required to show satisfactory mechanical strength and rigidity matching that of the implant site, shape fidelity, and proper ultrastructure (pore size) to support constructs bioactivity (diffusion of oxygen, carbon dioxide, and nutrients).^{124–127}

Since identifying the optimal cell-laden bioink formulation is the crucial step for successful bioprinting, several formulations have been attempted (Tables 3 and 4). In example, considering a bioink for extrusion-based bioprinting, it is initially in a bulk resting state, then it experiences a transition to a high shear condition while passing through the nozzle, and finally it is required to assume a new and stable resting shape after extrusion. All these transitions must take place in a respectful manner toward cells.¹²³

Despite the large number of biomaterials for TE and regenerative medicine, many of them are not compatible with 3D bioprinting strategies.¹²⁸ Only through adequate materials selection and modulating concentration, molecular weight, and crosslinking strategy, the elastic moduli of the bioinks can be tuned¹⁰⁷ with direct impact on the functionality of the final printed tissues and organ. As discussed above, the materials investigated for meniscal cell-laden bioinks include SF, gelatin, alginate, cellulose, GelMA, decellularized extracellular matrix (dECM), hyaluronic acid (HA), glycerol, alginate, collagen, gellan gum (Tables 3 and 4). Due to high-water content, good swelling characteristics, biocompatibility, biodegradability, and the presence of cell-binding sites, natural hydrogels are attractive for TE purposes. Optimal cells performances have been demonstrated with relatively soft and printable inks¹²³ which can also induce stem cells differentiation toward specific lineages by virtue of intrinsic and specific features.¹²⁹ However, hydrogels do not display significant strength and shape fidelity compared to synthetic polymers, representing a critical feature to manage. Despite variations in temperature and pressures as well as introduction of additives that may help in rheology modulation/control, the presence of cells within the bioink represents a stringent limit in the window of processing.¹²³ Higher viscosity assures for higher printing fidelity; however, it also leads to increased shear stress, which may impact the cells suspended in the bioink. Moreover, crosslinking strategies (i.e. thermal, chemical, physical, or enzymatic strategies also combined) could influence cells viability too, thus representing a further issue to manage. Most importantly, cell embedding itself (i.e., cell density) significantly affects the rheology of the final hydrogel: the volume occupied by cells is precluded to the hydrogel, likely exerting an effect on cross-linking efficiency and viscoelastic properties.¹²⁷

Formulating a cell-laden bioink is a delicate multistep phase which will be finally responsible for tissue construct efficiency. Intense efforts must be devoted toward the identification of a formula guaranteeing a proper equilibrium between bioink intrinsic characteristics, cellular density/survival along with the bioprinter technology adopted. Once identified the core material/materials, preliminary tests are mandatory for evaluation of different concentrations and ratios to gain satisfactory results in term of physicochemical features, printability, rheological and mechanical traits, cells distribution, and survival. In this

context, also bioprinter settings (temperature, pressure, flow rate, nozzle type, crosslinking strategy) should be tested and eventually adjusted leading to an efficient formulation and a promising tissue substitute.

Referring to the cell-laden bioinks for meniscal tissue bioprinting (Tables 3 and 4) both simple (only one core material + cells)^{130–134} and complex (core material + additives + cells)^{97,135–139} bioinks were experienced. According to our knowledge, collagen was the preferred hydrogel to formulate “simple” bioinks.^{131,132,134} Acting on concentration and temperature it is possible to control gelation. However, the use of alginate^{130,133} (crosslinking by 1% CaCl₂ solution) and dECM¹³² (crosslinking by temperature) was also reported. Regarding “complex” bioinks, alginate was combined with gelatin and cellulose nanofibers in different proportions (crosslinking by 0.1% w/v CaCl₂); higher gelatin content and cellulose nanofiber presence allowed for higher viscosity.⁹⁷ Similarly, Markstedt et al.¹³⁸ improved shape fidelity of an alginate bioink through nanofibrillated cellulose (cross-linking by 90 mM CaCl₂) while Narayanan et al.¹³³ by PLA nanofibers (crosslinking by 1% CaCl₂ solution). Romanazzo et al.¹³⁷ mixed alginate with meniscal dECM (crosslinking by 48/92 mM CaCl₂). Other composite cell-laden bioink formulations were that reported by Sun et al.,¹³⁶ using gelatin + fibrinogen + hyaluronic acid + glycerol encapsulating PLGA microparticles carrying TGFβ3 or CTGF; Jian et al.,¹³⁵ combining GelMA with pig meniscal dECM (crosslinking by blue light, 405 nm); Costa et al.,¹³⁹ proposing a sequential co-printing gellan gum/fibrinogen + porcine meniscus cells and SF methacrylate: here, gellan gum and fibrinogen lead to a stable hydrogel by a combination of ionic and enzymatic cross-linking while SF methacrylate lead to beta-sheet formation along culture time.

As for cell densities, the values are reported in Tables 3 and 4.

Synthetic and natural materials for meniscal scaffolds printing, conditioning, and bioprinting

Polymers or hydrogel precursors eventually enriched in biological factors including cells have been widely investigated for effective development of 3D printed/bioprinted meniscal scaffolds. Both synthetic (PCL,^{12,15,25,27,135,137,140–149} also combined with polyurethane PU/PCL¹³²; polycarbonate urethane¹⁵⁰; silicone elastomers i.e. Ecoflex30, Ecoflex50^{151,152}; poly(desaminotyrosyl-tyrosine dodecyl ester dodecanoate) (p(DTD DD))^{38,153,154}; poly(ethylene oxide-terephthalate)-copoly(butylene terephthalate) (PEOT/PBT)¹⁵⁵; polylactic acid (PLA)¹⁵⁶) and natural materials (protein-based hydrogels: collagen,^{38,131,132,134,150,153,154,156} gelatin,^{27,97,135,136,141,157} silk-fibroin^{139,140,142,146,157}; polysaccharides: agarose,^{27,141} alginate,^{97,130,133,137,138,156} hyaluronic acid,^{38,136,154} gellan gum¹³⁹; dECMs^{132,135,137,147}) have been exploited.

Synthetic materials

PCL. PCL is an aliphatic and biodegradable polyester.¹⁵⁸ It has a rather low melting temperature of 59°C–64°C and a glass transition temperature of about –60°C with a degree of crystallinity up to 69% resulting in high toughness. These features, together with its rheological properties and mechanical behavior (relatively low tensile strength, 23–25 MPa; elastic modulus, 330–360 MPa), make it adequate to be widely used in melt-based extrusion printing.^{159–161} PCL has been extensively explored for biomedical applications by virtue of biocompatibility and a slow degradation rate (i.e. 2–3 years) mainly due to its hydrophobicity.¹⁵⁸ It has been also evaluated in combination (e.g. PCL-biphasic calcium phosphates).¹⁶² In vivo, its resorption is mediated by the lipase enzyme secreted in the interstitial fluid by cells.

PCL is a material of choice for 3D printed meniscal scaffolds fabrication by the extrusion-based AM technique: bare^{12,15,25,143,144,148} and bioactivated (additives^{27,140–142,146,147} or bioinks^{135–137}) PCL supports with different shapes (i.e. cylinder scaffolds,^{12,143,148} prism-like,^{27,141,144,156} cuboid-like,¹⁴² coliseum-like,²⁷ meniscus-like^{15,25,135,136,140,141,145,147,149}) have been widely reported. Different molecular weights have been used, with a lower reported limit of 43,000 Da^{132,143} and an upper limit of 90,000 Da.¹⁴¹ As for nozzle inner diameter, the interval range was 200–516 μm . Simple grid-like meshes and more complex strands designs were both supported by the polymer (Tables 1, 2 and 4).

PUs. PUs are elastomers made through polyaddition of three basic components: diisocyanate, oligodiols (i.e. macrodiol or polyol), and a chain extender (diol or diamine).^{160,163} Specifically, the isocyanate can either be aromatic (higher reactivity and better mechanical properties) or aliphatic (less toxic and more stable to light). Kim et al.¹⁶⁴ described the use thermoplastic PU for fabrication of a 3D printed implantable drug delivery device. As for the oligodiols, these include polyether, polyester, or polycarbonate (PC). PC-based PUs (i.e. PCU) are more durable, with good mechanical properties, hydrolytic resistance, and low friction properties.^{165,166} Zhu et al.,^{167,168} focused on design and biomechanical characterization of PCU-based porous meniscal structures fabricated using triply periodic minimal surfaces (TPMS). Precise control over structure configuration seems to be beneficial to adjust mechanical stiffness of the meniscal implant.

To obtain polymers with intermediate characteristics, they can be blended or copolymerized.^{159,169,170} In meniscus 3D printing, the rate of hydrolysis of PCL has been adjusted through a blend with medical grade PU that is Carbothane PC-3575A (Lubrizol, USA),¹³² widely investigated for the fabrication of long-term implants. For PU/PCL blends the phase transition temperature decreases as PU content increases.¹⁷¹

Through a fused filament fabrication (FFF) approach, Abar et al.¹⁵⁰ prepared different PCU prism-shaped scaffolds characterized by a varying in plane pore-size (i.e.

0/100/200/400/600/800 μm). To do that, the nozzle temperature ranged from 220°C to 212°C, progressively. The temperature of the print bed was set at 40°C and printing occurred at a speed of 360 mm/min using a nozzle with a 0.4 mm inner diameter.

Silicone elastomers. Silicone elastomers Ecoflex (Smooth-On Inc., Macungie, PA, USA) are aliphatic–aromatic co-polyesters. They display an excellent flexibility and relatively fast degradation, without significant toxicological effects. Scant data are reported for their use in biomedicine.¹⁷²

Ecoflex 30 and Ecoflex 50 use in 3D printing of prosthesis is recent: Luis et al.^{151,152,173} fabricated cube/cylinder-like and/or meniscus-like structures through a pneumatic extrusion 3D printer; the experimental setup described by the Authors used nozzles with a diameter of 20–21 G/0.51 mm and a T of the nozzle and of the print bed in the range of 60°C–80°C and 80°C–110°C, respectively.^{152,173} The average porosity achieved was that of 0.27%–0.13% (Ecoflex 50) and 0.35%–0.18% (Ecoflex 30) suggesting the fabrication of high-density 3D-printed silicone scaffolds.¹⁷³

p(DTD DD). Poly(desaminotyrosyl-tyrosine dodecyl ester dodecanoate) (p(DTD DD)) belongs to tyrosine-derived polyarylates developed in the 2003 by Bourke and Kohn.¹⁷⁴ Considering the mechanical properties required to a meniscal scaffold, p(DTD DD) shows the most interesting potential among the polyarylates. Degradation does not produce toxic molecules.¹⁷⁵

As for meniscal scaffolds development, Ghodbane et al.^{38,153,154} fabricated p(DTD DD) printed devices through a pneumatic extrusion approach. Specifically, p(DTD DD) was printed at 160°C at 1.2–4.5 mm/s at a pressure of 8.9–9 bar using 0.4–0.5 mm inner diameter needle; the porosity achieved was of 69.9% \pm 8.0%.

PEOT/PBT. Poly(ethylene oxide-terephthalate)-co-poly(butylene terephthalate) (PEOT/PBT) are thermoplastic elastomers made of a soft segment (i.e. PEOT) and a hard segment (i.e. PBT). Varying the copolymer composition, the PEOT/PBT physical properties can be broadly tuned. The PBT melting temperature increases both with increasing PBT content and with increasing PEOT block length in the copolymer.^{176,177} Also, mechanical and swelling behaviors can change according to the composition of PEOT/PBT copolymers showing variations in tensile strengths from 8 to 23 MPa and in elongations at break from 500% to 1300%.¹⁷⁸ As for degradation, it can occur through hydrolysis and oxidation (in vivo ascribable to macrophages) and can be relatively slow. Long-term effects of degradation in the body are not well known.¹⁷⁹

PEOT/PBT meniscus-like scaffolds were prepared by Moroni et al.¹⁵⁵; the polymer, placed in a syringe and heated at 190 °C, was extruded at a speed of 300 mm/s (pressure, 5 bar) through a needle with a diameter of

Table 1. Synthetic 3D printed bare scaffolds.

Authors and references	Printing method/parameters	Printing material	Additives or biotink	Shape and/or dimensions	Cells	Scaffold characterization studies	In vitro cells/scaffold interactions	In vivo studies
Zhou et al. ¹²	MRI of rabbit leg, 3D CAM/CAD (Mimics, Materialize), FFF 3D printer. Parameters: Nozzle Ø: 317 µm, print T: 130°C; speed: 0.75 mm/s; P: 800 kPa.	PCL Mw 80,000 Da	—	Cylinder scaffolds, 30 × 30 × 2.5 mm; 6.0 × 2.5 mm 236.5 ± 23.8 µm MESH: layer-by-layer, 0°–90° direction	- Rat MFCs (Passage: 2–5) - Rat BM-MSCs (Passage: 2–5)	- SEM - Water contact angle - Degradation - Mechanical behavior, compression	Static culture - Cell viability/proliferation - Cell morphology and attachment	—
Zhang et al. ¹⁵	MRI of rabbit leg 3D CAD (Mimics, Materialize), FFF 3D Printer. Parameters: Nozzle Ø: 317 µm, print T: 130°C; speed: 0.75 mm/s; P: 800 kPa.	PCL Mw 74,000 Da	—	Meniscus-like 215 µm 61.5% MESH: printed fibers Ø, 300 µm; space, 200 µm	- Rabbit BM-MSCs (Passage: 3)	—	—	Orthotopic implant (rabbits) [± cells] 24 h static culture before implant End point: 12, 24 weeks - Synovial fluid (analysis of IL-1 and TNF-α) - Implants (gross evaluation, histology for structure, COL, proteoglycans, IHC for COL III) - Cartilage (gross evaluation, SEM, histology for structure, COL II, scoring) - Mechanical behavior, tensile test
Zhang et al. ²⁵	3D CAD meniscus scaffolds FFF 3D printer Parameters: Nozzle Ø: 317, 516, 516 µm; print T: 130°C; speed: 0.75, 0.85, 0.6 mm/s; P: 800 kPa.	PCL Mw 74,600 Da	—	Meniscus-like 215, 320, 515 µm/ 61.5%, 63.1%, 64.2% MESH: printed fibers Ø, 304, 315, 328 µm; space, 200, 300, 500 µm	- Rabbit BM-MSCs (Passage: 2–3)	- Surface wettability - Mechanical behavior, tensile/compression	Static culture - Cell adhesion, viability and proliferation - DNA content, GAG, COL III - Gene expression (fibrochondrogenesis-COL I/II, aggrecan; osteogenesis-ALP; hypertrophy—COLX) - If for COL III deposition - Mechanical behavior, tensile/compressive/elastic moduli	Orthotopic implant (rabbit) [– cells] End point: 12 weeks - Gross morphology - histology and IHC (proteoglycans, COL I/III, COL II) - Cartilage score (ICRS)
Huebner et al. ¹⁴³	3D CAD of scaffolds 3D bioprinter (Bioplotter, EnvisionTEC). Parameters: Nozzle internal Ø: 200 µm; speed: 0.4 mm/s; P: 0.6 N/mm ² .	PCL Mw 43,000 Da	—	Cylinder, 7.5 × 5 mm 100/400 µm (interstrand space) MESH: 32 layers in 0°/90° strand laydown pattern	—	- Microarchitecture optical characterization	—	Subcutaneous implant (rat) End-point: 4, 12 weeks - Histochemical staining (% matrix density, % COL alignment, orientation index) - Mechanical characteristics via AFM
Bahcecioglu et al. ¹⁴⁴	3D Bioprinter (Bioscaffolder-system, SYS + ENG). Parameters: print T: 150°C; strand orientation: 0°–90°; strand distance: 1 mm.	PCL Mw 50,000 Da	—	Prism, 4 × 4 × 3 mm 700 µm MESH: 0°–90° strand orientation and 1 mm strand distance	- Pig MFCs (Passage: 2)	- Mechanical behavior, compression - SEM	Static and dynamic culture (compression) - DNA content - Cell viability - Cell metabolic activity - COL content - sGAG content - Histology and IHC (COL I/II) - Mechanical behavior, compression	—
Warren et al. ¹⁴⁸	3D CAD (Solid Works 2015, Waltham, MA) 3D Bioprinter (Bioplotter, EnvisionTEC). Parameters: Nozzle Ø: 200 µm; print T: 120°C; speed: 0.4 mm/s; P: 0.6 N/mm ² .	PCL Mw 43,600 Da	—	Cylinder, 7.5 × 5 mm MESH: 213/222/208 µm strand with and 112/185/408 µm interstrand space	—	—	—	Subcutaneous implant (rats) End point: 4, 8, 12 weeks - Histology (COL, cell density, %matrix fill and density, quantification of % area with COL fiber alignment, F-actin)

(Continued)

Table 1. (Continued)

Authors and references	Printing method/parameters	Printing material	Additives or biotink	Shape and/or dimensions	Cells	Scaffold characterization studies	In vitro cells/scaffold interactions	In vivo studies
Luis et al. ¹⁵¹	3D CAD meniscus scaffolds Pneumatic extrusion 3D printer. Parameters: Nozzle Ø: 20–21G; T: 40°C–80°C (Nozzle) and 80°C–110°C (Print Bed)	Ecoflex30 and Ecoflex50 Silicone elastomers	—	Meniscus-like, 4.08 ± 0.14 cm × 2.08 ± 0.19 cm MESH: —	—	- Surface and cross-sectional morphology - Mechanical behavior, compression	—	—
Luis et al. ¹⁵²	3D CAD Custom pneumatic printer. Parameters: Needle: 21G; speed: 4800 mm/min; flow: 0.5 mL/min.	Ecoflex30 and Ecoflex50 Silicone elastomers	—	Meniscus-like, 4 × 2 × 1 cm MESH: regular, striated, laminated layer by layer fibrillar appearance	- L929, fibroblasts (Passage: N.R.)	- Surface characterization by SEM, surface profilometry, absorption test, XPS, FTIR, TGA, DSC, DTG - Mechanical properties, extrinsic stiffness and equilibrium modulus - Numerical analyses	- Cell viability/cytotoxicity assay - Mechanical behavior, compression	—
Moroni et al. ¹⁵⁵	CT and MRI 3D porcine menisci scaffolds 3D CAD (Rhynoceros®) Extrusion 3D Bioprinter (Bioplotter, EnvisionTEC) Parameters: Needle Ø: 400 µm; T: 190°C; speed: 300 mm/s; P: 5 bar	PEOT/PBPT	—	Meniscus-like (solid or hollow fibers) 70%–80% MESH: bottom and top, 0°/45°/90°/135° angle deposition architecture; middle part, 0°/90° angle deposition structure	—	- Mechanical stresses, shear stresses, and characteristics of stress concentrated area - Mechanical compressive test; SEM	—	—
Zhu et al. ¹⁶⁷	MR/CT of human knee; Materialize magics 20.03 software (Materialize) Parameters: N.R.	PCU	—	Anatomical shape of the meniscus 37%; 41%; 45%; 47% MESH: TPMS structures - primitive surface - gyroid surfaces	—	- Compression stresses, shear stresses, and characteristics of stress concentrated area - Mechanical compressive test; SEM	—	—
Zhu et al. ¹⁶⁸	MR/CT of human knee; Materialize magics 20.03 software (Materialize) Parameters: N.R.	PCU	—	Anatomical shape of the meniscus Pore size: 800/700/600/450/650/550/500/400 µm 63.3%; 53.7%; 44.3%; 34.5%; 56.2%; 56.9%; 57.2% 58.2% MESH: surface layer, lamellar layer, circumferential fibers, and radial fibers	—	- Mechanical compressive test; SEM	—	—
Luis et al. ¹⁷³	3D CAD heat-cured extrusion-based technology, Parameters: Nozzle Ø: 510 µm; T: 60°C (Nozzle) and 100°C (Print Bed); extrusion rate: 0.5 mL/min	Ecoflex30 and Ecoflex50 Silicone elastomers	—	Meniscus-like, 4 × 2 × 1 cm Ecoflex50: 0.27%–0.13% Ecoflex30: 0.35%–0.18% MESH: —	- L929, fibroblasts (Passage: N.R.)	- X-ray CT - Mechanical tests, compression	- Cytotoxicity assay	—

AFM: atomic force microscopy; ALP: alkaline phosphatase; BM-MSC: bone marrow mesenchymal stem cells; CAD: computer aided design; CAM: computer aided manufacturing; cm: centimeters; COL: collagen; CTGF: connective tissue growth factor; Da: Dalton; dECM: decellularized extracellular matrix; FFF: fusion filament fabrication; G: gauge; GAG: glycosaminoglycans; GelMA: gelatin methacrylate; HA: hyaluronic acid; hASCs: human adipose derived stem cells; IF: immunofluorescence; iPSCs: Infrapatellar fat pad stem cells; IHC: immunohistochemistry; IL: interleukin; kPa: kilopascal; kPa: kilopascal; MFCS: meniscal fibrochondrocytes; Micro-CT: micro computed tomography; mL/min: milliliters/minute; mm: millimeters; mm/s: millimeters/second; MPa: megapascal; MRI: magnetic resonance imaging; Mw: molecular weight; N.R.: not reported; N/mm: Newton/millimeter; N/mm²: Newton/square millimeter; P: pressure; PCL: ϵ -polycaprolactone; PCU: polycarbonate urethane; PEOT/PBPT: Poly(ethyleneoxide terephthalate)/poly(butylene terephthalate); PLA: poly lactic acid; PLGA: poly lactic-co-glycolic acid; PU: polyurethane; s: second; SEM: scanning electron microscopy; SOX9: SRY-Box Transcription Factor 9; T: temperature; TGF β 3: transforming growth factor beta 3; TNF- α : tumor necrosis factor-alpha; °C: centigrades; µm: micrometers; Ø: diameter.

Table 2. Synthetic 3D printed conditioned scaffolds.

Authors and references	Printing method/parameters	Printing material	Additives or bioink	Shape and/or dimensions — Pore size μm /porosity%	Cells	Scaffold characterization studies	In vitro cells/scaffold interactions	In vivo studies
Bahcecioglu et al. ²⁷	3D CAD (SketchUp, Google). 3D Bioprinter (Bioscaffolder, SYS + ENG). Parameters. Strand orientation: 0/90°; strand distance: 1 mm; w/wo shifting (offset: 0.5 mm) and w/wo circumferential strands. Pig knee MRI scanned on a 3T scanner; lateral meniscus CAD (Mimics, Materialize); 3D Bioprinter (Bioscaffolder, SYS + ENG).	PCL Mw 50,000 Da	- GelMA + cells suspension (impregnation) - GelMA- Agarose + cells suspension (impregnation)	- Square prism, $10 \times 10 \times 3$ mm; - Rectangular prism, $30 \times 10 \times 3$ mm; - Coliseum, $26 \times 8 \times 5$ mm $810 \pm 40 \mu\text{m}$ MESH: Scaffolds w/wo circumferential strands + non-shifted designs + shifted design	- Human fibrochondrocytes (Passage: 3)	- SEM - Mechanical behavior, compressive/tensile load	Static culture - Cell viability - COL I/II deposition, immunostaining	—
Ghodbane et al. ³⁸	3D Bioprinter (Bioplotter, EnvisionTEC), Pneumatic extrusion. Parameters. Needle inner \varnothing : 400 μm ; print T: 160°C; speed: 1.2 mm/s; P: 8.9 bar.	p(DTD DD)	Collagen-hyaluronate sponge infusion	Anterior-posterior length: 32 mm; medial-lateral length: 24 mm 69.9% \pm 8.0% MESH: successive layers of circumferential and radial filaments	—	- Determination of percent polymer and COL-hyaluronan - Porosity - Mechanical behavior, confined compressive creep, circumferential tensile testing - Suture retention test - In situ contact stress test	—	—
Li et al. ¹⁴⁰	3D CAM/CAD of rabbit medial meniscus (SolidWorks, Autodesk), 3D-Bioprinter (Bioplotter, EnvisionTEC). Parameters. Nozzle \varnothing : 300 μm ; T: 130°C; speed: 7.0 mm/s; P: 0.8 MPa.	PCL Mw 80,000 Da	SF crosslinking + synovial MSCs specific affinity peptide	- Medial meniscus model of a wedged shaped arc disk 300 μm MESH: PCL bundles alternately oriented along the circumferential and perpendicular direction in a bionic manner	- Rat synovial derived MSCs (Passage: 3)	- SEM - Degradation in vitro - Frictional force of interface - Mechanical behavior, compression - FTIR	Static culture - Cell viability - Cell morphology - Biochemical assays (GAG, COL I/II) - Gene expression (COL I/II, SOX9, aggrecan) - Synovial derived MSCs recruitment in vivo	Orthotopic implant (rat) [- cells] Synovial MSCs recruitment (rabbit) [- cells] End point: 12, 24 weeks - Gross evaluation (meniscus) - Cartilage evaluation - SEM (cartilage) - Inflammatory response (histology, IL-1, TNF- α , synovial and synovial fluid) - Biomechanical behavior, compressive/tensile load

(Continued)

Table 2. (Continued)

Authors and references	Printing method/parameters	Printing material	Additives or biolink	Shape and/or dimensions	Cells	Scaffold characterization studies	In vitro cells/scaffold interactions	In vivo studies
Baheccigioglu et al. ⁴¹	3D CAD (SketchUp, Google) 3D Bioprinter (Bioscaffolder system, SYS + ENG). Parameters: Strand orientation: 0/90°; strand distance: 1 mm.	PCL M _w 70,000–90,000 Da	- Agarose (impregnation) - GelMA (impregnation) - Agarose + cells suspension (impregnation of inner region) and GelMA + cells suspension (impregnation of outer region)	- Prism, 4 × 4 × 3 mm - Meniscus-like, outer Ø: 30 mm, height at periphery: 5 mm, inner Ø: 10 mm 751 ± 43 µm (PCL) in xy-direction and 97 ± 40 µm in z-direction, filled with hydrogel MESH: strand distance, 1 mm; strand orientation, 0/90°; average strand Ø, 2.11 ± 18 µm 5 mm ³	- Pig MFCs (Passage: 2)	- Mechanical behavior, compressive/tensile load	Static and dynamic culture (compression) - Cell viability - Biochemical assays (DNA, sGAGs, hydroxyproline, and COL content) - IF (COL I/II)	—
Cengiz et al. ⁴²	3D Bioprinter (Bioplotter, EnvisionTEC) Parameters: Needle Ø: 22G metallic; print T: 110°C; P: 5.5 bar.	PCL M _w 45,000 Da	Entrapped SF (8 or 16 wt%) in PCL	697.1 µm, 61.1% (PCL); 278.7 µm, 54.6% (PCL + 8%SF); 287.2 µm, 50.0% (PCL + 16%SF) MESH: parallel strands 1.2 mm apart from each other (layers); layer-wise alternating strand directions of 90° and 0° (3D cubic cage)	- Human mesenchymal cells (Passage: 5) - Human IPFSCs (Passage: 4)	- Micro-CT - SEM - Water uptake - Mechanical behavior, compression	Static culture - Cell adhesion/migration (SEM) - Cell viability - Proliferation - Staining for filamentous actin	Subcutaneous implant (nude mice) [± cells] 7 d static culture before implant End point: 4 weeks - Micro-CT - Histological analyses for tissue infiltration, COL matrix, vessels, inflammation
Nakagawa et al. ⁴⁵	MRI of ovine meniscus CAD reconstruction of sheep medial meniscus 3D Bioprinter (Bioplotter, Envision TEC), Parameters: T: 120°C; microstrands: 300 µm; microchannels: 100 µm.	PCL M _w 65,000 Da	Recombinant human CTGF (outer/middle zones) and recombinant human TGF-β3 (inner/middle zones) incorporation in PLGA	Meniscus-like 100/200 µm MESH: layer path, 300 µm microstrands, 100 µm microchannels	—	—	—	Orthotopic implant (sheep) End-point: 6, 12 months - MRI and MRI score - Macroscopic analysis - Histological analysis of meniscal, articular cartilage, and synovial tissues - Meniscal histological score (size, morphology, integrity, integration to the capsule, cellularity, cell morphology, COL organization, matrix staining)
Cengiz et al. ⁴⁶	3D Bioprinter (Bioplotter, EnvisionTEC), Parameters: Print T: 110°C; P: 5.5 bar.	PCL M _w 45,000 Da	SF reinforced in the middle on the transverse plane with PCL	5 m ³ 242.1 ± 7.6 µm 76.9% ± 0.5% MESH: layer-wise alternating strand directions of 45° and 135°; 2 mm inter-strands distance	- Human mesenchymal cells (Passage: 5) - Human ADSCs from IPF (Passage: 4)	- SEM - Micro-CT - Water uptake - Suture retention test - X-ray diffraction behavior, compression - In vitro enzymatic degradation	Subcutaneous implant (nude mice) [± cells] 7 d static culture before implant End point: 4 weeks - Histological analyses for biocompatibility, tissue infiltration, new vessels	—

(Continued)

Table 2. (Continued)

Authors and references	Printing method/parameters	Printing material	Additives or bioink	Shape and/or dimensions	Cells	Scaffold characterization studies	In vitro cells/scaffold interactions	In vivo studies
Chen et al. ⁴⁷	Micro-CT of rabbit menisci 3D CAD of scaffolds FFF 3D printing. Parameters, N.R.	PCL Mw 45,000Da	- Pig meniscal dECM injection and crosslinking - Pig meniscal dECM injection and crosslinking + cells	— Pore size μm /porosity% - Wedge-shaped porous scaffold, $10 \times 4 \times 1 \text{ mm}$ 1000 μm MESH: circumferential fibers spacing of 1000 μm , adjacent radial fibers angle of 18°, fiber diameters of 250 μm	- Rabbit MFCs (Passage: 3)	- Water contact angle, - FTIR - SEM - Mechanical behavior, compressive/tensile load	—	Subcutaneous implant (rats) [- cells] End point: 1 week, 1 month - Histology for inflammatory and immune responses Orthotopic implant (rabbit) [\pm cells] 24 h static culture before implant End point: 3, 6 months - Morphologic observation - Histology (cartilage) - IHC (COL I/II) - Ishida Score menisci - COL and GAG content - Mechanical behavior, compressive/tensile load - Image assessment (X-ray, MRI) - Kellgren–Lawrence and WOMMS grading
Lee et al. ⁴⁹	Laser Scan of human/sheep Meniscus 3D CAD 3D Bioprinter (Bioplotter, EnvisionTEC). Parameters, print T: 120°C.	PCL Mw 65,000Da	Tethering of CTGF and TGF- β 3 incorporated in PLGA microstrands	Meniscus-like 100 μm MESH: (a) interfilid strands and interconnecting microchannels with 100 μm \varnothing + circumferentially aligned fibers added (human meniscus scaffold); (b) 300 μm microstrands and 100 mm microchannels (sheep meniscus scaffold)	- Human BM or synovium MSCs (Passage: 2–3)	—	Static culture - Cell recruitment - Fibrocartilage matrix formation	Orthotopic implant (sheep) [- cells] End point: 12 weeks - Mechanical behavior (dynamic compression, pull-out strength, friction coefficient, stress relaxation, tensile test)
Abar et al. ⁵⁰	3D CAM/CAD (Fusion 360), FFF 3D printer (Taz 5, Luizbot). Parameters. Nozzle \varnothing : 400 μm ; print T: 212°C–220°C; bed T: 40°C; speed: 360 mm/min.	PCU	Collagen hydrogel infill	Prism, $105 \times 55 \times 1.66 \text{ mm}$ 0/100/200/400/600/800 μm MESH: first layer, a solid printed in diagonal pattern; next four layers, rectilinear infill pattern	- NIH/3T3, fibroblasts in aqueous or COL solution (Passage: N.R.)	- Light microscopy - Micro-CT - Mechanical behavior, tensile testing	Static culture - Cell proliferation and distribution	—

(Continued)

Table 2. (Continued)

Authors and references	Printing method/parameters	Printing material	Additives or biolink	Shape and/or dimensions Pore size μm /porosity%	Cells	Scaffold characterization studies	In vitro cells/scaffold interactions	In vivo studies
Ghodbane et al. ¹⁵³	3D Bioprinter (Bioplotter, EnvisionTEC). Pneumatic extrusion. Parameters: Nozzle inner \varnothing : 500 μm ; T: 160 °C; P: 9 bar; speed: 2 and 4.5 mm/s.	p(DTD DD)	Collagen infusion	Anterior-posterior length: 32mm, medial-lateral length: 24mm MESH: successive layers of circumferential and radial filaments 69.9% \pm 8.0%	—	- Orientation characterization (XRD) - Mechanical behavior, circumferential tensile stiffness and ultimate tensile load	—	—
Ghodbane et al. ¹⁵⁴	3D Bioprinter (Bioplotter, EnvisionTEC). Pneumatic extrusion. Parameters: Needle inner \varnothing : 400 μm ; print T: 160 °C; speed: 1.2mm/s; P: 8.9 bar.	p(DTD DD)	Collagen hyaluronate sponge infusion	Anterior-posterior length: 32mm, medial-lateral length: 24mm MESH: successive layers of circumferential and radial filaments 69.9% \pm 8.0%	—	—	—	Orthotopic implant (sheep) End point: T2, 24 weeks Histology for magnitude and type of tissue ingrowth, tissue thickness and integrity, surface features, cell density, vascularization, inflammatory response; IF for COL I/II; quantification of COL and sGAGs; cartilage histological analysis
Gupta et al. ¹⁵⁶	3D CAM/CAD of scaffolds (Fusion 360, Autodesk), FFF 3D printer (Taranula 3D printer). Parameters: print T: 200 °C; speed: 20mm/s.	PLA	- COL crosslinking - alginate - oxidized alginate Self-healing interpenetrating network hydrogel	Square prism, 10 \times 10 \times 3 mm 400 μm MESH: layer by layer with orthogonal orientation of fibers between successive layers. Fiber diameter, 200 μm ; fiber spacing in each layer, 400 μm	- Human UC-MSCs (Passage: N.R.)	- Cytotoxicity - Degree of carboxylation - Mechanical behavior, compression - Contact angle - Characterization of hydrogel - Impregnated scaffolds (in vitro degradation, swelling ratio)	Static culture - Cell viability/proliferation/morphology - Differentiation End point: 14, 28 days - Biocompatibility - Micro-CT - Histology (tissue architecture, COL content, GAG)	Subcutaneous implant (rats) [— cells] 28 d of static differentiation before implant End point: 14, 28 days - Biocompatibility - Micro-CT - Histology (tissue architecture, COL content, GAG)
Yang et al. ²²⁴	3D printer (Regenovo 3D Bio-Architect Sparrow). Parameters: Print T: 17 °C-22 °C; needle inner \varnothing 260 μm ; print bed T: 0 °C	N-acryloylsemicarbazide/gelatin	Polydopamine coated-ZIF-8	- Printed grid, 66 \times 56 \times 0.87 mm - Printed porous cuboid, 40 \times 20 \times 2.1 mm MESH: 6 layers grid	- L929 mouse fibroblasts - Rabbit MFCs (Passage: 3)	- Mechanical characterization, tensile/compressive wear, resistance against femur, tearing tests, suture strength - Swelling behavior - Biocompatibility	- In vitro antibacterial activity (Staphylococcus aureus and Escherichia coli)	—

ADSCs: adipose-derived stem cells; BMI: bone marrow; CAD: computer aided design; CAM: computer aided manufacturing; CO: collagen; CTGF: connective tissue growth factor; Da: Dalton; dECM: decellularized extracellular matrix; FFF: fusion filament fabrication; FTIR: Fourier-transform infrared spectroscopy; G: gauge; GAG: glycosaminoglycans; GelMA: gelatin methacrylate; IF: immunofluorescence; IFP: infrapatellar fat pad; IL: interleukin; IFPSCs: infrapatellar fat pad stem cells; IHC: immunohistochemistry; MFCs: meniscal fibrochondrocytes; Micro-CT: micro computed tomography; mm: millimeters; mm/min: millimeters/minute; mm/s: millimeters/second; MPa: megapascal; MRI: magnetic resonance imaging; MSC: mesenchymal stem cells; Mw: molecular weight; N.R.: not reported; p(DTD DD): poly(desaminotyrosyl-tyrosine dodecyl ester dodecanoate); P: pressure; PCL: ϵ -polycaprolactone; PCU: polycarbonate urethane; PLGA: poly lactic-co-glycolic acid; PU: polyurethane; SEM: scanning electron microscopy; SF: silk fibroin; sGAG: sulfated glycosaminoglycans; SOX9: SRY-Box transcription factor 9; T: temperature; TGF β 3: transforming growth factor; beta 3; UC: umbilical cord; w/wo: with/without; wt: weight; XRD: X-ray diffraction analysis; μm : micrometers; °C: centigrades; \varnothing : diameter.

400 μm . The described system set up allowed for fabrication of scaffolds with a 70%–80% porosity, achieved by the fine plotting the of the fibers orientation.

PLA. PLA is the homopolymer of L-lactide, the cyclic dimer of lactic acid existing in the two optical isoforms D(–) and L(+); its properties depend on isomers content (i.e. poly(L-lactide) (PLLA) and poly(D-lactide) (PDLA))¹⁸⁰; thus, controlling PLA stereochemical architecture, and in turn molecular weight (Mw) (high Mw PLA crystallizes at low crystallization temperatures¹⁸¹), it is possible to modulate the processing temperatures, crystallization speed (PLA is a slowly crystallizing material¹⁸²), crystallinity degree, and mechanical properties.^{182,183} PLA products are affected by polymer crystallinity and crystalline morphology. Semicrystalline PLA exhibits at room temperature a tensile modulus of about 3 GPa, a tensile strength between 50 and 70 MPa with an elongation at break of 1%–5% depending on blend.^{170,184} In vivo, PLA degradation is first hydrolytic and then the soluble oligomers are metabolized by cells¹⁸⁵; thus, lactic acid enters tricarboxylic acid cycle and is excreted as water and carbon dioxide.¹⁸⁶ PLA can take 10 months to 4 years to degrade, according to its intrinsic characteristics (i.e. chemical composition, porosity, and crystallinity—in turn influencing tensile strength) but also depending on the implantation site.^{183,187} Mechanical properties can be improved through fabrication of combined scaffolds (e.g. PLA/Ti) matching the requirements of biological end-use destination.¹⁸⁸

According to our knowledge, the use of PLA in the perspective of 3D printed meniscal scaffolds fabrication was only reported by Gupta et al.¹⁵⁶ and Narayanan et al.¹³³ A square prism-like structure¹⁵⁶ (simple orthogonal geometry) and a meniscus-like structure¹³³ (intercalating layers of circumferentially oriented/linear parallel strands) were fabricated by FFF strategy. In both the cases, the synthetic 3D printed polymeric support was functionalized with natural hydrogels (collagen, alginate and oxidized alginate)¹⁵⁶ or bioink (alginate + hASCs or alginate + PLA nanofibers + hASCs)¹³³ to induce cells adhesion and proliferation in vitro.

Natural materials

Collagen. Collagen is the main ECM structural protein broadly represented in the musculoskeletal soft tissues (e.g. tendons, ligaments, knee menisci); different collagen types exist, differentiated by their complexity and specific structural characteristics. Collagen has tissue-matching physicochemical properties, together with high biocompatibility and binding sites (Arg-Gly-Asp, RGD sequence) for cellular attachment mediated by integrins^{124,133,189}; moreover, as showed by Gupta et al.,¹⁵⁶ it also displays a critical role in cellular chondrogenic differentiation. Additionally, Abar et al.,¹⁵⁰ reporting about a porous PCU scaffold infilled

with collagen, stated the potentiality of this approach not only to promote cell adhesion and proliferation but also to improve the integration of the device in the host tissue, reducing the risk for implant dislocation and failure, typically reported for solid PCU in orthopedics.

The combination of collagen with hyaluronate contributed to mechanical features of p(DTD DD) scaffolds also inducing robust integration and fibrochondrocytic ingrowth after orthotopic implant.³⁸

Collagen, combined directly with cells, was also reported as a fundamental constituent of bioinks,^{131,132,134} mimicking the ECM environment. The main weakness of collagen is amenable to low mechanical properties and possible shrinkage in response to cellular activity.¹⁹⁰ To overcome this limit, it can be chemically modified through photoactive methacrylate groups, assuring an increase in the storage modulus after irradiation.¹⁹¹ Additionally, another strategy may reside in modulating concentration; Rhee et al.¹³¹ experimented different collagen concentrations to prepare a bioink enriched with meniscal fibrochondrocytes (10×10^6 cells/mL), with optimal results working between 15 and 17.5 mg/mL. Concentrations higher than 20 mg/mL and lower than 7.5 mg/mL were poorly printed.

Partial hydrolysis of collagen produces another soluble protein-based polymer, gelatin.

Gelatin. Gelatin shows lower antigenicity than collagen. It gives rise to hydrogels in a temperature-dependent manner (remains in the gel state below 37 °C) or in a concentration-dependent manner; it shows RGD motifs promoting interaction with cells. Its use in printing has been reported at a wide range of concentrations, also combined with a methyl acrylate group, leading to the photopolymerizable hydrogel GelMA.^{124,192}

GelMA¹⁴¹ or GelMA + fibrochondrocytes²⁷ were used as conditioning hydrogels to impregnate PCL 3D printed scaffolds. Compared to PCL nude supports, the presence of GelMA determined fibrochondrocytes proliferation, and high levels of collagen type I/II mRNA suggesting the bioactive potential ascribable to it; biologic recognition is likely due to presence of RGD sequences on gelatine. Significantly, as GelMA was recognized to be fibrogenic, complex meniscal printed scaffolds with zonal variations were prototyped by Bahcecioglu et al.¹⁴¹ to emulate the anisotropic behavior of the native meniscus (outer region with GelMA, fibrogenic potential; inner region with agarose, chondrogenic potential). Moreover, incorporation of hydrogels also exerted a protective effect on cells under dynamic stress together with a reduction in cartilage degeneration.¹⁴¹

Gelatin-based bioinks were broadly described. Bandyopadhyay and Mandal¹⁵⁷ prepared a formulation with also SF than used to fabricate a meniscus tri-layered model with a complex mesh (circumferential and radial lamellar layers); 7% w/v gelatin + 1.5% w/v SF was identified as an adequate blended formulation due to quick gelation of SF

within 20 min as well as for good shear-thinning and self-standing characteristics after extrusion. Luo et al.⁹⁷ compared different bioink formulations based on gelatin, alginate and cellulose nanofibers together with meniscal fibrochondrocytes (5×10^6 cells/mL): the results showed that only high-gelatin-containing alginate (HGA) + cellulose nanofibers and HGA bioinks guarantee for acceptable fidelity and integrity. Sun et al.¹³⁶ conditioned a PCL scaffold with a cell laden (goat bone marrow MSCs, 1×10^7 cells/mL) bioink made of gelatin (45 mg/mL), fibrinogen, hyaluronic acid and glycerol enriched in PLGA microparticles with growth factors.¹³⁶

GelMA was also adopted in bioink: Jian et al.¹³⁵ reported about a GelMA-based (10% w/v) formulation with meniscal dECM and meniscal fibrochondrocytes (1×10^6 cells/mL) for augmentation of PCL supports.

Silk fibroin. The SF biomolecule is composed of two proteins: hydrophobic fibroin and hydrophilic sericin.¹⁹³ It is a nondegradable material based on the US Pharmacopeia's definition; however, some reports consider it a degradable polymer. SF produces nontoxic aminoacids upon degradation, undergoing metabolism.¹⁹⁴ It is endowed with mechanical strength (surpassing many others biological materials), elasticity, biocompatibility, and controllable biodegradability; the properties of SF-derived scaffolds can be modulated by adjusting its secondary structure.¹⁹⁵ Li et al.¹⁴⁰ combined SF to PCL scaffolds through cross-linking, demonstrating its great contribution to balance both the biomechanical features and the degradation rate of the supports in vitro. Moreover, orthotopic implant in rabbit of PCL-SF supports showed new vessels formation (especially at the synovial edge) and collagen I deposition; recruitment, retention, and proliferation of synovial MSCs was also sustained.

In combination with gelatin¹⁵⁷ or as methacrylate, it was also used in bioink formulations.¹³⁹

Agarose. Agarose is a linear polysaccharide composed of alternating β -D-galactopyranose and anhydro- α -L-galactopyranose. It derives from red algae (*Rhodophyceae*) and seaweed and it is the major component of agar. The typical gel-like behavior is determined by temperature and/or concentration¹⁹³; thanks to its gelling property and the possibility for in situ polymerization, it is widely used in tissue engineering (TE).¹²⁵ As for meniscal scaffolds augmentation, agarose was used both alone¹⁴¹ and combined with GelMA + fibrochondrocytes²⁷ for printed PCL scaffolds conditioning. Both hydrogels exerted a protective effect on fibrochondrocytes under loading versus PCL alone; moreover, agarose impregnated constructs proved increased levels of GAGs and type II collagen in vitro. The blend GelMA-agarose exhibited higher levels of aggrecan expression compared to PCL.

Alginate. Alginate (or alginic acid) is a natural anionic polysaccharide refined from brown seaweed (e.g. *Laminaria hyperborea*, *Macrocystis pyrifera*, and *Ascophyllum nodosum*). This biopolymer is characterized by alternating blocks of α -1, 4-l-guluronic acid and β -1,4-d-mannuronic acid units; the ratio between them modulates the physicochemical/rheological properties of the hydrogel. Alginate structurally resembles the ECM glycosaminoglycans and is broadly used in biomedicine for biocompatibility, biodegradability, low cytotoxicity, mild gelation process, chemical versatility, and low cost.^{125,193} Alginate and oxidized alginate were used by Gupta et al.¹⁵⁶ for PLA 3D printed scaffolds conditioning. The natural polymer had a great influence on micro-mechanical properties and maintenance of structural integrity of the scaffold; moreover, as showed both in vitro and in vivo (subcutaneous implant) the presence of interpenetrating network hydrogels actively participated in ECM formation, inducing deposition of GAGs and collagen.

Alginate was reported as a component of complex bioinks formulations^{97,133,137,138}; similarly to agarose, chitosan and hyaluronic acid it can be used to improve the rheological and the biological properties of the bioinks¹²⁷; the GAG hyaluronic acid has been widely adopted together with alginate to enhance intrinsic properties of the descending supports¹⁹⁶; also nanocomposite hydrogel scaffolds were fabricated.¹⁹⁷ Different alginate concentrations were reported in the literature for 3D bioprinted meniscal scaffolds development (1.25% w/v,⁹⁷ 2.00% w/v,¹³⁸ and 2.5% w/w^{133,137}).

Alginate has also been reported as the sole constituent of the bioink together with cells.^{130,133}

Hyaluronic acid. Hyaluronic acid is a non-sulfated glycosaminoglycan composed of N-acetylglucosamine and glucuronic acid. Typically represented in the ECM, hyaluronic acid is particularly abundant in loose connective tissue. When dissolved in water, it shows remarkable hydrodynamic characteristics and viscous properties; retaining water, it displays a great role in tissue homeostasis and biomechanical integrity, thus making it a promising material for applications in tissue engineering (TE).^{124,198} It is possible to modulate hyaluronic acid characteristics through functionalization processes (e.g. sulfation, esterification, hydrazide modification, and cross-linking with glutaraldehyde) thus allowing for more rigid and stable, hydrophobic, and more resistant to enzyme decomposition hydrogels.¹⁹⁹ Ghodbane et al.,^{38,154} reported about collagen-hyaluronate sponges.

As for hyaluronic acid use in bioinks, it was also used as component of complex formulations.¹³⁶ Interestingly, it shows shear-thinning properties, together with an important supportive/protective role for cells during the extrusion process.²⁰⁰

Gellan gum. Gellan gum is a hydrophilic and high-molecular weight polysaccharide produced by bacteria. It is recognized as a good material for scaffolds development. Considering bioprinting, it has been combined with other polymers to prepare bioinks characterized by satisfactory rheology and shape fidelity. Its tunable mechanical properties are attractive for use in bioprinting.¹²⁴

According to our knowledge, only Costa et al.¹³⁹ reported its use in a complex bioink formulation for 3D bioprinted meniscal scaffolds fabrication.

Decellularized extracellular matrix. Decellularized extracellular matrix (dECM) hydrogels derive from tissues processed through chemical, physical, and enzymatic strategies to remove cells without damaging the ECM. Once the matrix is fully decellularized (verification by DNA quantification assays),²⁰¹ manipulation to prepare gels occurs.^{128,205}

Several Author focused on development of dECM for tissue engineering purposes,²⁰¹ including the development high-performance bioinks²⁰² dECM products can efficiently provide a distinctive environment capable of directing cell growth (e.g. Giobbe et al.²⁰³, Stocco et al.,²⁰⁴ Grandi et al.²⁰⁵) as they consist of the functional molecules secreted by the resident cells of each tissue. Thus, differently from hydrogels made of a single ECM component, dECM hydrogels maintain the biochemical complexity of the native tissues.²⁰⁶

Differences in proteins content can exist within each single tissue according to the region. In example, referring to menisci, extracted dECM exhibits different levels in collagens if considering the inner or the outer layer: inner meniscus has higher type II collagen than type I; whereas the outer region has higher type I collagen than type II; furthermore, the inner meniscus also displays higher levels of proteoglycans and TGF2/TGF3 than the outer meniscus ECM in turn showing richness in bFGF and insulin.^{137,207}

dECM enhancement with growth factors can also be adopted as a strategy to modulate tissue regeneration toward native-like features¹³⁷ favoring the establishment of original tissue anisotropy. Chen et al.¹⁴⁷ reported about a hybrid scaffold based on printed PCL and augmented with decellularized meniscal cartilage derived hydrogel both free and in presence of meniscal fibrochondrocytes (MFCs). The acellular matrix confirmed its ability to act as a functional cells' carrier; moreover, a percentage of 2% in hydrogel was identified as the most adequate to confer an optimal bioactive behavior to the support. Thereafter, according to orthotopic implant data in rabbits' knee, PCL + dECM + fibrochondrocytes explants displayed at 6 months post-implantation histological/biochemical and biomechanical features like native menisci.

Bioinks formulations including meniscal dECM were also described. According to our knowledge, their use is mainly restricted to bioactivation of 3D printed supportive

polymers. Jian et al.¹³⁵ combined it with GelMA and MFCs, Romanazzo et al.¹³⁷ mixed it with alginate and porcine infrapatellar fat pad stem cells (IFPSCs). Interestingly, Chae et al.¹³² proposed a bioink based only on pig meniscal dECM; the formulation, appearing like a gel, was adopted for PU/PCL 3D printed scaffolds biological activation.

Despite the intrinsic bioactive potential of dECM-based bioinks, intense efforts are required for the identification of adequate decellularization protocols. Often, chemical agents adopted for cells removal (as well as the number of decellularization cycles) can significantly alter the biological and mechanical properties of dECM thus affecting the effectiveness of the derived bioinks.^{202,208}

3D printing/bioprinting of meniscus: Issues in scaffolds design and development

AM techniques (mainly, FFF approach that is a material extrusion-based strategy) and 3D bioprinting methods (mainly, inkjet-based and extrusion-based 3D bioprinting) were broadly experienced, also in combination, with the aim to fabricate effective meniscal substitutes.

A prerequisite for satisfactory in vitro/in vivo outcomes and future translation in clinical practice of 3D printed scaffolds is optimization of print fidelity. Insufficient resolution can have a dramatic influence on the quality and functionality of the scaffold. Considering meniscus, intense efforts were made to mimic meniscal ultrastructural organization and distinct composition.^{27,38,130,131,135,136,140,141,150-153,155,157,209}

In fact, the typical structural inhomogeneity and anisotropy, despite assuring for the menisci physiological role,^{131,153} also represent important issues in scaffolds manufacture with implications in cellular repopulation. Elasticity/stiffness (i.e. the Young's modulus) of the support (partly amenable to porosity and ultrastructure) likely modulate cell spreading/morphology/function.^{68,210,211} More specifically, for stem cells a lineage-specific differentiation can be achieved when culture occurs on substrates matching the stiffness corresponding to native tissue.²¹¹

Porosity and pore interconnectivity determine scaffold's efficacy. Thus, together with the intrinsic mechanical properties of the material, the scaffold's microarchitecture has a key role as it affects cell behavior, ECM deposition/tissue formation and, in turn, the overall construct mechanics.^{25,212} Large pores promote cell migration into the scaffold, whereas small pores provide more surface area for cell attachment. A balance with biomechanical strength should be pursued considering that structural integrity typically diminishes along with an increased pore size.⁸⁸ 3D printing strategies help in fabrication of scaffolds characterized by interconnectivity and high-water absorption ability; acting on the diameter of the extrusion needle it is possible to modulate porosity.¹⁵⁷ However, to date, identification of the

most adequate porosity percentage (calculated as: (void space / total space) \times 100) and pore size for a specific tissue and cell type are a matter of discussion and hot topics of research.²¹²

Mikos and Temenoff²¹³ and later Rongen et al.²⁴ suggest that effective meniscal scaffolds should have a porosity percentage of 70% or higher; as for pore size, ranges of 150–500 μm and \sim 200 μm are referred to be adequate to allow meniscal tissue infiltration and cell proliferation/ECM deposition, respectively.^{25,214} In case of MSCs seeding or migration, 3D porous scaffolds may potentially also have a synergistic impact on their behavior; Zhao et al.²¹² reported for them a pore size of 200–300 μm as the most promising for growth, while a range of 300–450 μm for chondrogenic differentiation.

The porosity of the structure is strictly related to three geometrical variables; these include the distance between parallel layers, the number of columns on each layer and the radius of the columns.²¹⁵ However, spatial resolution is influenced by the specific technology and the processed material, whose characteristics would dramatically influence the printing performances too. In example, decreasing needle inner diameter allows to increase scaffold porosity but production of thin strands (27G needle) implies extremely slow printing times (even at high extrusion pressure) that likely may affect cells viability in case of bioinks + cellular elements use.

Desired porosity percentage, pore size, physical properties related to micro-structural morphology, degradation rate should be carefully evaluated in the pre-processing phase when designing the scaffold and selecting both the printing material and the fabrication technique. To date, different mesh geometries have been attempted for meniscal scaffolds fabrication (see Tables 1–4); critically considering all gathered results, there is consensus about complex networks efficacy (e.g. circumferentially-oriented fibers, held together by a 90° grid of fibers) than simpler grid structures. Composite meshes may withstand different mechanical stimuli and forces (shear, tension, and compression) with satisfactory outcomes once implanted *in vivo*.²⁰⁹ Intense research, also based on mathematical modeling methods, is devoted toward this direction. Interconnectivity, tortuosity, and high surface to volume ratio, can provide for scaffolds endowed with interesting mechanical/biological properties over the traditional designs. In this context, TPMS scaffolds seem promising for biomorphic and porous supports fabrication, also overcoming intrinsic limitations of materials as for PCU.^{167,168} In fact, TPMS supports can show pore architectures that are rearranged from a macro-scale to a nano-scale, responding to the biological properties of the native tissues, with a precise control over internal architectures and complex external anatomical shapes. Compared to the solid meniscal implants, TPMS scaffolds are favorable for reduction in stress extremes, stress concentration area, and

displacement of meniscal extrusion.^{167,168,216} Efforts are required in this field.

A further consideration regards the degradation rate of the scaffolds for meniscal tissue engineering (TE): it should be at least 12 months, which will allow for cells to grow and replace the support.²¹⁷

Methodologically, the workflow leading from the patient's need to the printed tissue include: (1) identification of the patient specific demand, coupling imaging techniques (MRI and Computed Tomography (CT) scans) and CAM/CAD 3D modeling; (2) digitalization of the 3D model by conversion into STL (Standard Triangulation Language) file; (3) slicing; (4) generation of the G-code file containing the geometries of each 2D layer from the 3D model; (5) printing of the materials; (6) post-manufacturing modifications^{150,218} (Figure 2).

To guarantee satisfactory outcomes in meniscal devices fabrication, great attention must be paid to the pre-processing (selection of materials, cells and customized construct design) and processing (choice of printing technique) phases; however, post-processing is a peculiar step too, aiming to scaffold structural optimization and, when required, maturation of the seeded/bioprinted support to allow for further cell growth, proliferation, and differentiation.²¹⁹ To this purpose, bioreactors may have a key role. These systems, together with provision of adequate and constant environmental parameters (pH, temperature, CO₂ concentration) favoring cell growth, also impart a convective flow to cell culture medium (mimicking the *in vivo* conditions) and assert mechanical forces on the cells improving tissue growth. Referring to the original articles included in this review, scaffolds culture in static conditions prevails (Tables 1–4). Only Bahcecioglu et al.^{141,144} compared scaffolds culture in static (no load) or dynamic (load) conditions in bioreactor: a dynamic compression at 10% strain for 4 weeks (1 Hz frequency, 1 h/day, 5 days/week) was applied on 3D printed PCL supports, hydrogel-based supports (not printed),¹⁴⁴ 3D printed PCL/hydrogel constructs¹⁴¹ gaining interesting results. It was showed that dynamic compression influences DNA content (cells proliferation) depending on the scaffold material; moreover, such stimulus could boost matrix proteins production even though catabolic effects on cells could occur at high strain levels. It descends that bioreactor-based tissue engineering strategies applied to meniscal scaffolds development may assure for interesting results allowing for further insights on physiological fibers alignment and zonal organization.¹³⁴

Type of scaffolds for meniscal regeneration

From an extensive revision of the literature, scaffolds for meniscal regeneration developed by 3D printing approaches can be categorized into four different groups: (a) synthetic 3D printed bare scaffolds; (b) synthetic 3D printed

Table 3. 3D bioprinted scaffolds.

Authors and references	Printing method/parameters	Printing material	Additives or bioink	SHAPE and/or DIMENSIONS PORE SIZE μm / POROSITY%	Cells	Scaffold characterization studies	In vitro cells/scaffold interactions	In vivo studies
Luo et al. ²⁷	3D MRI model of human medial meniscus 3D CAD Mimics software (Materialize 21, Belgium) 3D Custom Bioprinter Parameters: Needle \varnothing : 22G; print T: 25°C; bed T: 4°C; speed: 3 mm/s.	—	Bioink: gelatin + alginate + cellulose nanofibers (in different proportions) + cells (5×10^6 cells/mL)	- Square blocks ($15 \times 15 \times 2$ mm) - Meniscus-like ($48.3 \times 40.5 \times 8.28$ mm) MESH: 40% infill rate and rectilinear filling pattern	Rabbit MFCs (Passage: 3–4)	- Rheological characterization [– cells] - Printability [– cells] by SEM	Static culture - Cell viability and metabolic activity - Histology (calcium, COL, GAG) and IHC (COL I/III)	—
Narayanan et al. ³⁰	MRI of medial knee meniscus 3D CAD (Materialize, Mimics) 3D Bioprinter (Bioplotter, EnvisionTEC GmbH, Germany) Parameters: - STUDY 3: nozzle \varnothing : 200 μm ; print T: 50°C (Nozzle); speed: 18 mm/s; P: 0.12 N/mm - STUDY 4: nozzle \varnothing : 300 μm ; print T: 37°C (Nozzle); speed: 12 mm/s; P: 0.03 N/mm	—	Bioink: Alginate + cells (5×10^6 cells/mL)	- $20 \times 20 \times 3$ mm - Meniscus-like MESH: laydown orientation, $0^\circ/90^\circ$ in three layers	hASCs (Passage: N.R.)	- Cell viability	—	—
Rhee et al. ³¹	CT scan of scaffolds 3D CAD (Solidworks; Dassault Systemes, Velizy France) 3D Custom Bioprinter. Parameters: bed T: 37°C.	—	COL hydrogel + cells (10×10^6 cells/mL)	- Shape/dimensions: anatomic shape scaffold (sheep meniscus; geometric shape scaffold—half cylinder) MESH: —	- Bovine MFCs (Passage: 0)	- Cell dispersion by confocal reflectance - Mechanical behavior, compression	Static culture - Cell viability	—
Filardo et al. ³⁴	MRI scans of a human volunteer. 3D CAD (Mimics, Materialize) 3D Inkjet Bioprinter (3D discovery printing tool, RegenHU). Parameters: print T: 37°C; speed: 12 mm/s; P: 0.2 bar.	—	Bioink: LifeInk 200, Collagen I bio-ink (Advanced Biomatrix) + cells (38×10^6 cells/mL)	Meniscus-like MESH: height for each layer, 0.25 mm, rectilinear pattern with 50% density	- Human BM-MSCs (Passage: 3–4)	—	Static culture - Cell viability	—

(Continued)

Table 3. (Continued)

Authors and references	Printing method/parameters	Printing material	Additives or bioink	SHAPE and/or DIMENSIONS — PORE SIZE μm / POROSITY%	Cells	Scaffold characterization studies	In vitro cells/scaffold interactions	In vivo studies
Markstedt et al. ¹³⁶	CT-scan of sheep meniscus models 3D CAD (Mimics, Materialize) Ink Jet Bioprinter (3D Discovery). Parameters: Nozzle \varnothing : 300 μm ; print T: 25°C; speed (10–20 mm/s); P: 20–60 kPa. 3D CAD model 3D custom bioprinter (integrated tissue-organ printing) Parameters: For Gellan gum/fibrinogen bioinks Nozzle \varnothing : 240 μm ; speed: 250 mm/min; P: 45–65 kPa For SF methacrylate bioinks Nozzle \varnothing : 300 μm ; speed: 250 mm/min; P: 450–550 kPa.	—	Bioink: Nanofibrillated cellulose and alginate + cells (1.5×10^6 cells/mL)	- Small grid, $7.2 \times 7.2 \text{ mm}^2$ - Large grid $38.5 \times 17.7 \text{ mm}^2$ - Solid disk 8 mm \varnothing , 1.5 mm high - Human ear, 22 mm (long axis) - Sheep meniscus 18 mm (long axis) MESH: grid shape	- Human nasoseptal chondrocytes (Passage: 1)	- Mechanical behavior, compression - Cytotoxicity	Static culture - Cell viability and distribution	—
Costa et al. ¹³⁹	3D custom bioprinter (integrated tissue-organ printing) Parameters: For Gellan gum/fibrinogen bioinks Nozzle \varnothing : 240 μm ; speed: 250 mm/min; P: 45–65 kPa For SF methacrylate bioinks Nozzle \varnothing : 300 μm ; speed: 250 mm/min; P: 450–550 kPa.	—	Bioink (sequential co-printing): Gellan gum/fibrinogen + cells and SF methacrylate (1.5×10^7 cells/mL)	$10 \times 10 \times 5 \text{ mm}^3$ constructs MESH: grid shape; interstrand distance, 500 μm	Porcine meniscus cells	- Rheological measurement - Swelling - Mechanical behavior, compression - Diffusion testing - SEM	Static culture - Cell viability and proliferation - Quantitative GAGs and COL contents - Histological analysis (COL I/II)	Subcutaneous implant (nude mice) [+ cells] Culture before implant, N.R. End point: 2, 5, 10 weeks Fibrocartilagenous tissue formation (COL I/II) - Gross appearance - Biomechanical analysis, compression - Histological analysis (GAG, COL I/II) - COL fibers alignment
Bandyopadhyay and Mandal, 2019 ¹⁵⁷	MRI of human knee 3D CAD (3D Slicer) 3D Bioprinter (BioX, Cellink). Parameters: print T: 25°C; bed T: 4–5°C; print speed: 6–8 mm/s; P: 185–200 kPa.	—	Bioink: SF_Gelatin	Meniscus tri-layered model, $6 \times 6 \times 1 \text{ mm}$ MESH: Circumferential layer (bottom), radial lamellar layer (medial), thin mesh layer (top)	- Porcine MFCs (Passage: 2)	- Swelling - Enzyme-assisted degradability - SEM - Mechanical behavior, compression	Static culture - Cell viability and proliferation - DNA and sGAG content - Total COL content - Gene expression studies (aggrecan, SOX-9, COL I α /II α) - Histological analysis (cell morphology, sulfated proteoglycans, total COL) - Immunogenic response (macrophage stimulation and IL-1 β release)	Subcutaneous implant (rats) [- cells] End point: 7, 14 days - Histological and IHC for biocompatibility (cellular and macrophages infiltration)

BM-MSCs: bone marrow mesenchymal stem cells; CAD: computer aided design; COL: collagen; G: gauge; GAG: glycosaminoglycans; hASCs: human adipose derived stem cells; IL: interleukin; kPa: kilopascal; MFCs: meniscal fibrochondrocytes; mL: milliliters; mm/s: millimeters/second; MRI: magnetic resonance imaging; N.R.: not reported; P: pressure; SEM: scanning electron microscopy; T: temperature; μm : micrometers; °C: centigrades; \varnothing : diameter.

Table 4. Synthetic 3D printed + 3D bioprinted composite scaffolds.

Authors and references	Printing method/parameters	Printing material	Additives or bioink	Shape and/or dimensions	Cells	Scaffold characterization studies	In vitro cells/scaffold interactions	In vivo studies
Chae et al. ¹³²	MRI of rabbit medial meniscus, 3D CAM/CAD, Custom built 3D cell-printing system. Parameters: T: 190°C (PU/PCL melting).	PU/PCL (60/40) Mw 43,000–50,000Da	Bioink: - Collagen + cells + TGfβ - Pig meniscal dECM + cells (5 × 10 ⁶ cells/mL)	- Grid-like, 5 × 5 × 1 mm - Meniscus-like 600 μm MESH: strand width, 250 μm, layer by layer stacking	- Human BM-MSCs (Passage: 4–5)	—	Static culture - Cell viability and proliferation - Fibrochondrogenic gene expression (COL1A2, COL2A1, COLXA1, and aggrecan) - IF for COL1/2, aggrecan, COLX	Subcutaneous implant (mice) [– cells] End point: 1, 2, 4, 8 weeks - Histology and IHC (capsular thickness, foreign body giant cells, macrophages) Biocompatibility Subcutaneous implant (nude mice) [± cells] Both no culture before implant and static culture (7 d) before implant End point: 4, 8, 12, 16 weeks - Chondrogenicity, histology for cartilage, IHC for COL2 - Mechanical behavior; tensile test
Narayanan et al. ¹³³	MRI scan of medial meniscus 3D CAD (SolidWorks 2015, Dassault Systèmes, Waltham, MA; Magics (Mimics Software, Materialize v19)) 3D Bioprinting (BioplotterRP) Parameters. - Acellular alginate nanofibers and alginate nanofibers + hASC Nozzle Ø: 810 μm; print T: 37°C; speed: 5 mm/s; P: 0.02 N/mm ² - Acellular Alginate and Alginate + hASC; nozzle Ø: 810 μm; print T: 37°C; speed: 15 mm/s; P: 0.02 N/mm.	PLA	Bioink: Alginate + cells Alginate + PLA nanofibers + cells (1.375 × 10 ⁶ cells/mL)	Meniscus-like MESH: intercalating layers of circumferentially orientated and linear-parallel strand geometries; 20 layers (each 0.482 mm thick).	hASCs (Passage: N.R.)	- Dispersion of PLA nanofibers within the hydrogel - Compression test of acellular scaffolds	Static culture - Cell viability/proliferation - Histological analysis (cell distribution, COL secretion, chondrogenic differentiation, proteoglycan secretion)	—

(Continued)

Table 4. (Continued)

Authors and references	Printing method/parameters	Printing material	Additives or bioink	Shape and/or dimensions	Cells	Scaffold characterization studies	In vitro cells/scaffold interactions	In vivo studies
Jian et al. ³⁵	Micro-CT of sheep meniscus, 3D CAM/CAD (Mimics, Materialize), Dual nozzle 3D bioprinter (Biomaker, SunP Biotech). Parameters: Bed T: 20°C - Nozzle 1 (PCL): inner Ø: 400 µm; T: 85°C; speed: 5 mm/s. - Nozzle 2 (hydrogel): TT nozzle inner Ø: 500 µm; T: 20°C; speed: 5 mm/s.	PCL Mw ~65,000 Da	Bioink (dual nozzle): GelMA + pig meniscal dECM + cells (1 × 10 ⁶ cells/mL)	- Primary models, 5 × 5 mm - Meniscus-like, 5 × 5 × 2.5 mm, 1000 ± 50 µm (PCL) thus filled with bioink MESH: cross mesh, strand spacing (center to center) 1.5 mm	- Rabbit MFCs (Passage: 2–5)	- SEM - Biomechanical behavior, compression, tensile testing	Static culture - Cell viability	Subcutaneous implant (mice) [- cells] End point: 2, 3, 4 weeks - Degradation Orthotopic implant (sheep) [- cells] End point: 3, 6 months - Degradation in situ - Gross evaluation - Nanoindentation and hardness test - Variations in PCL Mw - Histological (COL I/III, GAGs) and IHC (COL I) analyses
Sun et al. ³⁶	3D CAD model of goat meniscus 3D Bioprinter (Opus System, Novaprint, China) Parameters: Needle Ø: 200 µm; layer thickness: 0.2 mm; speed: 180 mm/min.	PCL Mw N.R.	Bioink: Cell laden hydrogel (gelatin + fibrinogen + HA + glycerol) encapsulating PLGA microparticles carrying TGFβ3 or CTGF (1 × 10 ⁷ cells/mL)	Meniscus-like 21.5 × 15 × 3 mm 300 µm (microchannels between PCL fibers) MESH: composite structure, cell-laden hydrogel (~100 µm Ø) + PCL (~200 µm Ø); fibers spacing, 350 µm	Goat BM-MSCs (Passage: 2)	- SEM - Printability - Microspheres distribution - Release kinetics of TGFβ3 and CTGF and quantification - Biomechanical behavior (tensile modulus, aggregate modulus, ultimate tensile strength, radial strength, bidirectional tensile testing in radial and circumferential directions, compressive testing)	Static culture - Cell viability - Cell anchoring/proliferation/ - Cytotoxicity - Zonal MSCs differentiation - Histology for ECM deposition (proteoglycans, COL I/III) - Expression of chondrogenic and fibrochondrogenic marker (SOX9, COL1A1, COL2A1)	Orthotopic implant (goat) [+ cells] No culture before implant End point: 24 weeks - Mobility - Histology (Cell phenotype and tissue integrity, COL I/III, proteoglycans) IHC (COL I/III) - Cartilage and osteochondral evaluation - ICRS and Mankin grading
Romanazzo et al. ³⁷	CAD 3D modeling of scaffolds 3D Bioprinter (Bioplotter, RegenHU). Parameters: PCL Needle Ø: 25G; bed T: 65°C; P: 4 MPa. Bioink needle: 25G; P: 2 MPa	PCL Mw 45,000 Da	Bioink: Alginate + pig meniscus dECM + cells (8 × 10 ⁶ cells/mL)	Printed construct on a coverslip About 1020 µm MESH: PCL microfibers with a ~0.36 mm thickness and ~1.02 mm spacing; layer by layer printing together with bioink	- Porcine FPSCs (Passage: 2)	—	Static culture - Mechanical behavior, stress-relaxation	—

BM: bone marrow; CAD: computer aided design; COL: collagen; G: gauge; GAG: glycosaminoglycans; hASCs: human adipose derived stem cells; IHC: immunohistochemistry; IL: interleukin; kPa: kilopascal; MFCs: meniscal fibrochondrocytes; MSC: mesenchymal stem cells; mm/min: millimeters/minute; mm/s: millimeters/second; MRI: magnetic resonance imaging; P: pressure; PU: polyurethane; SEM: scanning electron microscopy; SF: silk fibroin; sGAG: sulfated glycosaminoglycans; SOX9: SRY-Box transcription factor 9; T: temperature; °C: centigrades; Ø: diameter.

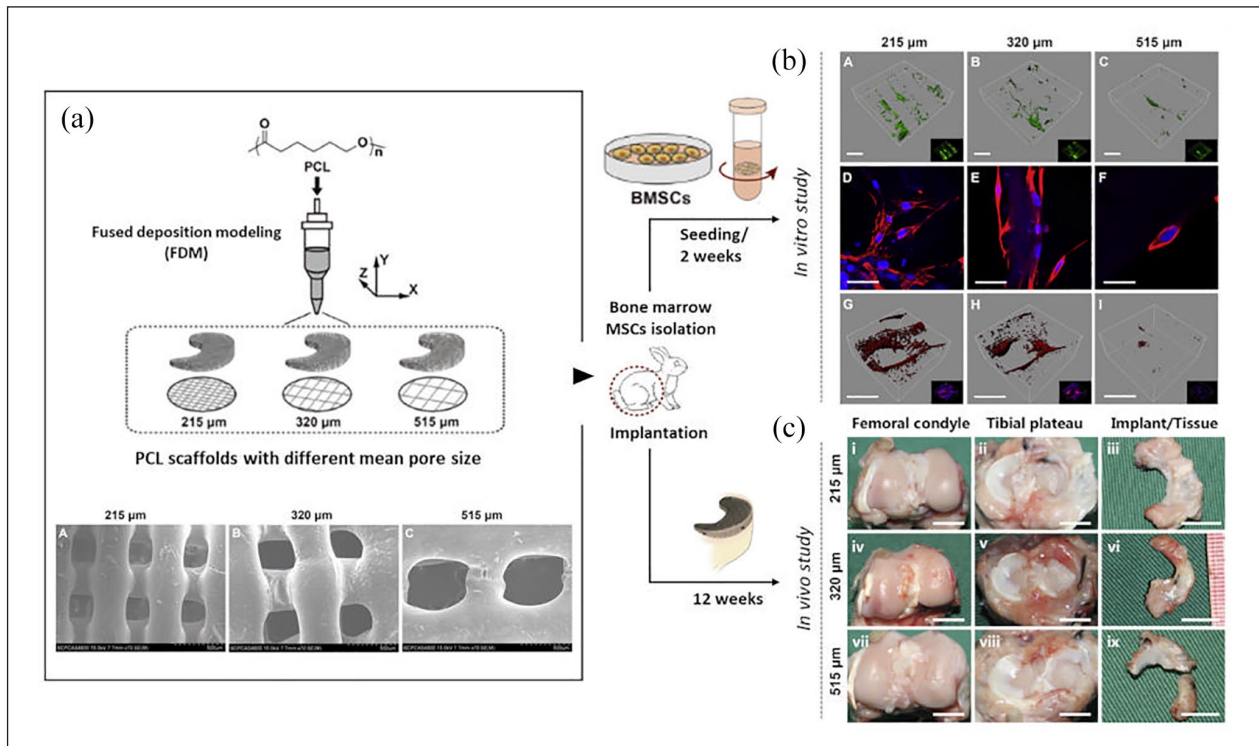


Figure 4. Synthetic 3D printed bare scaffolds, development and validation. (a) Schematic illustration of in PCL scaffolds printing method; (A–C) different mean pore sizes is also showed through SEM microimages. (b) Effect of scaffold mean pore size on bone marrow stem cells (BMSC) colonization and collagen II deposition. (A–C) Representative 3D microimages of BMSC colonization and collagen II deposition in scaffolds with various mean pore sizes; the surface area covered by live BMSCs was the greatest on the 215 μm scaffold in all three groups. Green fluorescence marked live BMSCs (scale bar: 300 μm). (D–F) BMSCs colonized and bridged neighboring fibers in the former group, while those placed on the latter were isolated; red fluorescence, cytoskeleton; blue fluorescence, nuclei (scale bar: 50 μm). (G–I) The largest areas of synthesized matrices around the pores were shown in the 215 μm scaffold compared with the other two scaffolds. Red fluorescence, collagen II (scale bar: 300 μm). (c) Macroscopic images of joints and implants 12 weeks after surgery; better outcomes were displayed by 215 μm scaffolds. Scale bar: 10 mm.

Source: Adapted and reprinted with permission from Zhang et al.²⁵ Copyright 2016 Elsevier.

conditioned scaffolds; (c) 3D bioprinted scaffolds; (d) synthetic 3D printed + 3D bioprinted composite scaffolds.

Specific references to the experimental studies discussed in the paragraphs below and referring to scaffold/cell types for meniscal reconstruction are reported in Tables 1 to 4.

Synthetic 3D printed bare scaffolds

Due to the apparently quiescent nature of meniscal cartilage, amenable to limited vascularization and low cell density, a few researchers searched for scaffolds able of bearing the joints load as a first prerequisite. In particular, PCL^{12,15,25,143,144,148} and Ecoflex30/50^{151,152} were investigated as materials for bare (i.e. free from biological conditionings and/or cells) 3D printed scaffolds, thus assayed through in vitro cell culture and/or in vivo implant (i.e. subcutaneous and/or orthotopic implant) to predict the biological response mediated by the construct alone, in perspective of meniscal TE approaches. Additionally, PCU was adopted for the development of porous meniscal

implant structures through triply periodic minimal surfaces¹⁶⁷ (Table 1; Figure 4).

Experimental evidence gathered on bare 3D printed PCL scaffolds highlighted their biological weakness. In fact, despite inducing MFCs adhesion/proliferation in vitro, these supports do not sustain high collagen production, correlating to PCL lack in bioactive sites.¹⁴⁴ Low collagen production after bare PCL scaffolds orthotopic implant was previously observed also by Zhang et al.¹⁵ who showed a higher cartilage degeneration in both femur and tibia and lower tensile and compressive characteristics ascribable to lower collagen content than that assured by MSCs-seeded PCL scaffolds.

Aware of PCL limitations, many efforts have been made over the years to improve the derived scaffolds potential; in particular, both ultrastructure and hydrophobicity have been extensively considered. Huebner et al.¹⁴³ and Warren et al.¹⁴⁸ and demonstrated that it is possible to control cell infiltration and obtain an oriented matrix deposition (i.e. aligned collagenous matrix) acting on PCL scaffold interstrand distances; in fact, lower interstrand distances

(100 μm) positively correlate with a higher collagen alignment percentage and, in turn, with a higher compressive elastic modulus.¹⁴³ As for the intrinsic PCL hydrophobicity, it can be modulated by simple soaking of PCL scaffolds in NaOH solution. The treatment also induces the formation of rough surfaces with pores, in turn improving the biological performances of the scaffold.¹²

Scaffold microarchitecture can deeply influence meniscal tissue formation as affecting endogenous and/or exogenous cell behavior²⁵; in vivo studies on animal model of meniscal injury (i.e. medial meniscectomy in rabbit; end point: 12 weeks) confirmed this assumption, also providing 215 μm as the optimal pore size to guarantee for superior in vivo results (i.e. increased type I and II collagen; chondroprotective effect).

Meniscal 3D printed prostheses based on bare Ecoflex are new devices requiring further investigation due to the novelty of (a) material use destination^{151,152}; (b) fabrication method, in relation to the intended use. In vitro data on Ecoflex-30 (low viscosity) and Ecoflex-50 (high viscosity) (Smooth-On Inc., Macungie, PA, USA) suggested their cytocompatibility (L929-fibroblasts) even though the seeded cells showed a spherical morphology instead of an elongated one, requiring further investigation. Additionally, fibroblasts clusters organization advocated to a possible correlation between surface roughness (similar for both Ecoflex-30/50) and a contact-inhibited growth.

As for mechanical behavior, these scaffolds showed resistance to cyclic loading and displayed mechanical features like native meniscus.

According to the experimental evidence, despite intense efforts in ameliorating design strategies,^{155,209} attempts to create bare scaffolds from synthetic materials have assured for limited achievements in terms of potential translational approaches. Urgent efforts must be devoted toward modifications able to orchestrate cells behavior within the scaffold thus promoting the regenerative process.

Synthetic 3D printed conditioned scaffolds (Impregnated)

As for most tissues, in meniscus TE the scaffold is the supporting construct that, acting as a guidance, is necessarily required for regenerating a new structure.²²⁰ Thus, it is expected to have strong mechanical properties to endure femur/tibia compressive load and circular hoop stress but also adequate features to promote cell adhesion/proliferation, creating a proper environment for cells to reside, and stem cells to differentiate, with also excellent permeability to nutrients and metabolites.^{12,88,147} Despite providing for shape-fidelity and self-supporting structures, the major challenge associated to polymers used in 3D printing is lack in biomimicry²²¹; without an adequate ECM-like microenvironment, regeneration likely fails.²²² To overcome this issue, conditioning of the supportive structure with bioactive elements has been widely investigated.

PCL, PCU, PU_PCL, p(DTD DD), and PLA scaffolds, endowed with intrinsic mechanical properties, have been conditioned (e.g. infusion/impregnation) with bioactive hydrogels based on natural polymers like collagen,^{38,150,153,154,156} GelMA and/or agarose,^{27,140} SF,^{140,142,146} alginate,¹⁵⁶ dECM.¹⁴⁷ Growth factors to increase scaffolds bioactivity was also sustained by Lee et al.¹⁴⁹ and Nakagawa et al.¹⁴⁵ (Table 2).

A complex scaffold made of a holding structure conditioned by a biological component must experience a dynamic equilibrium to be effective. The polymeric material acts as a reinforcement and is expected to bio-resorb slowly, supporting the developing tissue until its maturation and remodeling is occurred²²³; thus, the biological cues must create a temporary environment which degrades in balance with ECM proteins secretion by the embedded/colonizing cells.

Natural hydrogels were broadly used for synthetic polymeric scaffolds augmentation as they can reproduce native ECM-like environments. According to our knowledge, among these, protein-based hydrogels (collagen, gelatin, silk-fibroin), polysaccharides (agarose, alginate, hyaluronic acid), and dECMs have been adopted (Table 2; Figure 5).

Collagen, the main ECM structural protein, showed a critical role in cellular chondrogenic differentiation¹⁵⁶ and porous PCU scaffold infilled with it proved not only to promote cell adhesion and proliferation but also to improve the integration of the device in the host tissue, reducing the risk for implant dislocation and failure, typically reported for solid PCU in orthopedics.¹⁵⁰ Collagen combined with hyaluronate contributed to mechanical features of p(DTD DD) scaffolds also inducing robust integration and fibrochondrocytic ingrowth after orthotopic implant.³⁸ The development of collagen-hyaluronate sponges was reported by Ghodbane et al.^{38,154}

Gelatin combined with a methyl acrylate group (GelMA)^{124,192} was also used. Specifically, GelMA¹⁴¹ or GelMA + fibrochondrocytes²⁷ were adopted as conditioning hydrogels to impregnate PCL 3D printed scaffolds. Compared to PCL nude supports, the presence of GelMA determined fibrochondrocytes proliferation, and high levels of collagen type I/II mRNA suggesting the bioactive potential ascribable to it; biologic recognition is likely due to presence of RGD sequences on gelatine. Significantly, as GelMA was recognized to be fibrogenic, complex meniscal printed scaffolds with zonal variations were prototyped by Bahcecioglu et al.¹⁴¹ to emulate the anisotropic behavior of the native meniscus (outer region with GelMA, fibrogenic potential; inner region with agarose, chondrogenic potential). Moreover, incorporation of hydrogels also exerted a protective effect on cells under dynamic stress together with a reduction in cartilage degeneration.¹⁴¹

Li et al.¹⁴⁰ combined SF to PCL scaffolds through cross-linking, demonstrating its great contribution to balance both the biomechanical features and the degradation rate

of the supports *in vitro*. Moreover, orthotopic implant in rabbit of PCL-SF supports showed new vessels formation (especially at the synovial edge) and collagen I deposition; recruitment, retention, and proliferation of synovial MSCs was also sustained.

As for meniscal scaffolds augmentation, agarose was used both alone¹⁴¹ and combined with GelMA + fibrochondrocytes²⁷ for printed PCL scaffolds conditioning. Both hydrogels exerted a protective effect on fibrochondrocytes under loading versus PCL alone; moreover, agarose impregnated constructs proved increased levels of GAGs and type II collagen *in vitro*. The blend GelMA-agarose exhibited higher levels of aggrecan expression compared to PCL.

Alginate and oxidized alginate were used by Gupta et al.¹⁵⁶ for PLA 3D printed scaffolds conditioning; the natural polymer had a great influence on micromechanical properties and maintenance of structural integrity of the scaffold; moreover, as showed both *in vitro* and *in vivo* (subcutaneous implant) the presence of interpenetrating network hydrogels actively participated in ECM formation, inducing deposition of GAGs and collagen.

Chen et al.¹⁴⁷ reported about a hybrid scaffold based on printed PCL and augmented with decellularized meniscal cartilage derived hydrogel both free and in presence of MFCs. The acellular matrix confirmed its ability to act as a functional cells' carrier; moreover, a percentage of 20% in hydrogel was identified as the most adequate to confer an optimal bioactive behavior to the support. Thereafter, according to orthotopic implant data in rabbits' knee, PCL + dECM + fibrochondrocytes explants displayed at 6 months post-implantation histological/biochemical and biomechanical features like native menisci.

Interestingly, within this group, a singular type of meniscal substitutes can also be included, corresponding to 3D printed stiff antibacterial hydrogels. Yang et al.²²⁴ fabricated a stiff (2.69 MPa tensile stress; 26.25 MPa tensile Young's modulus) N-acryloylsemicarbazide (NASC)/gelatin support (gelatin was employed as a sacrificial material) with polydopamine coated-ZIF-8 anchored onto the scaffold surface. Together with their role as meniscal substitutes, these supports show a strong ability to minimize infection-induced implantation failure, representing a vanguard device with a twofold function: support in tissue regeneration and advanced drug-delivery system.²²⁴

3D bioprinted scaffolds

Printable bioinks are attractive for their ECM-like features assuring for biocompatibility, low cytotoxicity, high water content, porous structure, bioactive molecules, and cells incorporation. Thus, bioink development is a crucial step as its composition and structure will significantly affect the behavior/phenotype/differentiation of incorporated/seeded/tissue resident cells in turn strongly modulating

tissue regeneration. In example, alginate and agarose bioinks support the development of hyaline-like cartilage tissue; while GelMA based-bioinks favor cartilaginous tissue formation.¹²⁹

Typically, the components of a bioink are (1) the cells, (2) the biopolymer (representing the prevalent portion of the bioink),¹³¹ and (3) the additives, modulating the bioprinting materials' rheological properties and thus guaranteeing for resolution, shape fidelity, structural stability, and functional characteristics^{133,225}; as for the additives, there is no accordance in concentrations (Table 3).

Rhee et al.¹³¹ developed scaffolds based on highly-concentrated collagens (15 and 17.5 mg/mL gels) bioinks mixed with bovine MFCs. The supports showed to overcome the mechanical limitations of collagen gels (1–3 mg/mL) commonly used in bioprinting, displaying a linear increase of the compressive modulus according to collagen concentration. The scaffolds also maintained geometric fidelity over 10 days in culture and collagen fibers allowed for cells homogeneous distribution within the support. A promotion of cell growth/spreading with the increase in collagen concentration was also observed; despite heated bioink deposition (37°C), a minimal effect on cell viability occurred. Similarly, also Filardo et al.¹³⁴ manufactured a meniscus-like scaffold using a commercial highly concentrated Type I Collagen bioink (LifeInk 200—Advanced Biomatrix, San Diego, California) here added with human bone-marrow MSCs. In accordance with previous evidence by Rhee et al.,¹³¹ the method assured for cell viability and homogeneous cellular distribution within the support, which was successfully cultured up to 28 days.

Markstedt et al.¹³⁸ set up novel bioinks composed of nanocellulose and alginate. In particular, a formulation composed of nanofibrillated cellulose/alginate (80:20) combined with human nasoseptal chondrocytes proved its suitability for 3D bioprinting, guaranteeing for homogeneous cell distribution (i.e. successful mixing), cell viability, and biocompatibility. Printability of alginate in combination with human adipose derived stem cells was also possible as later showed by Narayanan et al.¹³⁰ in a study demonstrating efficacy of dielectric impedance spectroscopy as a label-free non-destructive monitoring approach for quality of 3D constructs (both during and after biofabrication).

More recently, cellulose nanofibers mixed with gelatine-alginate thermal responsive bioinks + MFCs were prepared by Luo et al.⁹⁷ The bioink showed capacity in maintaining long-term cellular viability with also encouraging mechanical performances attributable to physicochemical interactions; hydroxyl surface groups of cellulose and alginate can interact with carbonyl and amine groups in gelatin thus forming hydrogen bonds. ECM proteins content *in vitro* (GAG, type II/X collagens) was like that of native meniscus.

Costa et al.¹³⁹ prepared by coprinting a cell-laden (i.e. meniscus cells) gellan gum/fibrinogen composite bioink +

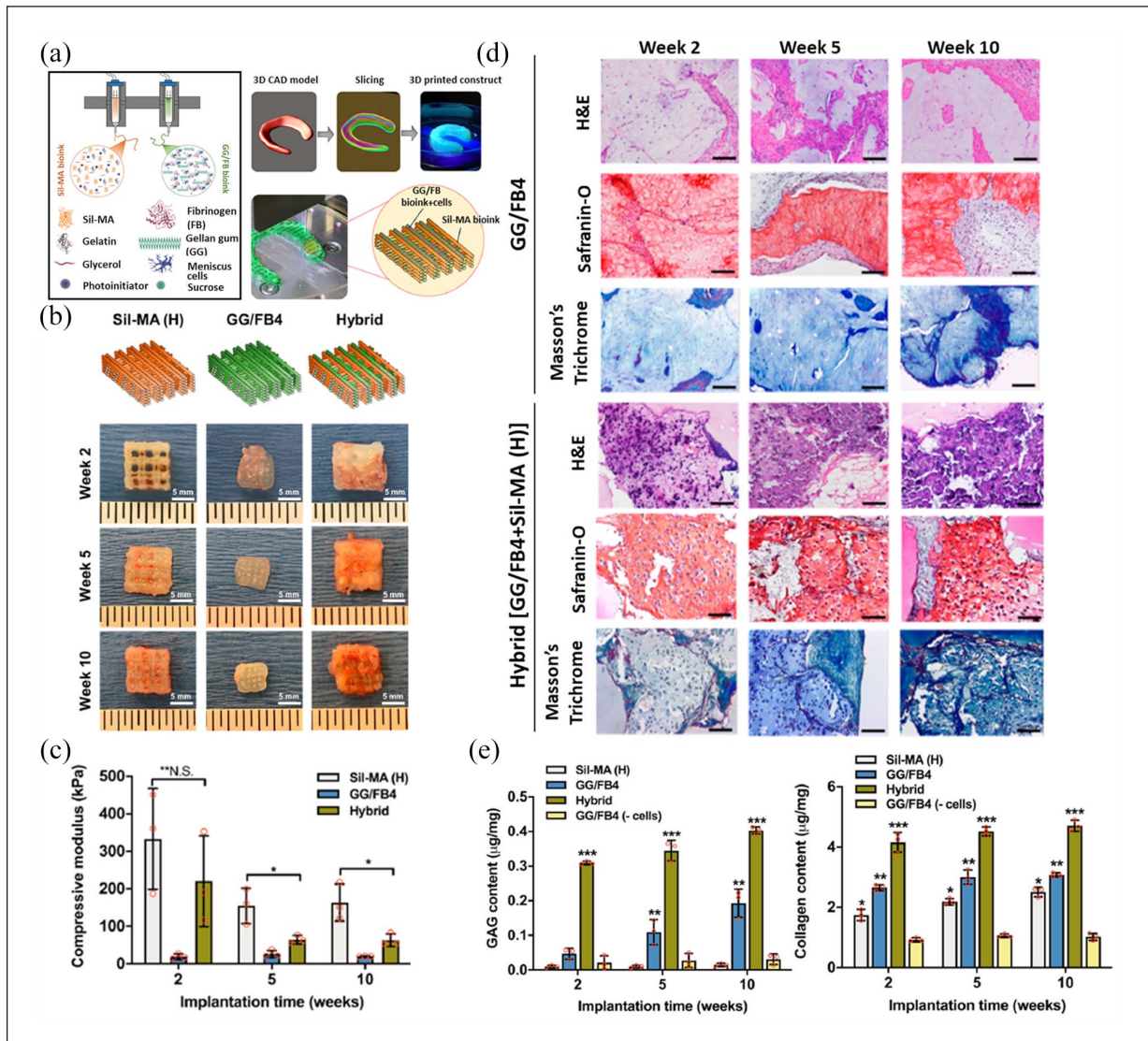


Figure 6. 3D bioprinted scaffolds. (a) Schematic representation of 3D bioprinted scaffolds obtained coprinting a cell-laden (i.e. porcine meniscus cells) gellan gum/fibrinogen (GG/FB4) composite bioink together with a silk fibroin methacrylate (Sil-MA (H)) bioink. An interleaved crosshatch pattern was obtained. (b) Scheme of the printed patterning used for 3D bioprinted constructs fabrication. Explants gross appearance at 2, 5, and 10 weeks after subcutaneous implantation in nude mice: the hybrid constructs maintained their original dimension along time. In contrast, a reduction of dimension was detected in the GG/FB4 group at 2 weeks from surgery. (c) Compressive elastic modulus of 3D bioprinted constructs at 2, 5, and 10 weeks after subcutaneous implantation: Sil-MA (H) and hybrid (220.0 constructs) showed a higher compressive modulus compared versus the GG/FB4 at 2 weeks from surgery. At 5 weeks after implantation, a significant decrease in mechanical strength occurred in the Sil-MA (H) and hybrid groups. At 10 weeks of implantation, the compressive modulus of the constructs was maintained. (d) Histological images of 3D bioprinted constructs after 2, 5, and 10 weeks of implantation (scale bars: 200 µm): the formation of fibrocartilage-like tissue was observed in the GG/FB4 and hybrid constructs. GAG and collagenous matrix production were confirmed by Safranin O and Masson's Trichrome staining, respectively. (e) Quantification of GAG and collagen production of the bioprinted constructs at 2, 5, and 10 weeks after subcutaneous implantation: increase in GAG and collagenous matrix production was observed along time. The hybrid constructs sustained the deposition of a considerably higher amount of GAGs and collagen versus the other groups, at 10 weeks after implantation.

Source: Adapted and reprinted with permission from Costa et al.¹³⁹ Copyright 2020 American Chemical Society.

SF methacrylate bioink. While the gellan gum/fibrinogen component provided to create a favorable environment for cell viability, the SF methacrylate bioink contributed to biomechanical behavior and structural integrity. More

importantly, this hybrid system allowed for fibrocartilaginous tissue formation without a dimensional change in a mouse subcutaneous implantation model also showing collagen fibers allignment (Figure 6).

Finally, Bandyopadhyay and Mandal¹⁵⁷ reported about a SF-gelatin blended 3D bioprinted scaffold; no cells were included here during printing despite the Authors referred to as “bioink.” The support was developed to mimic the internal and bulk architecture of the menisci; thus, it was characterized by a tri-layer ultrastructure (grid/concentric/lamellar infill) which displayed satisfactory swelling properties, in vitro degradation profile and stability at compression. Moreover, in vitro cell studies and in vivo subcutaneous implant of the acellular scaffold demonstrated immune-compatibility and its ability in promoting cell growth and ECM proteins secretion.

The main issue associated to hydrogels is that they are mechanically weak, lacking in viscosity and cross-linking ability to retain 3D structure without collapsing and mimic the biomechanics of tissues.^{98,138,226,227} Ideally, a bioink should possess proper mechanical, rheological, chemical, and biological characteristics; however, hydrogel-only scaffolds do not meet the mechanical requirements of meniscus scaffolds leading researchers to combine them with synthetic polymers^{138,147}.

Synthetic 3D printed + 3D bioprinted composite scaffolds

To date, despite 3D bioprinting techniques have evolved significantly, to develop fully functional tissues/organs for transplantation through this approach would be premature.²²⁸ Biomimetic bioinks often lack in mechanical strength thus proving to be not adequate as the sole material of a printed tissue.²²² To overcome this issue, Sun et al.,¹³⁶ Chae et al.,¹³² and Romanazzo et al.¹³⁷ combined 3D printing of the supportive polymer and 3D bioprinting of the cell-laden bioink, in sequence. Interestingly, a dual-nozzle + multi-temperature printing system was recently proposed for menisci by Jian et al.¹³⁵ (Table 4; Figure 7).

All Authors used PCL as supporting material^{135–137}; Chae et al.¹³² adopted the blend PU/PCL while Narayanan et al.,¹³³ preferred PLA. As for the bioactive component, different printable bioinks were prepared including alginate + adipose stem cells or alginate + PLA nanofibers + adipose stem cells¹³³; alginate + meniscal dECM + infrapatellar stem cells¹³⁷; gelatin + fibrinogen + HA + glycerol + bone marrow MSCs + TGFβ/CTGF PLGA microparticles¹³⁶; collagen + bone marrow MSCs + TGFβ or meniscal dECM + bone marrow MSCs¹³²; GelMA + meniscal dECM + MFCs¹³⁵ (Table 4).

Referring to the mechanical behavior, Romanazzo et al.,¹³⁷ reported a 100-fold increase in stiffness for the printed bioink in presence of PCL reinforcement, reaching a similar order of magnitude to native meniscus. Moreover, viability of the cells was maintained, suggesting that the adopted process-parameters and shear stress were acceptable. Sun et al.¹³⁶ also verified the mechanical behavior of the bioprinted scaffolds in vitro before in vivo

implantation. Here, the presence of growth factors in the bioink was recognized as the key element to provide mechanical strength to the construct (i.e. high tensile modulus, aggregate modulus, ultimate tensile strength, radial strength). Regional variations in biomechanical behavior in vitro also suggested the achievement of functional heterogeneity typical of native menisci. Chae et al.¹³² assessed the tensile properties of the constructs after subcutaneous implant; in particular, the cell-laden meniscal dECM scaffolds were implanted both after printing and after 1 week of in vitro chondrogenic priming. All constructs maintained their original shape without evident deformation; the tensile properties (maximum load to failure, elastic and ultimate strength, and toughness) in all groups gradually increased due to host cell infiltration and tissue ingrowth. Moreover, the tensile properties of the meniscal dECM-based constructs were higher than those of the collagen + TGF constructs and the tensile properties of the primed meniscal dECM group were higher than those of the meniscal dECM group.

Multi-nozzle printing was interestingly reported by Jian et al.¹³⁵; mechanical characterization studies' results showed lower compressive and tensile moduli in presence of the hydrogel. However, the compression modulus of the construct was higher than that of the human meniscus and the tensile modulus was close to that of the meniscus in the radial direction. However, as for circumferential tensile modulus there was still a large difference.

As concluded by all the Authors, the combination of different techniques is effective for achieving meniscal higher-level biomimetic scaffolds, without affecting cell viability. Despite the “ideal” scaffold has not been achieved yet, and intense efforts are still required especially in material science, this strategy seems extremely promising.

Cell types in printed meniscal scaffolds

For meniscal replacement, the use of cell-free scaffolds is commonly considered a first choice; it would provide for off-the-shelf devices and ensure for no further costs and eventual risks associated with cell manipulation, also including bacterial contamination and phenotype loss. In addition, regulatory limitations that could hinder translation into clinical practice are thus avoided.^{134,229} In cell-free implants, the tissue resident cells must be capable of reaching the site of injury and colonize the supporting structure.^{26,149} Pre-clinical studies outcomes considering orthotopic implant of conditioned cell-free 3D printed scaffolds were reported in the literature.^{135,145,147,154} Here, the Authors aimed to assess resident cells migration and the biological response in situ (i.e. lesion recovery) elicited by PCL scaffolds laden with growth factors (i.e. connective tissue growth factor and TGFβ),¹⁴⁵ GelMA + pig meniscal dECM¹³⁵ or injected with meniscal dECM.¹⁴⁷

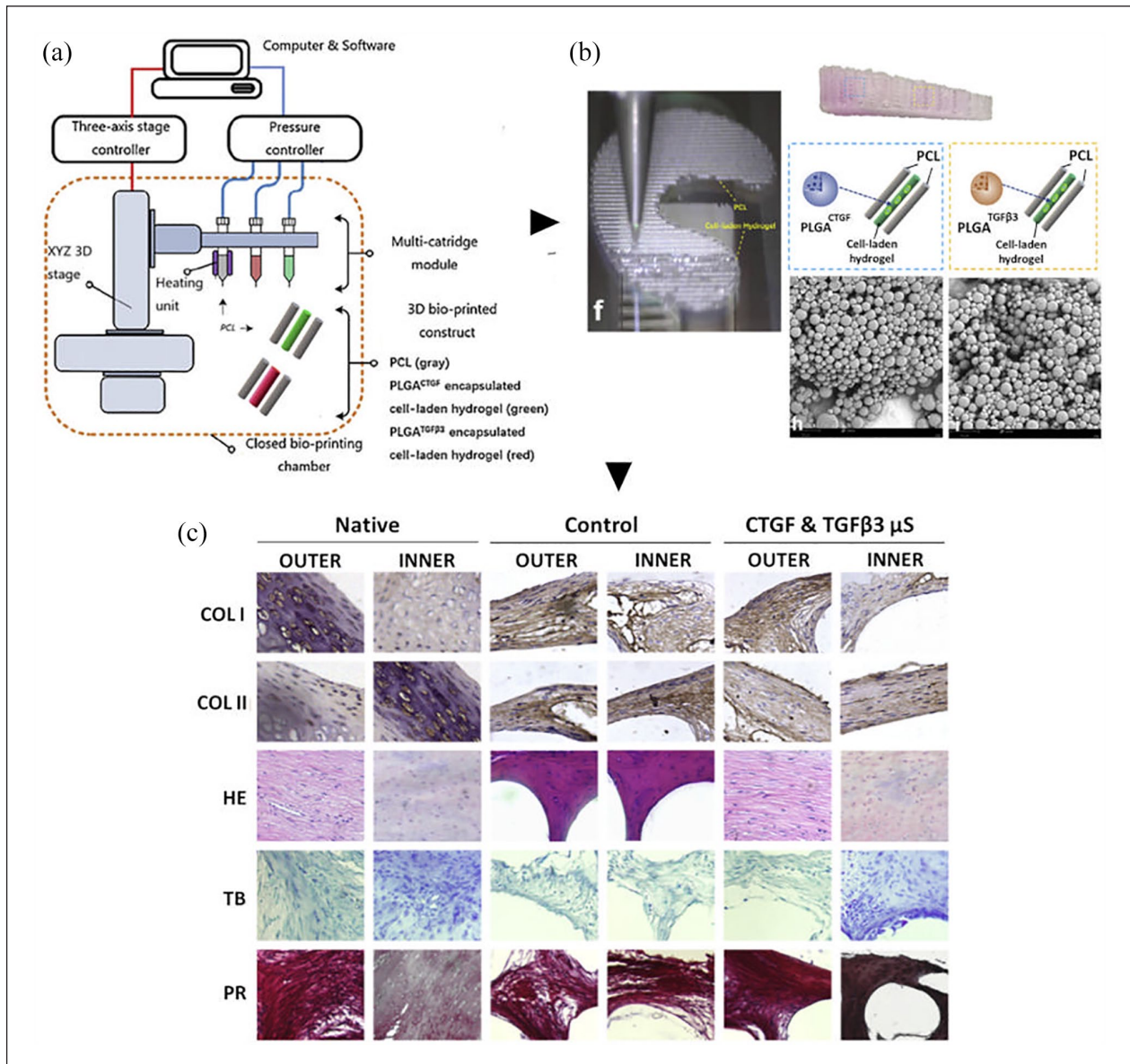


Figure 7. Synthetic 3D printed + 3D bioprinted composite scaffolds. (a) Schematic illustration of bioprinted protein-releasing mesenchymal stem cells (MSC)-laden hydrogel-PCL composite constructs for meniscus regeneration in goats. (b) 3D-bioprinted meniscus scaffold for implantation (f). Schematic illustration of MSC cell-laden hydrogel encapsulating PLGA microparticles carrying CTGF (blue box) or TGFβ3 (yellow box) in different regions, between PCL fibers; printing occurred from different syringes; (H–I) SEM images of PLGA μS showing a less than 5 μm diameter for CTGF (h) and TGFβ3 (i) respectively. (c) Regeneration of the goat meniscus at 24 weeks after implantation. Zonal matrix phenotype analysis in engineered versus native tissue. Tissue sections were stained by immunohistochemistry for collagen type I and II (COL-I and -II) presence or by hematoxylin and eosin (H&E) for cells distribution and tissue integrity; toluidine blue (TB) staining occurred for assessment of proteoglycans deposition while picrosirius red (PR) for COLI and COLIII verification. Histological evaluation of the regenerated meniscus in the CTGF & TGFβ3 group revealed matrix phenotypes and distribution resembling those in the native tissue. Source: Adapted and reprinted with permission from Sun et al.¹³⁶ Copyright 2019 Elsevier.

Also p(DTD DD) scaffolds infused with collagen-hyaluronan were considered.¹⁵⁴ However, according to experimental comparative studies, it seems that cell augmentation might provide for superior regenerative potential¹³⁴ than cell-free constructs, which likely lead to a worse repair due to insufficient ECM production in turn getting to inferior mechanical performances.^{147,220}

Identification of the most adequate cell population for meniscal reconstruction is crucial for a satisfying outcome in regeneration, despite it also represents a significant challenge amenable to the specific physiological role of the tissue. As meniscus is a load-bearing structure, the cells must be able to adhere/proliferate overcoming compressive and shearing motion and, in case of mature cells,

also preserve the specific fibrochondrogenic phenotype. This feature was in example addressed by Bahcecioglu et al.¹⁴¹ showing that a dynamic compression at 10% strain has no significant effect on MFCs viability but can affect cell proliferation rate in case of no protecting hydrogel (i.e., alginate).

Regarding cell sources for meniscal tissue regeneration, the most reported include specific resident cells referred to as meniscocytes^{139,142,146} or MFCs^{12,27,97,131,135,141,144,147,157} and MSCs^{12,15,25,130,132–134,136,137,140,146,149,156} (Tables 1–4).

Meniscocytes/meniscal fibrochondrocytes

The main advantage residing on tissue constructs derived from meniscus cells is their better histocompatibility.²³⁰ Cells of both human-origin^{27,142,146} and animal-origin^{12,97,131,135,139,141,144,147,157} were assayed in combination with PCL scaffolds^{12,144} (eventually conditioned^{20,135,141,142,146,147}), or hydrogels/bioinks^{97,131,139,157} as solely scaffold. Specifically, cell printing was accomplished by Luo et al.,⁹⁷ Jian et al.,¹³⁵ Rhee et al.,¹³¹ and Costa et al.¹³⁹; others preferred seeding once the supportive scaffold was developed.

The primary aim of in vitro cell studies is to evaluate cells/scaffolds interactions; assays considering meniscocytes/MFCs adhesion and migration, distribution, viability, and the maintenance of specific cell morphology are mandatory.^{12,27,97,131,135,139,142,157} However, confirming cell bioactivity in terms of ECM production is also imperative. To this purpose, gene expression studies (Aggrecan, SOX-9, COL I α /II α) and evaluation of specific ECM proteins content/presence (total collagen, collagen I/II deposition, GAGs, hydroxyproline) were taken into consideration.^{27,97,139,141,144,157}

Furtherly, ex vivo pre-seeded scaffolds were implanted subcutaneously in nude mice^{139,142,146} or orthotopically in rabbits.¹⁴⁷ After 4 weeks of subcutaneous implant, Cengiz et al.^{142,146} highlighted the ability of the constructs to promote tissue infiltration, blood vessels formation, newly formed collagenous ECM with only mild inflammatory cells invasion. Indeed, seeded/unseeded (control group) implants displayed here similar outcomes; the Authors suggested that seeding higher cells number and/or extending ex vivo culture time may lead to different results.¹⁴² Conversely, Costa et al.¹³⁹ displayed different in vivo events: at 10 weeks from surgery, constructs with cells showed higher ECM production with higher levels of GAGs and collagens, whose fibers also appeared aligned as in native tissue.

The subcutaneous site and the knee joint site are different environments; it descends that ectopic implant can provide data on biocompatibility but for outcomes in terms of support effectiveness and tissue regeneration, orthotopic implant is indispensable.¹⁴² According to our knowledge, only Chen et al.¹⁴⁷ considered the performances of pre-seeded scaffolds once implanted in the meniscus of a rabbit

animal model of injury (i.e. total medial meniscectomy). Briefly, PCL-hydrogel-MFCs scaffolds (hydrogel: meniscal dECM) were compared to PCL scaffolds and PCL-hydrogel scaffolds. At 3 and 6 months all supports showed meniscus regeneration, but histological structure, biochemical contents, and biomechanical performance were superior in presence of cells, highlighting their significant role in regeneration and, in turn, also in chondroprotection; because of the major size of the regenerated tissue, more effective biomechanical properties with adequate load transmission and stabilization occurred. Together with MFCs, the Authors also speculated a possible recruitment in vivo of stem cells (from synovia, bone marrow, infrapatellar fat pad, or peripheral blood) mediated by bioactive cues secreted by MFCs or identifiable in the dECM.

Among primary cells also nasoseptal chondrocytes were used as constituents of a bioink based on nanofibrillated cellulose and alginate; in vitro cell viability and homogeneous distribution were confirmed within the supports however no further evaluation was performed for bioactivity.¹³⁸ In this context, Lehoczy et al.²³¹ proved nasal cartilage as an interesting alternative source of chondrocytes, overcoming the limit of chondrocytes from debrided knee cartilage, that show a reproducibly poor capacity to chondro-differentiate.

Satisfactory regenerative results from in vitro/preclinical studies using meniscocytes/MFCs would indicate the possibility to implant autologous primary cells. This strategy is broadly accepted and described in several TE approaches for other joint compartments, especially for articular cartilage (e.g. Stocco et al.,²³² Migliorini et al.²³³). However, in the perspective of future clinical application, some considerations/reflections are due. To guarantee effective scaffold colonization, seeding at high density is required: (1) primary cells display a poorer proliferation ability than stem cells; (2) sufficient tissue must be processed for primary cells isolation (debrides? larger sampling?); (3) meniscocytes/MFCs, whether isolated from patients affected by a chronic and/broad lesion, might be primed by the inflammatory environment thus acquiring cellular alterations which could affect proliferation and tissue regeneration.^{68,146,234,235} Only results descending from long-term studies follow-up will help in the identification of the most effective strategy for satisfactory outcomes.

Mesenchymal stem cells

In case of meniscal lesions approached through TE strategies, stem cells figure out as a keystone¹⁴² by virtue of: (i) self-renewal and highly proliferative potential; (ii) reduced immunogenicity versus mature cells (as lacking Human Leukocyte Antigen (HLA) class II expression)²⁶; (iii) active secretion of local anti-proliferative mediators reducing/suppressing inflammation and in vivo immune response (immunomodulatory role)²³⁶; (iv) ability to

differentiate toward different lineages including cartilage, bone, muscle, fat.

To date, several sources of MSCs have been considered for meniscus repair through 3D printing; these include bone marrow^{12,15,25,132,134,136,149} synovia,^{140,149} umbilical cord,¹⁵⁶ lipoaspirate,^{130,133} infrapatellar fat pad^{137,142,146}; however, according to our knowledge, only few studies actually considered their mixture/dispersion in bioinks followed by direct printing^{130,132–134,136,137} rather preferring a subsequent seeding on the bare-synthetic/conditioned 3D printed scaffold.^{12,15,25,140,142,146,149,156}

Printability of MSCs (i.e. preservation of viability and stemness) needs attention²³⁷; biological and printing requirements (often opposite) must both be met for successful outcomes and transability to production floor^{130,134} as cells could be affected by fluid shear stress intensity/duration in turn increasing the number of cells undergoing necrosis. In this scenario, damaged cells can release trophic factors which seem to exert negative effect on viability and differentiation of the resident cells.²³⁸ A great awareness about this issue has been demonstrated by Narayanan et al.¹³⁰ providing evidence on dielectric impedance spectroscopy as a label free method to in-process monitoring the adequacy of the printing strategy (number of cells, percentage of viability, proliferation).

From a methodological perspective, the studies involving MSCs printing need to confirm the suitability of the approaches. No detrimental effect on MSCs viability was highlighted by several Authors^{130,132–134,136} referring to the conditions they adopted. In addition, Sun et al.¹³⁶ and Chae et al.¹³² also assessed and confirmed the differentiated cells bioactivity in vitro through evaluation of ECM proteins expression and deposition; for a broad appraisal of the bioactive potential of the scaffold, Sun et al.¹³⁶ also performed the orthotopic implant. The in vivo outcome of the developed anisotropic support (i.e., protein-releasing MSCs-laden hydrogels with a synthetic PCL) was evaluated at 24 weeks from surgery (i.e. animal model: goat; total meniscectomy) by histological and immunohistochemical analyses. The results confirmed the preliminary in vitro data on zonal expression of type I, II collagen but also highlighted that MSC-derived meniscus chondrocytes can generate and maintain anisotropic and stable phenotypes in vivo, after transplantation. Furtherly, the 3D bioprinted meniscus into goat knees proved ability in long-term chondroprotection.

To comprehend the effective contributory role in regeneration guaranteed in vivo by MSCs, the study by Zhang et al.¹⁵ is enlightening (animal model: rabbit; total meniscectomy of the medial meniscus). Briefly, the Authors considered the orthotopic implant of PCL 3D printed menisci subsequently laden with BM-MSCs (seeding 24 h before surgery) versus bare-PCL scaffolds. As for the main study results, the cell-laden scaffolds displayed significantly higher integration with the joint, significantly better fibrocartilaginous tissue formation (resembling the native

meniscus in matrix composition/cellularity), lower cartilage degeneration, retained mechanical strength. Moreover, better lower foreign body reaction was identified in the cell-seeded group confirming MSCs immunoregulatory behavior. Interestingly, this study also validates the potential of allogenic MSCs for meniscal TE.

As for subcutaneous implants of ex-vivo seeded scaffolds with MSCs, only two studies were reported.^{142,146} Despite presence of human IFPSCs did not show significantly different outcomes versus cell-free scaffolds in terms of tissue infiltration and vessels formation, the Authors convey that cell seeding gives rise to benefit.

At last, orthotopic implants of 3D printed cell-free scaffolds, previously validated by in vitro MSCs seeding, were also performed.^{25,140,149}

Surgical strategies in preclinical studies and future perspectives

Animal models of meniscal injury for orthotopic implant of 3D printed devices

In this evolving phase for meniscal devices development, pre-clinical studies considering orthotopic implant of the 3D printed scaffolds provide important data to broadly describe, study, and ameliorate the biological and biomechanical behavior of these substitutes.

According to our knowledge, different animal species were included in in vivo studies evaluating the 3D printed meniscal scaffolds outcomes. Specifically, sheep,^{135,145,149,154} goat,¹³⁶ rabbits,^{15,25,140,147} and rats¹⁴⁰ were adopted. As for rats, surgery specifications were not reported.

Meniscal surgery in sheep

After administration of general anesthesia, sheep were approached in supine position. Patella was luxated or subluxated after medial parapatellar arthrotomy^{149,154} or lateral patellar arthrotomy.¹⁴⁵ Hence, joint flexure and condylectomy allowed for medial meniscus exposure preserving ligaments. Slightly differently, Jian et al.¹³⁵ reported to have performed two apertures (5 mm) which were drilled in the anterior horn of the medial meniscus and in the anterior horn of the lateral meniscus, after patella dislocation.

Partial meniscectomy led to resection of all but about 10%¹⁴⁴ or 20%¹⁴⁹ of the meniscal outer zone; or 80% of the medial meniscus.¹⁵⁴ Thereafter, the meniscal defect was repaired through implant and suture of the graft; the joint capsule, the subcutaneous tissue and the skin were sutured layer by layer.

To reduce sudden or extended movements, Nakagawa et al.¹⁴⁵ and Lee et al.¹⁴⁹ housed the sheep in small pens. Only after complete condylectomy recovery, sheep were group-housed in progressively large paddocks.

No limitations of movement were imposed to sheep by Ghodbane et al.¹⁵⁴ and Jian et al.¹³⁵

As reported by Nakagawa et al.,¹⁴⁵ the anatomic shape and the contour of the menisci are quite similar among animals regardless of age. Differences can occur in the anterior-posterior length.

Meniscal surgery in goats

Surgery on goats was reported by Sun et al.¹³⁶ Similarly for sheep, after anesthesia, medial parapatellar approach was performed; the patella was luxated medially and joint flexure allowed for medial meniscus exposure followed by total meniscectomy with ligaments preservation. Joint capsule and subcutaneous tissue were closed separately through continuous absorbable suture.

No immobilization method was reported after surgery.

Meniscal surgery in rabbits

Once anesthetized, an anteromedial¹⁴⁰ or medial^{15,25} parapatellar incision was performed. Thereafter, different strategies were reported. Li et al.¹⁴⁰ cut the medial collateral ligament for medial meniscus exposure; hence, total medial meniscectomy occurred followed by implant suture to the capsule of the meniscal rim, and the anterior and posterior horns were fixed by the tibial bony tunnel. Zhang et al.^{15,25} detached the medial meniscus without injuring the ligament and sutured the scaffold to the adjacent synovium and the ligamentous structures. After suture of the medial collateral ligament, the wound was closed in layers. Chen et al.¹⁴⁷ also performed a total medial meniscectomy except 5% of the external rim were then implanted; to preserve joint stability, the ligaments were not injured or disconnected.

No immobilization method was reported after surgery.^{15,25,140,147}

Body donation as a resource for research and development in 3D printed meniscal scaffolds fabrication

The most significant issue in 3D printed meniscal scaffolds development relies on fabrication of mechanically efficient devices fitting well the defect area and supporting loading and fixation without giving rise to ruptures and dislocations. Certainly, substitutes good performances also depend on the injury severity and location: orthopedic surgeon's responsibility must combine clinical information, radiological image, and clinical experience aiming to individualize meniscal tears management and considering factors related to both the patient and lesion.²³⁹

Considering the state-of-the-art on meniscal substitutes fabrication, possibility to reproduce clinical practice environment is extremely tempting as supporting a complete

high surgical education but also transversal integration between different professional figures. Combination of different specific backgrounds and skills (clinicians, surgeons, researchers) may promote future translation to clinic of optimized 3D printed meniscal devices (still a challenge). In this setting, it descends the precious role that may be attributed to Body Donation Programs: a resource for simulation of clinical scenario allowing to get in touch with surgical issues from both surgeons and researchers (actively involved in devices fabrication) perspective. In example, Body Donation Program currently active at the University of Padua and allowing for collection of donated cadavers and body parts surgically removed,^{240,241} largely proved what stated above.^{62,242-247}

According to our knowledge, the cadaver-based approach for the evaluation of 3D printed meniscal substitutes performances has never been proposed previously and it may represent a tempting further strategy for devices evaluations to be interposed between pre-clinical studies and implant in human. Hence, in the light of the above considerations, the cadaver could be considered as a patient, allowing to lay the foundations for a 2.0 customized surgery based on effective interplay between clinicians and researchers thus providing for scaffolds that fully meet patients' needs overcoming the limitations of current devices.

Corpses or lower limbs from Donation Programs could be a fundamental tool also in meniscal substitutes development, allowing for optimization in scaffold design, surgery, and implant validation. Ideally, in a cadaver-based research approach, corpses or lower limbs could undergo 3-T clinical MR scan and CT scan of the knee for data acquisition; thus, 3D reconstruction of the knee joint by DICOM image segmentation could be performed. Manual image segmentation should be developed by a multidisciplinary team composed of experienced orthopedic, anatomist, radiologist, and biomedical engineer; accuracy in image segmentation will minimize variations in the models. After data conversion into STL file, followed by conversion in a G-code file containing the geometries of each 2D layer from the 3D model, 3D printing could occur. Once the scaffold will be fabricated according to the preferred strategy (i.e. 3D printing/3D bioprinting), surgeon could attempt different surgical approaches for implant, also experimenting and comparing vanguard techniques. Additionally, this step could guarantee for direct assessment of device handling characteristics. At the end, after implantation, the cadaver could again undergo MR and CT scans for fitting evaluations in normal and flexed positions. Other tests could include mechanical evaluations for knee kinematics and load stress, providing for significant advance in the ability to simulate and quantitatively study the effects related to 3D printed scaffolds implantation (Figure 8). It descends that the precious value attributed to the cadaver in this context likely relies in its possible role

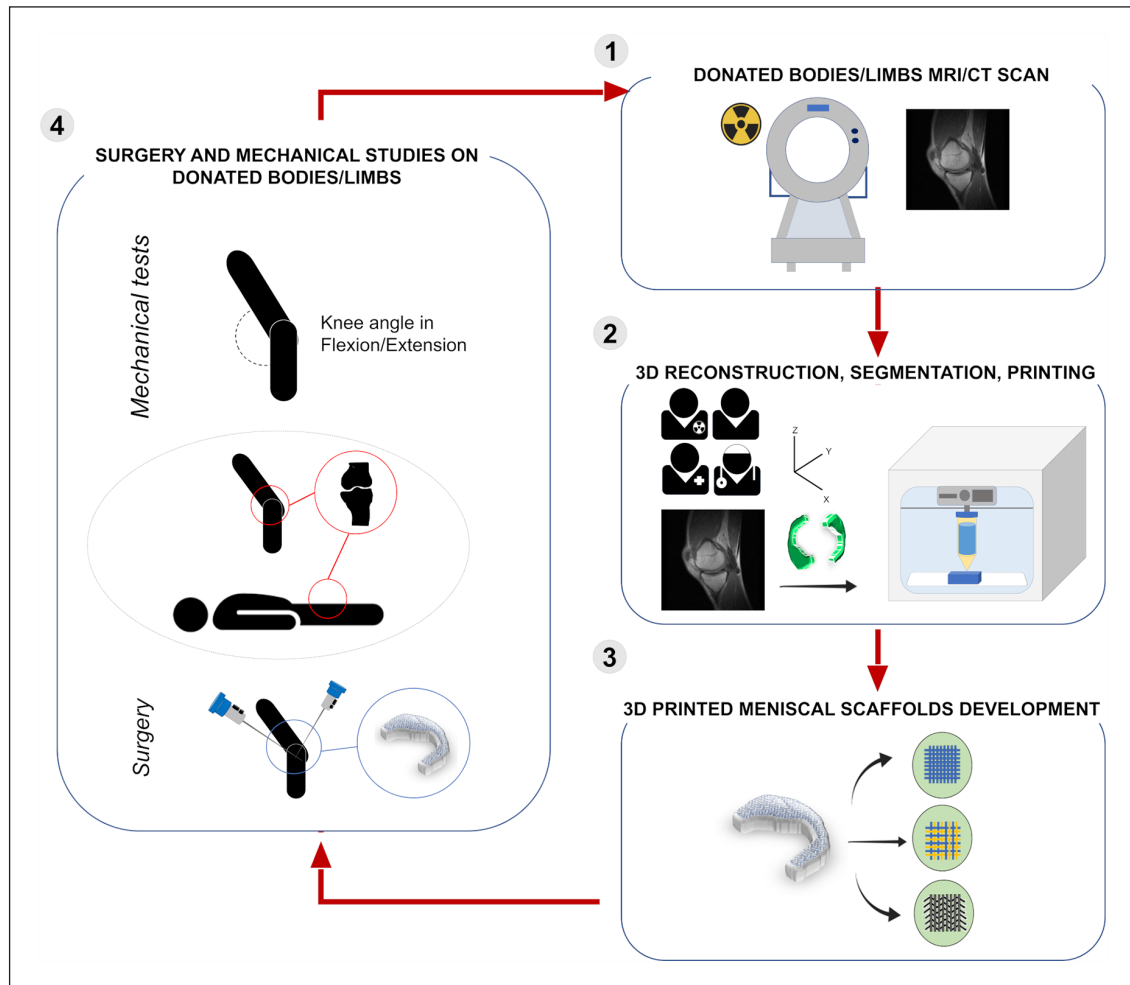


Figure 8. From donated bodies and limbs to effective 3D printed meniscal scaffolds development: a workflow proposal. After meniscal scaffolds development by 3D printing/bioprinting, based on MRI/CT scan images, the performances of the constructs may be evaluated by a cadaver-based approach. Donated bodies may represent a precious resource for reliable studies on meniscal substitutes manipulability, mechanics, and fitting, thus constituting an intermediate step toward their future use in clinical practice.

as intermediate between pre-clinical studies and clinical practice.

Conclusions and final considerations

The urgent need for effective meniscal scaffolds, overcoming the limitations of available devices or surgical strategies, has prompted intense research in TE. The development of different bioactive scaffolds has been reported in the literature, taking advantage from several different fabrication methods including lyophilization, solvent leaching, solvent casting and particulate leaching, lamination technique, electrospinning.³⁹ Repopulation of commercial collagen type I supports with MFCs²⁴⁸ and preparation of decellularized meniscal ECMs^{201,249} have also been considered. In this dynamic context, the field of 3D printing/bioprinting is gaining wide attention, highlighting the tremendous potential of these technologies. When applied in

medicine, 3D printing approaches can provide for complex and customized devices responding to both surgeon and patient requirements, solving the problems of traditional transplantation, assuring for production in high speed, and resolution with also cost and risk potential benefits for patients.²⁵⁰ However, despite the increased ability of TE to mimic the native environment, and the great potential of printing strategies, which type of scaffold is best suited for meniscus is still pending. Several challenges need to be still solved.

- (1) *Technique.* The development of printed constructs is affected by a plethora of technical factors. Among these, material viscosity, shear-thinning properties, identification of the most adequate cross-linking strategy, maintenance of 3D shape and cell viability after ink/bioink deposition, temperature, resolution in turn related to the diameter

of the needle, which might result in some restrictions on material viscosity and affect the shear-stress induced during the dispensing process.

- (2) *Scaffolds*. Currently, no biomaterial with adequate mechanical strength, outstanding biocompatibility and promoting the activity of cells after printing have been identified. As for bioinks, critical challenges include printability, adequate solidification to guarantee structural fidelity, mild curing process for cells protection, proper mechanical strength for stability in vivo. Several gelation attempts and hydrogels have been investigated for extrusion-based bioprinting, but none of those fully satisfies all above requirements.²⁵¹ Additionally, when selecting the printing material, a compromise is often required between one showing adequate features in supporting the specific cells phenotype and one with desired printing characteristics.¹¹²

To manage this issue, polymeric (mainly PCL) and biological materials (bioinks) have been combined thus developing augmented scaffolds with tunable (but still not clearly defined) characteristics.²⁵² PCL is an intriguing material for meniscal scaffolds fabrication by virtue of its degradation rate. In vivo it loses its molecular weight considerably slower than other aliphatic polyester²¹⁷; however, it has substantial hardness and insufficient flexibility.¹³⁵ As for dECMs as conditioning components, their potential is significant but decellularization process can significantly ruin/alter physical properties and bioactivity.

Considering scaffolds design/fabrication, complex circumferential ink/bioink deposition should be preferred to the most experienced layer-by-layer approach to mimic the arrangement of the collagen fibers in the native meniscus.¹³⁵ Commonly reported grid-based structures may fail in meeting the mechanical requirements of meniscus, especially once implanted in vivo. However, obtaining of an architecture reproducing the native collagen fibers orientation still represents a significant issue in meniscal scaffold fabrication justifying the not fully satisfactory results achieved so far and suggesting the need of intense efforts toward this direction.

Ideal devices are required to be endowed with adequate mechanics, bioactivity, and easy supply. To address this purpose, meniscus microstructure analysis is of great importance and a challenge too; the irregularity of the diameter and cross-linking pattern of the fibers in the ECM cause difficulties in the identification of a proper method for ultrastructural characterization. Moreover, few 3D printer and printing materials are adequate to satisfy the requirement for nano-scale printing accuracy. Spatial resolution is strongly influenced by the specific technology and the processed material. Insufficient resolution can dramatically affect both the quality and functionality of the scaffold.²⁰⁹

To counteract this issue, thus capturing the complexity of native tissues, a new hybrid technology combining cellular microtissues, biomaterials, and 3D printing is emerging. Spheroids are 3D spatial arrangements of cells that can be recognized as scaffold-free microtissues.²⁵³ Acting as tissues building blocks, they can be combined with a photo-crosslinkable hydrogel and subsequently bioprinted to obtain spheroids-based 3D bioprinted scaffolds. Supporting the creation of cell–cell contacts and cell–extracellular matrix (ECM) interactions these structures can mimic the natural environment. Despite, according to our knowledge, meniscus has never been specifically approached in this manner, experimental data reported for articular cartilage tissue engineering^{249,254–256} suggest that it may represent an extremely promising future perspective also in this field.

- (3) *Cells*. Considering cell sources, both MFCs and MSCs have been used for 3D printed scaffolds repopulation. MFC could be interesting for meniscal TE due to adequate fibrochondrogenic differentiation potential and their ability to form collagen fibers resembling in thickness and orientation that of native meniscus. Moreover, MFCs were associated to a less tendency to form bone precursors leading to calcifications than MSCs. However, isolation of an adequate amount of MFCs from surgically removed debris is a great issue. In vivo, MFCs reside in a dense ECM which is only about 0.1%–0.12% of the wet weight of normal meniscus. Additionally, also partial meniscectomy allows for limited cells isolation thus requiring in vitro monolayer cell expansion with the concrete risk of dedifferentiation and reduced ability in secreting typical proteins of the ECM along with passages in 2D culture. In particular, significant downregulation of mRNA expression levels of type II collagen and aggrecan, with an increased gene expression of type I collagen occur.²⁵⁷ To date there is no consensus on the ideal cell source for meniscus regeneration.²⁵⁸

Another significant consideration regards the complex environment in which the MFCs reside, mainly characterized by combined hypoxia and dynamic loading. Intriguingly, hypoxia (regardless of loading) promotes accumulation of hyaline cartilage while dynamic compression (regardless of oxygen tension) induces a matrix remodeling associated to *SOX9* and *COL1A1* upregulation.²⁴⁸ As these two conditions were demonstrated to exert a priming role on cells behavior it descends that they are essential features to bear in mind when validating the bioactivity of a new meniscal scaffold.

- (4) *Pre-clinical studies*. A further consideration regards in vivo studies on animal models of meniscal lesion. According to our knowledge, no study on 3D

printing/bioprinting considers inflammation which, conversely, could be a characterizing feature in patients undergoing meniscal repair surgery. Experimental evidence considering meniscal injury context supports a significant local increase in the inflammatory mediators TNF-alpha and IL-6 (as well as of IL-6 in the synovial membrane close to the injury) with a role in the initiation of articular cartilage degeneration.²⁵⁹ An inflamed status likely affects tissue regeneration and cells viability/responsiveness; in particular, stem-cells are susceptible to local stimuli and may be primed by the presence of a pathological/inflamed environment.

Preclinical studies allow to predict the biological behavior of the 3D printed scaffolds even more when cellular elements are included. Thus, resorting to them is important for the researcher to modulate, ameliorate, change, or confirm the adequacy of fabrication protocols leading to effective devices. However, from surgeon perspective, looking toward 3D printed scaffolds implant in patients, surgical training on human bodies could be particularly appealing also allowing for full integration with researcher activity and guaranteeing for excellence results in the field.

Acknowledgements

The authors would like to thank “Consortio per la Ricerca Sanitaria” (CORIS) of the Veneto Region, Italy (L.i.f.e.L.a.b. Program) for financial support (grant number DGR1017, July 17, 2018) and Department of Physics and Astronomy “G. Galilei”, University of Padova, Padova, Italy for technical support in meniscal imaging by Two-Photon Microscopy.

The authors express their deepest gratitude to the people who participate in the Body Donation Program “Donation to Science” of the University of Padova, thanks to whom this research was possible. We hope that the results of these efforts are useful to the entire scientific community, and hence honor the memory of those who donate their bodies.

Author contributions

All authors were involved in drafting the article or revising it critically for important intellectual content, and all authors approved the final version to be published. All authors read and approved the final manuscript.

Declaration of conflicting interests

The author(s) declared no potential conflicts of interest with respect to the research, authorship, and/or publication of this article.

Ethics statement

Human tissue samples here used were obtained from bodies joined to Body Donation Program “Donation to Science” of Padova University recognized as Veneto Region Reference Center for the preservation and use of gifted bodies (Deliberation of the Regional Council of the Veneto Region No. 245, Mar 8th,

2019; No. 389897), in accordance with the national laws, and the ethical standards of the regional/ national research committees, as well as with the 1964 Helsinki declaration and its later amendments or comparable ethical standards. Written informed consent was provided to join the Body Donation Program. As for the Magnetic Resonance Images, the patients’ informed consent was obtained too.

Funding

The author(s) disclosed receipt of the following financial support for the research, authorship, and/or publication of this article: This research was funded by the ‘Consortio per la Ricerca Sanitaria’ (CORIS) of the Veneto Region, Italy (L.i.f.e.L.a.b. Program), grant number DGR1017, July 17, 2018.

ORCID iDs

Andrea Porzionato  <https://orcid.org/0000-0003-3025-4717>

Enrico De Rose  <https://orcid.org/0000-0001-7647-1990>

References

1. Makris EA, Hadidi P and Athanasiou KA. The knee meniscus: structure-function, pathophysiology, current repair techniques, and prospects for regeneration. *Biomaterials* 2011; 32: 7411–7431.
2. Shriram D, Praveen Kumar G, Cui F, et al. Evaluating the effects of material properties of artificial meniscal implant in the human knee joint using finite element analysis. *Sci Rep* 2017; 7: 6011.
3. Rey-Rico A, Cucchiari M and Madry H. Hydrogels for precision meniscus tissue engineering: a comprehensive review. *Connect Tissue Res* 2017; 58: 317–328.
4. Cavanaugh JT. Rehabilitation of meniscal injury and surgery. *J Knee Surg* 2014; 27: 459–478.
5. Fox AJS, Wanivenhaus F, Burge AJ, et al. The human meniscus: a review of anatomy, function, injury, and advances in treatment. *Clin Anat* 2015; 28: 269–287.
6. Kennedy MI, Strauss M and LaPrade RF. Injury of the Meniscus root. *Clin Sports Med* 2020; 39: 57–68.
7. Katz JN, Brophy RH, Chaisson CE, et al. Surgery versus physical therapy for a meniscal tear and osteoarthritis. *New Engl J Med* 2013; 368: 1675–1684.
8. Kwon H, Brown WE, Lee CA, et al. Surgical and tissue engineering strategies for articular cartilage and meniscus repair. *Nat Rev Rheumatol* 2019; 15: 550–570.
9. Chen M, Gao S, Wang P, et al. The application of electrospinning used in meniscus tissue engineering. *J Biomater Sci Polym Ed* 2018; 29: 461–475.
10. Hutchinson ID, Moran CJ, Potter HG, et al. Restoration of the meniscus: form and function. *Am J Sports Med* 2014; 42: 987–998.
11. Winkler PW, Rothrauff BB, Buerba RA, et al. Meniscal substitution, a developing and long-awaited demand. *J Exp Orthop* 2020; 7: 55.
12. Zhou Z-X, Chen Y-R, Zhang J-Y, et al. Facile strategy on hydrophilic modification of poly(ϵ -caprolactone) scaffolds for assisting tissue-engineered meniscus constructs in vitro. *Front Pharmacol* 2020; 11: 471.
13. Buma P, Ramrattan NN, van Tienen TG, et al. Tissue engineering of the meniscus. *Biomaterials* 2004; 25: 1523–1532.

14. Pereira H, Frias AM, Oliveira JM, et al. Tissue engineering and regenerative medicine strategies in meniscus lesions. *Arthroscopy* 2011; 27: 1706–1719.
15. Zhang Y, Li P, Wang H, et al. Research progress on reconstruction of meniscus in tissue engineering. *J Sports Med Phys Fitness* 2017; 57: 595–603.
16. Twomey-Kozak J and Jayasuriya CT. Meniscus repair and regeneration: a systematic review from a basic and translational science perspective. *Clin Sports Med* 2020; 39: 125–163.
17. Diez-Escudero A, Harlin H, Isaksson P, et al. Porous polylactic acid scaffolds for bone regeneration: a study of additively manufactured triply periodic minimal surfaces and their osteogenic potential. *J Tissue Eng* 2020; 11: 2041731420956541.
18. Mei Q, Rao J, Bei HP, et al. 3D bioprinting photocrosslinkable hydrogels for bone and cartilage repair. *Int J Bioprinting* 2021; 7: 367.
19. Arguchinskaya NV, Beketov EE, Kisel AA, et al. The technique of thyroid cartilage scaffold support formation for extrusion-based bioprinting. *Int J Bioprinting* 2021; 7: 348.
20. Yi HG, Choi YJ, Jung JW, et al. Three-dimensional printing of a patient-specific engineered nasal cartilage for augmentative rhinoplasty. *J Tissue Eng* 2019; 10: 2041731418824797.
21. Han J, Kim DS, Jang H, et al. Bioprinting of three-dimensional dentin-pulp complex with local differentiation of human dental pulp stem cells. *J Tissue Eng* 2019; 10: 2041731419845849.
22. Jain S, Yassin MA, Fuoco T, et al. Engineering 3D degradable, pliable scaffolds toward adipose tissue regeneration; optimized printability, simulations and surface modification. *J Tissue Eng* 2020; 11: 2041731420954316.
23. Sällström N, Capel A, Lewis MP, et al. 3D-printable zwitterionic nano-composite hydrogel system for biomedical applications. *J Tissue Eng* 2020; 11: 2041731420967294.
24. Rongen JJ, van Tienen TG, van Bochove B, et al. Biomaterials in search of a meniscus substitute. *Biomaterials* 2014; 35: 3527–3540.
25. Zhang Z-Z, Jiang D, Ding J-X, et al. Role of scaffold mean pore size in meniscus regeneration. *Acta Biomater* 2016; 43: 314–326.
26. Bilgen B, Jayasuriya CT and Owens BD. Current concepts in meniscus tissue engineering and repair. *Adv Health Mater* 2018; 7: e1701407.
27. Bahcecioglu G, Bilgen B, Hasirci N, et al. Anatomical meniscus construct with zone specific biochemical composition and structural organization. *Biomaterials* 2019; 218: 119361.
28. Zhang X and Zhang Y. Tissue engineering applications of three-dimensional bioprinting. *Cell Biochem Biophys* 2015; 72: 777–782.
29. Markes AR, Hodax JD and Ma CB. Meniscus form and function. *Clin Sports Med* 2020; 39: 1–12.
30. Fox AJ, Bedi A and Rodeo SA. The basic science of human knee menisci: structure, composition, and function. *Sports Health* 2012; 4: 340–351.
31. Brindle T, Nyland J and Johnson DL. The meniscus: review of basic principles with application to surgery and rehabilitation. *J Athl Train* 2001; 36: 160–169.
32. Day B, Mackenzie WG, Shim SS, et al. The vascular and nerve supply of the human meniscus. *Arthroscopy* 1985; 1: 58–62.
33. Amoczky SP and Warren RF. Microvasculature of the human meniscus. *Am J Sports Med* 1982; 10: 90–95.
34. Danzig L, Resnick D, Gonsalves M, et al. Blood supply to the normal and abnormal menisci of the human knee. *Clin Orthop Relat Res* 1983; 172: 271–276.
35. Gray JC. Neural and vascular anatomy of the menisci of the human knee. *J Orthop Sports Phys Ther* 1999; 29: 23–30.
36. Zimny ML, Albright DJ and Dabezies E. Mechanoreceptors in the human medial meniscus. *Acta Anat* 1988; 133: 35–40.
37. Lin Y, Zhang K, Li Q, et al. Innervation of nociceptors in intact human menisci along the longitudinal axis: semi-quantitative histological evaluation and clinical implications. *BMC Musculoskelet Disord* 2019; 20: 338.
38. Ghodbane SA, Patel JM, Brzezinski A, et al. Biomechanical characterization of a novel collagen-hyaluronan infused 3D-printed polymeric device for partial meniscus replacement. *J Biomed Mater Res Part B Appl Biomater* 2019; 107: 2457–2465.
39. Guo W, Liu S, Zhu Y, et al. Advances and prospects in tissue-engineered meniscal scaffolds for meniscus regeneration. *Stem Cells Int* 2015; 2015: 517520.
40. López-Franco M and Gómez-Barrena E. Cellular and molecular meniscal changes in the degenerative knee: a review. *J Exp Orthop* 2018; 5(1): 11.
41. Verdonk PC, Forsyth RG, Wang J, et al. Characterisation of human knee meniscus cell phenotype. *Osteoarthritis Cartilage* 2005; 13: 548–560.
42. Declercq HA, Forsyth RG, Verbruggen A, et al. CD34 and SMA expression of superficial zone cells in the normal and pathological human meniscus. *J Orthop Res* 2012; 30: 800–808.
43. Kopher RA, Penchev VR, Islam MS, et al. Human embryonic stem cell-derived CD34+ cells function as MSC progenitor cells. *Bone* 2010; 47: 718–728.
44. Cai D, Marty-Roix R, Hsu HP, et al. Lapine and canine bone marrow stromal cells contain smooth muscle actin and contract a collagen-glycosaminoglycan matrix. *Tissue Eng* 2001; 7: 829–841.
45. Tan G-K and Cooper-White JJ. Interactions of meniscal cells with extracellular matrix molecules: towards the generation of tissue engineered menisci. *Cell Adh Migr* 2011; 5: 220–226.
46. Krupkova O, Smolders L, Wuertz-Kozak K, et al. The pathobiology of the meniscus: a comparison between the human and dog. *Front Vet Sci* 2018; 5: 73.
47. Masouros SD, McDermott ID, Amis AA, et al. Biomechanics of the meniscus-meniscal ligament construct of the knee. *Knee Surg Sports Traumatol Arthrosc* 2008; 16: 1121–1132.
48. McNulty AL and Guilak F. Mechanobiology of the meniscus. *J Biomech* 2015; 48: 1469–1478.
49. Flandry F and Hommel G. Normal anatomy and biomechanics of the knee. *Sports Med Arthrosc* 2011; 19: 82–92.
50. Chia HN and Hull ML. Compressive moduli of the human medial meniscus in the axial and radial directions at equilibrium and at a physiological strain rate. *J Orthop Res* 2008; 26: 951–956.

51. Donahue TLH, Hull ML, Rashid MM, et al. The sensitivity of tibiofemoral contact pressure to the size and shape of the lateral and medial menisci. *J Orthop Res* 2004; 22: 807–814.
52. Matar HE, Duckett SP and Raut V. Degenerative meniscal tears of the knee: evaluation and management. *Br J Hosp Med* 2019; 80: 46–50.
53. Paletta GAJ, Manning T, Snell E, et al. The effect of allograft meniscal replacement on intraarticular contact area and pressures in the human knee: a biomechanical study. *Am J Sports Med* 1997; 25: 692–698.
54. Seedhom BB and Hargreaves DJ. Transmission of the load in the knee joint with special reference to the role of the Menisci: Part II: Experimental results, discussion and conclusions. *Eng Med* 1979; 8: 220–228.
55. Kurosawa H, Fukubayashi T and Nakajima H. Load-bearing mode of the knee joint: physical behavior of the knee joint with or without menisci. *Clin Orthop Relat Res* 1980; 149: 283–290.
56. Wirth CJ. The meniscus — structure, morphology and function. *Knee* 1994; 1: 171–172.
57. Jerosch J and Prymka M. Proprioception and joint stability. *Knee Surg Sports Traumatol Arthrosc* 1996; 4: 171–179.
58. Malliou P, Gioftsidou A, Pafis G, et al. Proprioception and functional deficits of partial meniscectomized knees. *Eur J Phys Rehabil Med* 2012; 48: 231–236.
59. Marzo JM. Medial meniscus posterior horn avulsion. *J Am Acad Orthop Surg* 2009; 17: 276–283.
60. Cook AE, Cook JL and Stoker AM. Metabolic responses of Meniscus to IL-1 β . *J Knee Surg* 2018; 31: 834–840.
61. Belluzzi E, Stocco E, Pozzuoli A, et al. Contribution of infrapatellar fat Pad and synovial membrane to knee osteoarthritis pain. *Biomed Res Int* 2019; 2019: 6390182.
62. Macchi V, Stocco E, Stecco C, et al. The infrapatellar fat pad and the synovial membrane: an anatomic-functional unit. *J Anat* 2018; 233: 146–154.
63. Favero M, Belluzzi E, Trisolino G, et al. Inflammatory molecules produced by meniscus and synovium in early and end-stage osteoarthritis: a coculture study. *J Cell Physiol* 2019; 234: 11176–11187.
64. Tsujii A, Nakamura N and Horibe S. Age-related changes in the knee meniscus. *Knee* 2017; 24: 1262–1270.
65. Muncie JM and Weaver VM. The physical and biochemical properties of the extracellular matrix regulate cell fate. *Curr Top Dev Biol* 2018; 130: 1–37.
66. Battistelli M, Favero M, Burini D, et al. Morphological and ultrastructural analysis of normal, injured and osteoarthritic human knee menisci. *Eur J Histochem* 2019; 63: 2998.
67. Stocco E, Belluzzi E, Contran M, et al. Age-dependent remodeling in infrapatellar fat pad adipocytes and extracellular matrix: a comparative study. *Front Med* 2021; 8: 661403.
68. Stocco E, Barbon S, Piccione M, et al. Infrapatellar fat Pad stem cells responsiveness to microenvironment in osteoarthritis: from morphology to function. *Front Cell Dev Biol* 2019; 7: 323.
69. Stärke C, Kopf S, Petersen W, et al. Meniscal repair. *Arthroscopy* 2009; 25: 1033–1044.
70. Dangelmajer S, Familiari F, Simonetta R, et al. Meniscal transplants and scaffolds: a systematic review of the literature. *Knee Surg Relat Res* 2017; 29: 3–10.
71. Faucett SC, Geisler BP, Chahla J, et al. Meniscus root repair vs meniscectomy or nonoperative management to prevent knee osteoarthritis after medial meniscus root tears: clinical and economic effectiveness. *Am J Sports Med* 2019; 47: 762–769.
72. Yoon KH and Park KH. Meniscal repair. *Knee Surg Relat Res* 2014; 26: 68–76.
73. Beaufils P, Becker R, Kopf S, et al. Surgical management of degenerative meniscus lesions: the 2016 ESSKA meniscus consensus. *Knee Surg Sports Traumatol Arthrosc* 2017; 25: 335–346.
74. Pujol N and Beaufils P. Save the meniscus again! *Knee Surg Sports Traumatol Arthrosc* 2019; 27: 341–342.
75. Rocha de Faria JL, Pavão DM, Cruz RS, et al. Vertical continuous meniscal suture technique. *Arthrosc Tech* 2020; 9: e1335–e1340.
76. Rocha de Faria JL, Pavão DM, Villardi AM, et al. Continuous meniscal suture technique of the knee. *Arthrosc Tech* 2020; 9: e791–e796.
77. Chahla J, Serra Cruz R, Cram TR, et al. Inside-Out meniscal repair: medial and lateral approach. *Arthrosc Tech* 2016; 5: e163–e168.
78. Barbon S, Stocco E, Grandi F, et al. Biofabrication of a novel leukocyte-fibrin-platelet membrane as a cells and growth factors delivery platform for tissue engineering applications. *J Tissue Eng Regen Med* 2018; 12: 1891–1906.
79. Di Liddo R, Bertalot T, Borean A, et al. Leucocyte and platelet-rich fibrin: a carrier of autologous multipotent cells for regenerative medicine. *J Cell Mol Med* 2018; 22: 1840–1854.
80. DePhillipo NN, LaPrade RF, Zaffagnini S, et al. The future of meniscus science: international expert consensus. *J Exp Orthop* 2021; 8: 24.
81. Monibi FA, Bozynski CC, Kuroki K, et al. Development of a micronized meniscus extracellular matrix scaffold for potential augmentation of meniscal repair and regeneration. *Tissue Eng Part C Methods* 2016; 22: 1059–1070.
82. Trentacosta N, Graham WC and Gersoff WK. Meniscal allograft transplantation: state of the art. *Sports Med Arthrosc* 2016; 24: e23–e33.
83. Stevenson C, Mahmoud A, Tudor F, et al. Meniscal allograft transplantation: undersizing grafts can lead to increased rates of clinical and mechanical failure. *Knee Surg Sports Traumatol Arthrosc* 2019; 27: 1900–1907.
84. Southworth TM, Naveen NB, Tauro TM, et al. Meniscal allograft transplants. *Clin Sports Med* 2020; 39: 93–123.
85. Houck DA, Kraeutler MJ, Belk JW, et al. Similar clinical outcomes following collagen or polyurethane meniscal scaffold implantation: a systematic review. *Knee Surg Sports Traumatol Arthrosc* 2018; 26: 2259–2269.
86. Sun J, Vijayavenkataraman S and Liu H. An overview of scaffold design and fabrication technology for engineered knee meniscus. *Materials* 2017; 10: 29.
87. Hansen R, Choi G, Bryk E, et al. The human knee meniscus: a review with special focus on the collagen meniscal implant. *J Long Term Eff Med Implants* 2011; 21: 321–337.
88. Smith BD and Grande DA. The current state of scaffolds for musculoskeletal regenerative applications. *Nat Rev Rheumatol* 2015; 11: 213–222.

89. Schüttler KF, Pöttgen S, Getgood A, et al. Improvement in outcomes after implantation of a novel polyurethane meniscal scaffold for the treatment of medial meniscus deficiency. *Knee Surg Sports Traumatol Arthrosc* 2015; 23: 1929–1935.
90. Baynat C, Andro C, Vincent JP, et al. Actifit® synthetic meniscal substitute: experience with 18 patients in Brest, France. *Orthop Traumatol Surg Res* 2014; 100: S385–S389.
91. Shemesh M, Shefy-Peleg A, Levy A, et al. Effects of a novel medial meniscus implant on the knee compartments: imaging and biomechanical aspects. *Biomech Model Mechanobiol* 2020; 19: 2049–2059.
92. Leroy A, Beaufils P, Favre B, et al. Actifit® polyurethane meniscal scaffold: MRI and functional outcomes after a minimum follow-up of 5 years. *Orthop Traumatol Surg Res* 2017; 103: 609–614.
93. Barber FA. Editorial commentary: polyurethane meniscal scaffold: a perfect fit or flop? *Arthroscopy* 2018; 34: 1628–1630.
94. Accadbled F, Pham TT, Lemoine CT, et al. Implantation of an actifit® polyurethane meniscal scaffold 18 Months after subtotal lateral meniscectomy in a 13-year-old male adolescent. *Am J Case Rep* 2020; 21: e920688.
95. Messner K. Meniscal regeneration or meniscal transplantation? *Scand J Med Sci Sports* 1999; 9: 162–167.
96. Park J, Wetzel I, Dréau D, et al. 3D miniaturization of human organs for drug discovery. *Adv Healthc Mater* 2018; 7: 1700551. DOI: 10.1002/adhm.201700551
97. Luo Y, Wei X and Huang P. 3D bioprinting of hydrogel-based biomimetic microenvironments. *J Biomed Mater Res Part B Appl Biomater* 2019; 107: 1695–1705.
98. Murphy SV, Skardal A and Atala A. Evaluation of hydrogels for bio-printing applications. *J Biomed Mater Res A* 2013; 101: 272–284.
99. Hölzl K, Lin S, Tytgat L, et al. Bioink properties before, during and after 3D bioprinting. *Biofabrication* 2016; 8: 032002. DOI: 10.1088/1758-5090/8/3/032002
100. Marga F, Jakab K, Khatiwala C, et al. Toward engineering functional organ modules by additive manufacturing. *Biofabrication* 2012; 4: 022001.
101. Owens CM, Marga F, Forgacs G, et al. Biofabrication and testing of a fully cellular nerve graft. *Biofabrication* 2013; 5: 045007. DOI: 10.1088/1758-5082/5/4/045007
102. Petcu EB, Midha R, McColl E, et al. 3D printing strategies for peripheral nerve regeneration. *Biofabrication* 2018; 10: 032001.
103. Sarker M, Naghieh S, McInnes AD, et al. Strategic design and fabrication of nerve guidance conduits for peripheral nerve regeneration. *Biotechnol J* 2018; 13: e1700635.
104. Mironov V, Trusk T, Kasyanov V, et al. Biofabrication: a 21st century manufacturing paradigm. *Biofabrication* 2009; 1: 022001.
105. Yurie H, Ikeguchi R, Aoyama T, et al. The efficacy of a scaffold-free bio 3D conduit developed from human fibroblasts on peripheral nerve regeneration in a rat sciatic nerve model. *PLoS One* 2017; 12: e0171448.
106. Ong CS, Yesantharao P, Huang CY, et al. 3D bioprinting using stem cells. *Pediatr Res* 2018; 83: 223–231.
107. Chartrain NA, Williams CB and Whittington AR. A review on fabricating tissue scaffolds using vat photopolymerization. *Acta Biomater* 2018; 74: 90–111.
108. Sekar MP, Budharaju H, Zennifer A, et al. Current standards and ethical landscape of engineered tissues-3D bioprinting perspective. *J Tissue Eng* 2021; 12: 20417314211027677.
109. Ng WL, Lee JM, Zhou M, et al. Vat polymerization-based bioprinting: process, materials, applications and regulatory challenges. *Biofabrication* 2020; 12: 022001.
110. Dou C, Perez V, Qu J, et al. A state-of-the-art review of laser-assisted bioprinting and its future research trends. *ChemBioEng Rev* 2021; 8: 517–534.
111. Gudapati H, Dey M and Ozbolat I. A comprehensive review on droplet-based bioprinting: past, present and future. *Biomaterials* 2016; 102: 20–42.
112. Fonseca AC, Melchels FPW, Ferreira MJS, et al. Emulating human tissues and organs: a bioprinting perspective toward personalized medicine. *Chem Rev* 2020; 120: 11128–11174.
113. Derby B. Bioprinting: Inkjet printing proteins and hybrid cell-containing materials and structures. *J Mater Chem* 2008; 18: 5717–5721.
114. Wijshoff H. The dynamics of the piezo inkjet printhead operation☆. *Phys Rep* 2010; 491: 77–177.
115. Nishiyama Y, Nakamura M, Henmi C, et al. Development of a three-dimensional bioprinter: construction of cell supporting structures using hydrogel and state-of-the-art inkjet technology. *J Biomech Eng* 2009; 131: 035001.
116. Chang R, Nam J and Sun W. Effects of dispensing pressure and nozzle diameter on cell survival from solid free-form fabrication-based direct cell writing. *Tissue Eng Part A* 2008; 14: 41–48.
117. Ozbolat IT and Hospodiuk M. Current advances and future perspectives in extrusion-based bioprinting. *Biomaterials* 2016; 76: 321–343.
118. Soman P, Chung PH, Zhang AP, et al. Digital microfabrication of user-defined 3D microstructures in cell-laden hydrogels. *Biotechnol Bioeng* 2013; 110: 3038–3047.
119. Li W, Mille LS, Robledo JA, et al. Recent advances in formulating and processing biomaterial inks for vat polymerization-based 3D printing. *Adv Healthc Mater* 2020; 9: 2000156.
120. Han X, Chang S, Zhang M, et al. Advances of hydrogel-based bioprinting for cartilage tissue engineering. *Front Bioeng Biotechnol* 2021; 9: 746564.
121. Naghieh S, Lindberg G, Tamaddon M, et al. Biofabrication strategies for musculoskeletal disorders: evolution towards clinical applications. *Bioengineering* 2021; 8: 123.
122. Saska S, Pilatti L, Blay A, et al. Bioresorbable polymers: advanced materials and 4D printing for tissue engineering. *Polymers* 2021; 13: 563.
123. Schwab A, Levato R, D'Este M, et al. Printability and shape fidelity of bioinks in 3D bioprinting. *Chem Rev* 2020; 120: 11028–11055.
124. Gungor-Ozkerim PS, Inci I, Zhang YS, et al. Bioinks for 3D bioprinting: an overview. *Biomater Sci* 2018; 6: 915–946.
125. Gillispie G, Prim P, Copus J, et al. Assessment methodologies for extrusion-based bioink printability. *Biofabrication* 2020; 12: 022003.
126. Lee SC, Gillispie G, Prim P, et al. Physical and chemical factors influencing the printability of hydrogel-based extrusion bioinks. *Chem Rev* 2020; 120: 10834–10886.
127. Veiga A, Silva IV, Duarte MM, et al. Current trends on protein driven bioinks for 3D printing. *Pharmaceutics* 2021; 13: 1444.

128. Hospodiuk M, Dey M, Sosnoski D, et al. The bioink: a comprehensive review on bioprintable materials. *Biotechnol Adv* 2017; 35: 217–239.
129. Daly AC, Critchley SE, Rencsok EM, et al. A comparison of different bioinks for 3D bioprinting of fibrocartilage and hyaline cartilage. *Biofabrication* 2016; 8: 045002.
130. Narayanan LK, Thompson TL, Shirwaiker RA, et al. Label free process monitoring of 3D bioprinted engineered constructs via dielectric impedance spectroscopy. *Biofabrication* 2018; 10: 035012.
131. Rhee S, Puetzer JL, Mason BN, et al. 3D bioprinting of spatially heterogeneous collagen constructs for cartilage tissue engineering. *ACS Biomater Sci Eng* 2016; 2: 1800–1805.
132. Chae S, Lee S-S, Choi Y-J, et al. 3D cell-printing of bio-compatible and functional meniscus constructs using meniscus-derived bioink. *Biomaterials* 2021; 267: 120466.
133. Narayanan LK, Huebner P, Fisher MB, et al. 3D-Bioprinting of Polylactic acid (PLA) nanofiber–alginate hydrogel bioink containing human adipose-derived stem cells. *ACS Biomater Sci Eng* 2016; 2: 1732–1742.
134. Filardo G, Petretta M, Cavallo C, et al. Patient-specific meniscus prototype based on 3D bioprinting of human cell-laden scaffold. *Bone Jt Res* 2019; 8: 101–106.
135. Jian Z, Zhuang T, Qinyu T, et al. 3D bioprinting of a biomimetic meniscal scaffold for application in tissue engineering. *Bioact Mater* 2021; 6: 1711–1726.
136. Sun Y, You Y, Jiang W, et al. Generating ready-to-implant anisotropic menisci by 3D-bioprinting protein-releasing cell-laden hydrogel-polymer composite scaffold. *Appl Mater Today* 2020; 18: 100469.
137. Romanazzo S, Vedicherla S, Moran C, et al. Meniscus ECM-functionalised hydrogels containing infrapatellar fat pad-derived stem cells for bioprinting of regionally defined meniscal tissue. *J Tissue Eng Regen Med* 2018; 12: e1826–e1835.
138. Markstedt K, Mantas A, Tournier I, et al. 3D bioprinting human chondrocytes with nanocellulose-alginate bioink for cartilage tissue engineering applications. *Biomacromolecules* 2015; 16: 1489–1496.
139. Costa JB, Park J, Jorgensen AM, et al. 3D bioprinted highly elastic hybrid constructs for advanced fibrocartilaginous tissue regeneration. *Chem Mater* 2020; 32: 8733–8746.
140. Li Z, Wu N, Cheng J, et al. Biomechanically, structurally and functionally meticulously tailored polycaprolactone/silk fibroin scaffold for meniscus regeneration. *Theranostics* 2020; 10: 5090–5106.
141. Bahcecioglu G, Hasirci N, Bilgen B, et al. A 3D printed PCL/hydrogel construct with zone-specific biochemical composition mimicking that of the meniscus. *Biofabrication* 2019; 11: 025002.
142. Cengiz IF, Maia FR, da Silva Morais A, et al. Entrapped in cage (EiC) scaffolds of 3D-printed polycaprolactone and porous silk fibroin for meniscus tissue engineering. *Biofabrication* 2020; 12: 025028.
143. Huebner P, Warren PB, Chester D, et al. Mechanical properties of tissue formed in vivo are affected by 3D-bioplotting scaffold microarchitecture and correlate with ECM collagen fiber alignment. *Connect Tissue Res* 2020; 61: 190–204.
144. Bahcecioglu G, Hasirci N, Bilgen B, et al. Hydrogels of agarose, and methacrylated gelatin and hyaluronic acid are more supportive for in vitro meniscus regeneration than three dimensional printed polycaprolactone scaffolds. *Int J Biol Macromol* 2019; 122: 1152–1162.
145. Nakagawa Y, Fortier LA, Mao JJ, et al. Long-term evaluation of meniscal tissue formation in 3-dimensional-printed scaffolds with sequential release of connective tissue growth factor and TGF- β 3 in an Ovine model. *Am J Sports Med* 2019; 47: 2596–2607.
146. Cengiz IF, Pereira H, Espregueira-Mendes J, et al. Sutureable regenerated silk fibroin scaffold reinforced with 3D-printed polycaprolactone mesh: biomechanical performance and subcutaneous implantation. *J Mater Sci Mater Med* 2019; 30: 63.
147. Chen M, Feng Z, Guo W, et al. PCL-MECM-Based hydrogel hybrid scaffolds and Meniscal fibrochondrocytes promote whole Meniscus regeneration in a rabbit meniscectomy model. *ACS Appl Mater Interfaces* 2019; 11: 41626–41639.
148. Warren PB, Huebner P, Spang JT, et al. Engineering 3D-bioplotting scaffolds to induce aligned extracellular matrix deposition for musculoskeletal soft tissue replacement. *Connect Tissue Res* 2017; 58: 342–354.
149. Lee CH, Rodeo SA, Fortier LA, et al. Protein-releasing polymeric scaffolds induce fibrochondrocytic differentiation of endogenous cells for knee meniscus regeneration in sheep. *Sci Transl Med* 2014; 6: 266ra171.
150. Abar B, Alonso-Calleja A, Kelly A, et al. 3D printing of high-strength, porous, elastomeric structures to promote tissue integration of implants. *J Biomed Mater Res A* 2021; 109: 54–63.
151. Luis E, Pan HM, Sing SL, et al. 3D direct printing of silicone meniscus implant using a novel heat-cured extrusion-based printer. *Polymers* 2020; 12: 1031. DOI: 10.3390/polym12051031
152. Luis E, Pan HM, Bastola AK, et al. 3D printed silicone meniscus implants: influence of the 3D printing process on properties of silicone implants. *Polymers* 2020; 12: 2136. DOI: 10.3390/polym12092136
153. Ghodbane SA, Murthy NS, Dunn MG, et al. Achieving molecular orientation in thermally extruded 3D printed objects. *Biofabrication* 2019; 11: 045004.
154. Ghodbane SA, Brzezinski A, Patel JM, et al. Partial meniscus replacement with a collagen-hyaluronan infused three-dimensional printed polymeric scaffold. *Tissue Eng Part A* 2019; 25: 379–389.
155. Moroni L, Lambers FM, Wilson W, et al. Finite element analysis of meniscal anatomical 3D scaffolds: implications for tissue engineering. *Open Biomed Eng J* 2007; 1: 23–34.
156. Gupta S, Sharma A, Vasantha Kumar J, et al. Meniscal tissue engineering via 3D printed PLA monolith with carbohydrate based self-healing interpenetrating network hydrogel. *Int J Biol Macromol* 2020; 162: 1358–1371.
157. Bandyopadhyay A and Mandal BB. A three-dimensional printed silk-based biomimetic tri-layered meniscus for potential patient-specific implantation. *Biofabrication* 2019; 12: 015003.
158. Siddiqui N, Asawa S, Birru B, et al. PCL-Based composite scaffold matrices for tissue engineering applications. *Mol Biotechnol* 2018; 60: 506–532.

159. Middleton JC and Tipton AJ. Synthetic biodegradable polymers as orthopedic devices. *Biomaterials* 2000; 21: 2335–2346.
160. Doppalapudi S, Jain A, Khan W, et al. Biodegradable polymers—an overview. *Polym Adv Technol* 2014; 25: 427–435.
161. Malikmammadov E, Tanir TE, Kiziltay A, et al. PCL and PCL-based materials in biomedical applications. *J Biomater Sci Polym Ed* 2018; 29: 863–893.
162. Ahn JH, Kim J, Han G, et al. 3D-printed biodegradable composite scaffolds with significantly enhanced mechanical properties via the combination of binder jetting and capillary rise infiltration process. *Addit Manuf* 2021; 41: 101988.
163. Marzec M, Kucińska-Lipka J, Kalaszczyńska I, et al. Development of polyurethanes for bone repair. *Mater Sci Eng C* 2017; 80: 736–747.
164. Kim SY, Han G, Hwang DB, et al. Design and usability evaluations of a 3D-printed implantable drug delivery device for acute liver failure in preclinical settings. *Adv Healthc Mater* 2021; 10: e2100497.
165. Inyang AO and Vaughan CL. Functional characteristics and mechanical performance of PCU composites for knee meniscus replacement. *Materials* 2020; 13: 1886. DOI: 10.3390/ma13081886
166. Griffin M, Castro N, Bas O, et al. The current versatility of polyurethane three-dimensional printing for biomedical applications. *Tissue Eng Part B Rev* 2020; 26: 272–283.
167. Zhu LY, Li L, Li ZA, et al. Design and biomechanical characteristics of porous meniscal implant structures using triply periodic minimal surfaces. *J Transl Med* 2019; 17: 89.
168. Zhu LY, Cheng M, Sun WC, et al. Influence of deformed primitive architecture on mechanical behavior of artificial porous meniscus. *Mater Des* 2020; 186: 108303.
169. Jain JP, Yenet Ayen W, Domb AJ, et al. Biodegradable polymers in drug delivery. In: Domb AJ and Kumar N (eds) *Biodegradable polymers in clinical use and clinical development*. New York: John Wiley & Sons, Inc., 2011: pp.1–58.
170. Gunatillake P, Mayadunne R and Adhikari R. Recent developments in biodegradable synthetic polymers. *Biotechnol Annu Rev* 2006; 12: 301–347.
171. Ashton JH, Mertz JA, Harper JL, et al. Polymeric endoaortic paving: mechanical, thermoforming, and degradation properties of polycaprolactone/polyurethane blends for cardiovascular applications. *Acta Biomater* 2011; 7: 287–294.
172. Wang A, Gan Y, Yu H, et al. Improvement of the cytocompatibility of electrospun poly[(R)-3-hydroxybutyrate-co-(R)-3-hydroxyvalerate] mats by Ecoflex. *J Biomed Mater Res A* 2012; 100: 1505–1511.
173. Luis E, Pan HM, Sing SL, et al. Silicone 3D printing: process optimization, product biocompatibility, and reliability of silicone meniscus implants. *3D Print Addit Manuf* 2019; 6: 319–332.
174. Bourke SL and Kohn J. Polymers derived from the amino acid L-tyrosine: polycarbonates, polyarylates and copolymers with poly(ethylene glycol). *Adv Drug Deliv Rev* 2003; 55: 447–466.
175. Tovar N, Bourke S, Jaffe M, et al. A comparison of degradable synthetic polymer fibers for anterior cruciate ligament reconstruction. *J Biomed Mater Res A* 2010; 93: 738–747.
176. Vanzanella V, Scatto M, Zant E, et al. The rheology of PEOT/PBT block copolymers in the melt state and in the thermally-induced Sol/Gel transition. Implications on the 3D-printing bio-scaffold process. *Materials* 2019; 12: 226. DOI: 10.3390/ma12020226
177. Klepić M, Fuoco A, Monteleone M, et al. Tailoring the thermal and mechanical properties of PolyActive(TM) poly(ether-ester) multiblock copolymers via blending with co(2)-phylic ionic liquid. *Polymers* 2020; 12: 890. DOI: 10.3390/polym12040890
178. Deschamps AA, Claase MB, Sleijster WJ, et al. Design of segmented poly(ether ester) materials and structures for the tissue engineering of bone. *J Control Release* 2002; 78: 175–186.
179. Deschamps AA, van Apeldoorn AA, Hayen H, et al. In vivo and in vitro degradation of poly(ether ester) block copolymers based on poly(ethylene glycol) and poly(butylene terephthalate). *Biomaterials* 2004; 25: 247–258.
180. Qi L, Zhu Q, Cao D, et al. Preparation and properties of Stereocomplex of poly(lactic acid) and its Amphiphilic copolymers containing glucose groups. *Polymers* 2020; 12: 760. DOI: 10.3390/polym12040760
181. Pan P, Zhu B, Kai W, et al. Polymorphic transition in disordered poly(l-lactide) crystals induced by annealing at elevated temperatures. *Macromolecules* 2008; 41: 4296–4304.
182. Auras R, Harte B and Selke S. An overview of polylactides as packaging materials. *Macromol Biosci* 2004; 4: 835–864.
183. Farah S, Anderson DG and Langer R. Physical and mechanical properties of PLA, and their functions in widespread applications: a comprehensive review. *Adv Drug Deliv Rev* 2016; 107: 367–392.
184. Aliotta L, Cinelli P, Coltelli MB, et al. Effect of nucleating agents on crystallinity and properties of poly (lactic acid) (PLA). *Eur Polym J* 2017; 93: 822–832.
185. Tokiwa Y and Calabia BP. Biodegradability and biodegradation of poly(lactide). *Appl Microbiol Biotechnol* 2006; 72(2): 244–251.
186. Darabian B, Bagheri H and Mohammadi S. Improvement in mechanical properties and biodegradability of PLA using poly(ethylene glycol) and triacetin for antibacterial wound dressing applications. *Prog Biomater* 2020; 9: 45–64.
187. Chen CC, Chueh JY, Tseng H, et al. Preparation and characterization of biodegradable PLA polymeric blends. *Biomaterials* 2003; 24: 1167–1173.
188. Lee J, Lee H, Cheon KH, et al. Fabrication of poly(lactic acid)/ti composite scaffolds with enhanced mechanical properties and biocompatibility via fused filament fabrication (fff)-based 3D printing. *Addit Manuf* 2019; 30: 100873.
189. Barczyk M, Carracedo S and Gullberg D. Integrins. *Cell Tissue Res* 2010; 339: 269–280.
190. Stepanovska J, Supova M, Hanzalek K, et al. Collagen bioinks for bioprinting: a systematic review of hydrogel properties, bioprinting parameters, protocols, and bioprinted structure characteristics. *Biomedicines* 2021; 9: 1137.

191. Gaudet ID and Shreiber DI. Characterization of methacrylated Type-I collagen as a dynamic, photoactive hydrogel. *Biointerphases* 2012; 7: 25.
192. Tetsuka H and Shin SR. Materials and technical innovations in 3D printing in biomedical applications. *J Mater Chem B* 2020; 8: 2930–2950.
193. Oliveira I, Carvalho AL, Radhouani H, et al. Promising biomolecules. *Adv Exp Med Biol* 2018; 1059: 189–205.
194. Farokhi M, Mottaghtalab F, Fatahi Y, et al. Overview of silk fibroin use in wound dressings. *Trends Biotechnol* 2018; 36: 907–922.
195. Yao D, Liu H and Fan Y. Silk scaffolds for musculoskeletal tissue engineering. *Exp Biol Med* 2016; 241: 238–245.
196. Jang TS, Jung HD, Pan HM, et al. 3D printing of hydrogel composite systems: recent advances in technology for tissue engineering. *Int J Bioprinting* 2018; 4: 126.
197. Chen S, Jang TS, Pan HM, et al. 3D freeform printing of nanocomposite hydrogels through in situ precipitation in reactive viscous fluid. *Int J Bioprinting* 2020; 6: 258.
198. Zhao F, He W, Yan Y, et al. The application of Polysaccharide biocomposites to repair cartilage defects. *Int J Polym Sci* 2014; 2014: 1–9. DOI: 10.1155/2014/654597
199. Collins MN and Birkinshaw C. Hyaluronic acid based scaffolds for tissue Engineering: a review. *Carbohydr Polym* 2013; 92: 1262–1279.
200. Petta D, D'Amora U, Ambrosio L, et al. Hyaluronic acid as a bioink for extrusion-based 3D printing. *Biofabrication* 2020; 12: 032001.
201. Porzionato A, Stocco E, Barbon S, et al. Tissue-Engineered grafts from human decellularized extracellular matrices: a systematic review and future perspectives. *Int J Mol Sci* 2018; 19: 4117. DOI: 10.3390/ijms19124117
202. Jeong W, Kim MK and Kang HW. Effect of detergent type on the performance of liver decellularized extracellular matrix-based bio-inks. *J Tissue Eng* 2021; 12: 2041731421997091.
203. Giobbe GG, Crowley C, Luni C, et al. Extracellular matrix hydrogel derived from decellularized tissues enables endodermal organoid culture. *Nat Commun* 2019; 10: 5658.
204. Stocco E, Barbon S, Dalzoppo D, et al. Tailored PVA/ECM scaffolds for cartilage regeneration. *Biomed Res Int* 2014; 2014: 762189. DOI: 10.1155/2014/762189
205. Grandi F, Stocco E, Barbon S, et al. Composite scaffolds based on intestinal extracellular matrices and oxidized polyvinyl alcohol: a preliminary study for a new regenerative approach in short bowel syndrome. *Biomed Res Int* 2018; 2018: 7824757. DOI: 10.1155/2018/7824757
206. Saldin LT, Cramer MC, Velankar SS, et al. Extracellular matrix hydrogels from decellularized tissues: structure and function. *Acta Biomater* 2017; 49: 1–15.
207. Rothrauff BB, Shimomura K, Gottardi R, et al. Anatomical region-dependent enhancement of 3-dimensional chondrogenic differentiation of human mesenchymal stem cells by soluble meniscus extracellular matrix. *Acta Biomater* 2017; 49: 140–151.
208. Placone JK, Mahadik B and Fisher JP. Addressing present pitfalls in 3D printing for tissue engineering to enhance future potential. *APL Bioeng* 2020; 4: 010901.
209. Zhu S, Tong G, Xiang JP, et al. Microstructure analysis and reconstruction of a meniscus. *Orthop Surg* 2021; 13: 306–313.
210. Engler AJ, Sen S, Sweeney HL, et al. Matrix elasticity directs stem cell lineage specification. *Cell* 2006; 126: 677–689.
211. Tse JR and Engler AJ. Stiffness gradients mimicking in vivo tissue variation regulate mesenchymal stem cell fate. *PLoS One* 2011; 6: e15978.
212. Zhao Y, Tan K, Zhou Y, et al. A combinatorial variation in surface chemistry and pore size of three-dimensional porous poly(ϵ -caprolactone) scaffolds modulates the behaviors of mesenchymal stem cells. *Mater Sci Eng C* 2016; 59: 193–202.
213. Mikos AG and Temenoff JS. Formation of highly porous biodegradable scaffolds for tissue engineering. *Electron J Biotechnol* 2000; 3: 23–24.
214. Klompmaker J, Jansen HWB, Veth RH, et al. Porous implants for knee joint meniscus reconstruction: a preliminary study on the role of pore sizes in ingrowth and differentiation of fibrocartilage. *Clin Mater* 1993; 14: 1–11.
215. Buj-Corral I, Bagheri A and Petit-Rojo O. 3D printing of porous scaffolds with controlled porosity and pore size values. *Materials* 2018; 11: 1532. DOI: 10.3390/ma11091532
216. Kapfer SC, Hyde ST, Mecke K, et al. Minimal surface scaffold designs for tissue engineering. *Biomaterials* 2011; 32: 6875–6882.
217. Zhang Z-Z, Jiang D, Wang S-J, et al. Scaffolds drive meniscus tissue engineering. *RSC Adv* 2015; 5: 77851–77859.
218. Guo H, Lv R and Bai S. Recent advances on 3D printing graphene-based composites. *Nano Mater Sci* 2019; 1: 101–115.
219. Teoh JH, Thamizchelvan AM, Davoodi P, et al. Investigation of the application of a Taylor-Couette bioreactor in the post-processing of bioprinted human dermal tissue. *Biochem Eng J* 2019; 151: 107317.
220. Niu W, Guo W, Han S, et al. Cell-Based strategies for Meniscus tissue engineering. *Stem Cells Int* 2016; 2016: 4717184.
221. McCormack A, Highley CB, Leslie NR, et al. 3D printing in suspension baths: keeping the promises of bioprinting afloat. *Trends Biotechnol* 2020; 38: 584–593.
222. Mandrycky C, Wang Z, Kim K, et al. 3D bioprinting for engineering complex tissues. *Biotechnol Adv* 2016; 34: 422–434.
223. Malda J, Visser J, Melchels FP, et al. 25th anniversary article: engineering hydrogels for biofabrication. *Adv Mater Weinheim* 2013; 25: 5011–5028.
224. Yang R, Fan C, Dou Y, et al. 3D printing stiff antibacterial hydrogels for meniscus replacement. *Appl Mater Today* 2021; 24: 101.
225. Nam SY and Park S-H. ECM based Bioink for tissue mimetic 3D bioprinting. *Adv Exp Med Biol* 2018; 1064: 335–353.
226. Xu C, Dai G and Hong Y. Recent advances in high-strength and elastic hydrogels for 3D printing in biomedical applications. *Acta Biomater* 2019; 95: 50–59.

227. Kang S-W, Kim J-S, Park K-S, et al. Surface modification with fibrin/hyaluronic acid hydrogel on solid-free form-based scaffolds followed by BMP-2 loading to enhance bone regeneration. *Bone* 2011; 48: 298–306.
228. Gu Z, Fu J, Lin H, et al. Development of 3D bioprinting: from printing methods to biomedical applications. *Asian J Pharm Sci* 2020; 15: 529–557.
229. Di Matteo B, Perdisa F, Gostynska N, et al. Meniscal scaffolds—preclinical evidence to support their use: a systematic review. *Open Orthop J* 2015; 9: 143–156.
230. Pillai MM, Gopinathan J, Selvakumar R, et al. Human knee meniscus regeneration strategies: a review on recent advances. *Curr Osteoporos Rep* 2018; 16: 224–235.
231. Lehoczy G, Wolf F, Mumme M, et al. Intra-individual comparison of human nasal chondrocytes and debrided knee chondrocytes: relevance for engineering autologous cartilage grafts. *Clin Hemorheol Microcirc* 2020; 74: 67–78.
232. Stocco E, Barbon S, Radossi P, et al. Autologous chondrocytes as a novel source for neo-chondrogenesis in haemophilias. *Cell Tissue Res* 2016; 366: 51–61.
233. Migliorini F, Berton A, Salvatore G, et al. Autologous chondrocyte implantation and mesenchymal stem cells for the treatments of chondral defects of the knee- a systematic review. *Curr Stem Cell Res Ther* 2020; 15: 547–556.
234. Collins NJ, Prinsen CA, Christensen R, et al. Knee injury and osteoarthritis outcome score (KOOS): systematic review and meta-analysis of measurement properties. *Osteoarthr Cartil* 2016; 24: 1317–1329.
235. Rocha FAC, Girão VCC, Nunes RM, et al. Cell sources of inflammatory mediators present in bone marrow areas inside the meniscus. *PLoS One* 2019; 14: e0226986.
236. Bouffé C, Bony C, Courties G, et al. IL-6-dependent PGE2 secretion by mesenchymal stem cells inhibits local inflammation in experimental arthritis. *PLoS One* 2010; 5: e14247.
237. Sun W, Starly B, Darling A, et al. Computer-aided tissue engineering: application to biomimetic modelling and design of tissue scaffolds. *Biotechnol Appl Biochem* 2004; 39: 49–58.
238. Snyder J, Rin Son A, Hamid Q, et al. Mesenchymal stem cell printing and process regulated cell properties. *Biofabrication* 2015; 7(4): 044106.
239. Doral MN, Bilge O, Huri G, et al. Modern treatment of meniscal tears. *EFORT Open Rev* 2018; 3: 260–268.
240. Macchi V, Porzionato A, Stecco C, et al. Body parts removed during surgery: a useful training source. *Anat Sci Educ* 2011; 4: 151–156.
241. Porzionato A, Macchi V, Stecco C, et al. Quality management of body donation program at the University of Padova. *Anat Sci Educ* 2012; 5: 264–272.
242. Dell'Amore A, Boscolo-Berto R, Schiavon M, et al. Human corpse model for video-assisted thoracoscopic lobectomy simulation and training. *Interact Cardiovasc Thorac Surg* 2020; 31: 632–637.
243. Iwanaga J, Ishak B, Saga T, et al. The Lumbar ligamentum flavum does not have two layers and is confluent with the interspinous ligament: anatomical study with application to surgical and interventional pain procedures. *Clin Anat* 2020; 33: 34–40.
244. Polese L, Lezoche E, Porzionato A, et al. Transanal ileo-proctostomy is feasible in human cadavers. *Colorectal Dis* 2014; 16: O367–O369.
245. Dal Moro F, Macchi V, Porzionato A, et al. RUG technique: replacement of the ureter with gonadal vein: a cadaveric study. *Minerva Urol Nefrol* 2019; 71: 85–91.
246. Porzionato A, Polese L, Lezoche E, et al. On the suitability of thiel cadavers for natural orifice transluminal endoscopic surgery (NOTES): surgical training, feasibility studies, and anatomical education. *Surg Endosc* 2015; 29: 737–746.
247. Polese L, Rizzato R, Porzionato A, et al. An evaluation of trans-anal rectoscopic-assisted minimally invasive surgery (ARAMIS): a new platform for transanal surgery. *Int J Colorectal Dis* 2020; 35: 1681–1687.
248. Szojka ARA, Li DX, Sopcak MEJ, et al. Mechano-hypoxia conditioning of engineered human meniscus. *Front Bioeng Biotechnol* 2021; 9: 739438.
249. Li H, Li P, Yang Z, et al. Meniscal regenerative scaffolds based on biopolymers and polymers: recent status and applications. *Front Cell Dev Biol* 2021; 9: 661802.
250. Zhang L, Yang G, Johnson BN, et al. Three-dimensional (3D) printed scaffold and material selection for bone repair. *Acta Biomater* 2019; 84: 16–33.
251. Zhou Y, Liao S, Chu Y, et al. An injectable bioink with rapid prototyping in the air and in situ mild polymerization for 3D bioprinting. *Biofabrication* 2021; 13: 045026.
252. Shen S, Chen M, Guo W, et al. Three dimensional printing-based strategies for functional cartilage regeneration. *Tissue Eng Part B Rev* 2019; 25: 187–201.
253. Dalton PD, Woodfield TBF, Mironov V, et al. Advances in hybrid fabrication toward hierarchical tissue constructs. *Adv Sci* 2020; 7: 1902953.
254. Yu Y, Moncal KK, Li J, et al. Three-dimensional bioprinting using self-assembling scalable scaffold-free “tissue strands” as a new bioink. *Sci Rep* 2016; 6: 28714.
255. Daly AC and Kelly DJ. Biofabrication of spatially organised tissues by directing the growth of cellular spheroids within 3D printed polymeric microchambers. *Biomaterials* 2019; 197: 194–206.
256. De Moor L, Fernandez S, Vercrusse C, et al. Hybrid bioprinting of chondrogenically induced human mesenchymal stem cell spheroids. *Front Bioeng Biotechnol* 2020; 8: 484.
257. Liang Y, Idrees E, Andrews SHJ, et al. Plasticity of human meniscus fibrochondrocytes: a study on effects of mitotic divisions and oxygen tension. *Sci Rep* 2017; 7(1): 2148.
258. Baker BM, Nathan AS, Huffman GR, et al. Tissue engineering with meniscus cells derived from surgical debris. *Osteoarthr Cartil* 2009; 17: 336–345.
259. Ogura T, Suzuki M, Sakuma Y, et al. Differences in levels of inflammatory mediators in meniscal and synovial tissue of patients with meniscal lesions. *J Exp Orthop* 2016; 3: 7.